TU Delft Delft University of Technology

M.Sc. Thesis

Effect of insertion and rotational velocity on friction between catheter and tissue

Author:
Tim van der Maas

Supervisors:
Ir. Dennis van Gerwen &
Dr. John J. van den Dobbelsteen

September 2, 2011

Faculty of Mechanical, Maritime and Materials Engineering
Delft University of Technology

PREFACE

This thesis includes the work and research done during the final stage of the study Biomedical Engineering. The research was performed at the Minimally Invasive Surgery and Interventional Techniques (MISIT) section which is within the BioMechanical Engineering (BME) department of Delft University of Technology. The reason for the experiment is the idea of developing a steerable needle existing of a flexible tube and a cutting device as was discussed in the literature report. The aspects that are of importance for the development of this needle were first investigated. One of the aspects is the friction force and this aspect was investigated during the experimental stage of the project.

During the graduation I came into contact with the field of research for the first time. This was challenging but nevertheless interesting. I've learned a lot and hope to use the gained knowledge in a career in the field of research. I am also interested in health care and for me the ideal situation would be a combination of research and health care.

I would like to thank my supervisors Ir. Dennis van Gerwen and Dr. John J. van den Dobbelsteen as well as my Professor Jenny Dankelman for their support. I also would like to thank Dr. Ir. A. van Beek for his eye opening view and explanations; Ir. T. Horeman for his support and motivation; A. van Dijke for his technical support and motivation; J. Dukker for producing the parts of the setup; Dr. Ir. Abbink for his view and support; P. Moore for the English grammar support. Finally I would like to thank Evianne, for her support and love during this exciting period.

Tim van der Maas, September 2011

LIST OF SYMBOLS

Symbol	Variable
Ω	rotational velocities in rev/s.
β	Percentage of the contact area that is separated by a lubricant.
δ	logarithm of overshoot.
ε	The continuous contribution of the leaf springs to the insertion force .
ζ	The damping ratio.
η	The viscosity of the lubricant.
λ	The coefficient for the lubricant profile.
μ	Friction coefficient.
μ_s	Friction coefficient for the area where the surfaces are in direct contact.
μ_m	Friction coefficient for the area that is separated by the lubricant.
ξ	the ratio between the smallest and largest film thickness.
ρ_{alu}	Density aluminum.
ρ_{water}	Density water.
τ	The torque.
ϕ	Tip rotation of the beam.
ω_0	The natural frequency of the system.
ω_n	Natural frequency.
A	The contact area (of the lubricant).
A_{pl}	Cross section area of plateau.
C	Scale factor.
C_{corr}	Additional correction factor.
C_{lOS}	Correction factor for overshoots larger than 100%
E	The modulus of elasticity.
F	The force acting on the tip of the beam.
$F_{cutting}$	The cutting force.
$F_{friction}$	The friction force.
$F_{fin}(x)$	$F_{lOS}(x)$ after correction.
$F_{insertion}$	The insertion force.
$F_{lOS}(x)$	Model of insertion force with overshoot larger than 100 %.
F_{smax}	The maximum force that may be applied to the force sensor.
F_{st}	The steady insertion force.
$F_{stiffness}$	The force required to deform the tissue and needle/catheter.
I_{st}	The steady current.
I	The moment of inertia.
L	Length of the beam.
M	The moment acting on the tip of the beam.

Symbol	Variable
N	Normal force.
$Vrot$	Rotational velocity.
$Vins$	Insertion velocity.
$Vres$	Resultant velocity.
Rt	Maximum surface roughness.
oscillation peaks.	
Ra	Average surface roughness.
S_b	Sliding friction during boundary lubrication.
S_v	Sliding friction during hydrodynamic lubrication.
S_{steady}	The steady value considered as the horizontal line between the upper and lower
T	Period.
T_{setl}	Settling time.
$U(k)$	The fourier transform of u(k).
$Y(t)$	The fourier transform of y(t).
b	The width.
b_{br}	With of bracket.
f	frequency.
h	The height.
h_0	The smallest film thickness.
h_1	The largest film thickness.
h_{br}	Height of bracket.
$h/l/b_{co}$	Height = length = width container.
k	The stiffness.
k_{leaf}	The stiffness of the leaf spring.
k_{lf1}	The stiffness of the first leaf spring.
k_{lf2}	The stiffness of the second leaf spring.
k_{sensor}	The stiffness of the force sensor.
l_{pl}	Length of plateau.
l_{br}	Length of bracket.
m	The mass of the system.
m_{cl}	Mass clamp.
m_{co}	Mass container.
r_{cath}	The radius of the catheter.
$u(k)$	An discrete input signal.
v	The displacement.
v_0	The stationary velocity between the two surfaces.
v_{pen}	The tangential velocity.
v_{smax}	The maximum deflection of the force sensor or maximum displacement of the plateau.
x	Displacement of the catheter.
$y(t)$	A continuous input or value.

LIST OF ABBREVIATIONS

ANOVA	Analysis of the Variance.
BME	BioMedical Engineering.
DFT	Discrete Fourier Transform.
MISIT	Minimally Invasive Surgery and Interventional Techniques.
NIDAQ	National Instruments Data Acquisition device.
VAF	Variance-Accounted-For.
WTC	Water holding Capacity.

CONTENTS

CHAPTER

1

CONCEPT PAPER

In the next chapter the concept paper is presented. This is the main part of the report. After reading the concept paper, a clear and concise answer should be obtained on the questions why the experiment is performed, how the experiment is performed, what the results are and what the findings are.

Effect of insertion and rotational velocity on friction between catheters and tissue

J.P. van der Maas

Abstract

Purpose: An accurate needle or catheter placement is essential for the success of many procedures like regional anesthesia or biopsy taking. The accuracy of the needle or catheter placement could be increased by application of a rotational motion, which reduces the tissue indentation and required insertion force, as is presented in this paper.
Materials and methods: A shortened catheter (5F/1.67 mm Pig angiographic, Boston Scientific, ref. 16391-41, 31 cm) strengthened by a carbon fiber which perfectly fits inside the catheter, was pulled through muscle tissue (pork tenderloin) over a distance of 125 mm in directions parallel or perpendicular to the muscle fibers. Insertion velocities of 1, 10 and 50 mm/s were applied in combination with 0, 114 and 572 RPM. The friction force between the tissue and catheter was measured by the use of a force sensor (Futek Lsb200, 2.5 N). In total 576 measurements were obtained using 16 tissue samples.
Results: The results show that the fiber orientation has no effect on the amount of friction. Also the insertion velocity on its own has little effect on the steady friction force. However, comparing the same combinations with different insertion velocities, differences in the amount of overshoot can be found. A higher insertion velocity normally result in higher overshoot. In contrast, the rotational velocity can affect both the overshoot as well as the final amount of friction. An increased rotational velocity normally results in a reduced overshoot. The steady insertion force is reduced when the tangential velocity is higher than the insertion velocity. A larger ratio results in a lower amount of friction. The reduction in steady insertion force can be as large as 97% when comparing the perpendicular insertions with 1 mm/s and without rotation with the perpendicular insertions with 1 mm/s and 572 RPM (0.76 N and respectively 0.021 N with $p = <0.001$) .
Conclusion: We conclude that friction forces between instrument and tissue can be reduced by application of a rotational motion especially when the tangential velocity is much larger than the insertion velocity. Hence, rotation of needles and catheters might reduce the effect of indentation and tissue movements and therefore increase the precision of needle or catheter placement.

1 Introduction

Needles are used in several percutaneous interventions such as biopsies, brachytherapies, anesthesia, cryo-ablation and thermo ablations [1]. The success of these interventions depends on the accuracy of needle placement [2]. Furthermore, not all places in the body can be reached due to obstructions, like bone, and vulnerable tissue [2, 3]. Nerves for example should be avoided at all times. More information is required about needle tissue interaction for the development of a steerable needle which can avoid obstructions or for realistic needle training devices [2, 4].

During insertion of a needle mainly three forces can be distinguished, cutting forces, friction forces and deformation forces [2] (appendix A). Cutting forces are essential to pierce through tissue. The interaction between tissue and needle shaft results in friction forces. The friction acts in the opposite direction of the needle displacement. The deformation of the needle and the tissue results in deformation forces. Experimental studies show that rotation during the insertion of a needle reduces friction force as well as tissue deformation [3, 5, 6, 7, 8]. Tissue deformation is influenced by the friction between the needle shaft and the surrounding tissue [5, 9]. This in turn results in an inaccurate needle placement and therefore treatment outcome [5, 9, 10]. Also it is found that the insertion force is affected by the insertion velocity [3, 5, 6, 7, 8].

Friction reduction can be of interest for the development of a steerable needle and can provide information about the friction force itself. With reduced friction, the ease of placement of a steerable needle is increased and the chance on difficulties like buckling reduces. Another application is for example layer recognition. When the friction is low compared to the cutting force, piercing through layers can be noticed more easily. A reduced friction also leads to a reduced tissue deformation which in turn can increase the accuracy of the needle placement.

Needles are used in all the mentioned existing studies, therefore cutting forces are involved which influence the insertion forces. Furthermore, the existing studies are performed with different phantoms, different needles and different velocities which makes it hard to compare the individual studies. For this reason cutting forces were eliminated in this study. Furthermore it provides an answer on the question if a friction reduction can also be found for catheter rotation.

Catheters are made of polymers instead of metal, hence they are normally more flexible than needles. The idea was to develop a needle which uses this property and is able to make curves with small radii. The needle consists of a catheter as shaft and a steerable cutting device as tip.

The goal of this experimental study is to clarify the relation between friction force and insertion and rotational velocities during the insertion of a catheter. It is expected that the fiber orientation of the tissue has no effect on the amount of friction. To verify this, also the influence of the fiber orientation on the friction force is investigated. Looking at friction models of boundary lubricated sliding and lubricate sliding (appendix C) it can be expected that any rotational velocity will reduce the friction force; that an increased insertion velocity will decrease the friction force; and that the friction is not affected by the fiber orientation in the tissue. The minimum and maximum film thickness is the same for both fiber directions, therefore it can be expected that the friction is also the same in both fiber directions. These hypotheses will be verified by the results of the experiment described in this paper which in turn can be used to improve percutaneous devices and training.

2 Method & Materials

During the insertion of a needle mainly three forces occur: cutting, friction and deformation forces. However only the friction force is of interest in this experiment. The other forces should not contribute to the force measurements. To avoid cutting forces and to avoid deformation forces as much as possible, a catheter (a straight tube made of a polymer), is pulled in a straight path through tissue. In this way cutting forces are eliminated and the catheter and tissue are only loaded in the direction of the movement.

The experiment and some background information are discussed in detail in this chapter.

2.1 The experiment

During the experiment, the insertion force and torque required to move the catheter through tissue are measured. The insertion velocity, rotational velocity and the tissue orientation will vary. It is important that other parameters do not influence the measurements and stay constant. During the next sections the choices concerning the experiment are discussed.

2.1.1 Experimental setup

The experimental setup consists of the catheter that was pierced through the tissue and attached to the motor shaft. The motor was attached to the plateau of a linear stage. This made it possible to apply a certain rotational and insertion velocity at the catheter.

The tissue was enclosed by a container, a commercial plastic storage box of 50x50x50 mm, which was attached to a plateau. This plateau was supported at each end by a leaf spring which made the plateau able to move almost freely (continuous contribution of 2% to measured force, see appendix F) forwards and backwards with the amount of deflection of the force sensor (0.13 mm).

The friction force between the catheter and tissue during forward movement resulted in a pulling force on the tissue. The pulling force was transmitted to the container which in turn was transmitted to the plateau which was supported by the leaf springs.

This force, the insertion force, was sensed by a force sensor which was statically undetermined attached between the plateau and the ground by the use of rot-ends. The torque was determined by measuring the current of the motor which is linearly proportional to the torque.

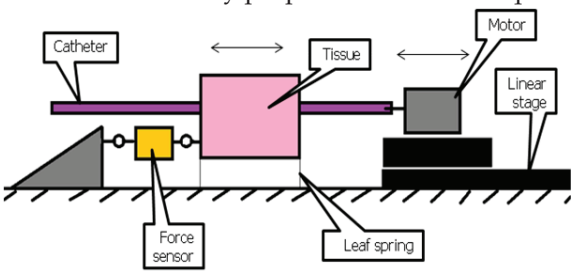

Fig. 1: Sketch of experimental setup.

Force sensor: An experiment was performed to determine the required range of the force sensor by measuring the force required to extract a deflectable puncture needle (15G/1,829 mm Daum ref. 10227) from beef and pork tenderloin (appendix B). Different sizes up to 100 mm and different phantom orientations were used and the results show that the force never exceeds

1.5 Newton. When a safety factor of 1.5 is used, forces up to 2.25 N can be suspected and a force sensor of 2.5 N (Futek Lsb200) in combination with a standard amplifier is chosen.

Motor: The required torque ($1.9\times10^{-}3$ Nm) of the motor is determined by the required insertion force (2.25 N) times the radius of the catheter (0.84 mm). The maximum speed that will be applied is 572 RPM which results in a required power of 0.11 Watt. However a motor of 0.75 Watt is chosen (Maxon RE10 0.75 W 256085) with a gear (GP10 A 16:1 218416) and encoder (MR S 16 c/t) in combination with a controller (LSC30/2 250521). This was the smallest motor gear combination that can be combined with an encoder and controller.

The small motor is attached on the plateau of the linear stage and has a low mass which makes it easier to accelerate. The motor was also used to measure the torque during the insertion because no suitable torque sensor could be found. For this reason the motor with the lowest torque constant ($2.14\times10^{-}3$ Nm/A) and direct current was chosen.

Current sensor: The current was measured by an Ametes CS0.25A-02 with a resolution of 0.1 mA which was connected between the controller and motor. The torque is determined by the net motor current (measured current minus the current with no load). The torque (τ) is linear proportional to the current:

$$\tau = \frac{\Psi \cdot (I_{st} - I_0)}{r_{cath}} \tag{1}$$

Where I_{st} the steady current, Ψ the torque constant, I_0 the no load current (23.4 mA) and r_{cath} the radius of the catheter.

Linear stage: The linear stage (Aerotech PRO115) that was available was used which is driven by a 120 Watt motor (Maxon EC 40 ref. 167181) in combination with a hall sensor (Scancon 2RMHF7500) and controller (Maxon DES 50/5 ref. 205679) which in turn was controlled by a dSPACE system (DS1104 R&D).

Temperature monitoring: During the experiment the temperature of the surface of the catheter at a distance of 1 cm from the tissue was monitored by an infrared temperature sensor (Optris LS LT). The sensor was controlled and read during the experiment by the use of a MATLAB computer program.

Setup monitoring: A Webcam (Creative Life! HD) in combination with an optical lens was used to monitor the front side of the container where the catheter exits the tissue. A movie for each run was stored separately.

Data acquisition & control: All sensors and actuators, except the temperature sensor, were connected to a data acquisition device (NI USB6008) which was connected to a laptop. Measuring and controlling was performed by the use of a MATLAB program running on the laptop.

The linear stage and motor can be controlled by applying a set voltage to the dSPACE system and respectively to the motor controller. A schematic wiring diagram is shown in figure 2. The dSPACE system was used to keep the stage at the velocity set by the data acquisition device. The motor controller did the same for the rotational velocity of the motor.

2.1.2 The phantom

The human body is almost completely covered by muscle tissue and muscle tissue comprises more than one third of the weight of an adult [11]. This makes it likely that muscle tissue is involved during needle insertions and pork tenderloin or pork muscle, direct from the abattoir was used as a phantom. Pigs are mammals like humans and pork tenderloin is commercially available. The pigs of about 6 to 7 months old, were aged for one day before the tenderloins were removed and packet vacuumed.

Muscle contain parallel arranged protein fibers (see figure 3) which carry the load [12]. These fibers are also present in other types of tissue like connective tissue. The arrangement of the fibers is important for the behavior of the tissue what in turn can effect the friction [12]. By choosing muscle tissue it is also possible to investigate the effect the fiber orientation on the friction during the catheter insertion.

During the one hour transport the tenderloins were left in the packages and unpacked at arrival. The pork tenderloins were stored at $7°C$ in boxes in a suspension of de-mineralized water with physiological salts to prevent dehydration. The used tenderloins were between 1 and 4 days old to make sure that the rigor mortis had stopped and the change of stiffness of the muscle over time is minimized (appendix E).

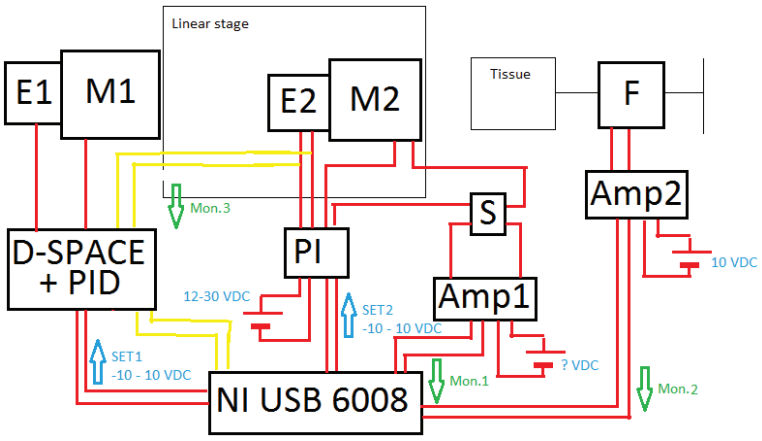

Legend

E1:	Encoder Motor linear stage
M1:	Motor linear stage
E2:	Encoder Motor for rotating the tube
M2:	Motor for rotating the tube
F:	Force sensor
Amp2:	Amplifier force sensor
PI:	Controller motor for rotating the tube
S:	Current sensor
Amp1:	Amplifier current sensor
SET1:	Setting voltage for set velocity linear stage
SET2:	Setting voltage for set rotational velocity tube
Mon.1:	Monitor current, -10 - 10 VDC
Mon.2:	Monitor Force, -10 - 10 VDC
Mon.3:	Monitor encoder signal

Fig. 2: Sketch of the wiring.

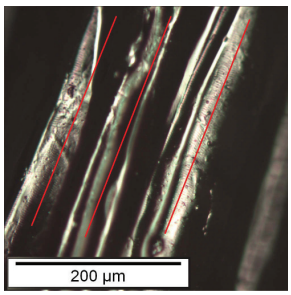

Fig. 3: Image of a cross-section of muscle tissue, pork tenderloin, with optical microscope and 50x magnification. The fibers are parallel arranged as indicated by the lines.

2.1.3 The catheter

The smallest available catheter (5F/1.67 mm Pig angiographic, Boston Scientific, ref. 16391-41) was used in the experiment. Small diameters decrease the flexural rigidity which makes it easier to follow a curvature which in turn is beneficial for a steerable needle.

However, for the experiment this is undesired since a very flexible catheter will bend under its own mass and hinder the insertion. To prevent this, the catheter is shortened to a length of 31 cm and strengthened by a carbon fiber which perfectly fits inside the catheter. Furthermore, a smaller diameter will harm the patients less compared to needles or catheters with a larger diameter [13].

Also the properties of the catheter are important for the type of friction. The exact material of the catheter was not specified by the manufacturer, however catheters are normally made of polymers such as polyethylene, polyurethane, polyvinyl chloride, Teflon and silicone elastomers [14]. A polymer consists of long shaped molecules and behaves viscoelastically like tissue [15].

The surface roughness is of importance for the amount and type of friction. The lubricant can be squeezed out easier when both surfaces are smooth. The same holds if both surfaces are relatively rough. In this case, the possibility exists that protrusion of the surfaces interlock which increases the amount of friction [16].

An analysis of the surface roughness of the catheter was performed (see figure 4) which shows a maximum roughness (Rt) of 4,59 μm and average roughness (Ra) of 0,79 μm. The different levels on the surface of muscle tissue reflected insufficient light therefore it was not possible to perform an analysis of the roughness of the muscle tissue.

However from the optical picture of figure 3 it can be expected that the muscle fibers have diameters of around 80 μm. The surface profile of the catheter shows distances of 20 μm between the peaks and so the fibers cannot be interlocked between the peaks. The surfaces are carried by the contact points and the lubricant can not be squeezed out completely. This will increase the lubricant layer and makes it more likely that a type of lubricated friction will occur.

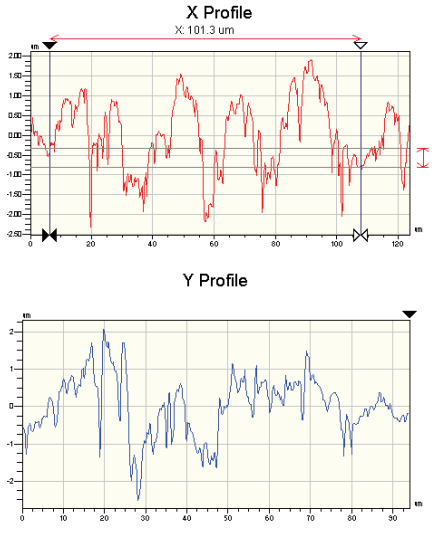

Fig. 4: Analysis of the surface of the catheter. A maximum roughness (Rt) of 4.59 μm and maximum average roughness (Ra) of 0.79 μm.

2.1.4 Insertion and rotational velocities

The choice of the rotational and insertion velocities were based on velocities used in experimental studies with needles found in literature. These experiments are performed with needles in different phantoms. Unfortunately, the results found during the literature search were inconsistent. For this reason a large range of velocities was used during the experiment with the tube.

Second, the effects of low and high velocities on the friction force were investigated. The velocities were chosen in such a way that some of the combinations results in roughly the same resultant velocity. For the experiment, the following settings were chosen:

Tab. 1: Settings for the experiment

Parameter	Settings
Fiber orientation	0 and 90°
Insertion velocity	1, 10 and 50 mm/s
Rotational velocity / tangential velocity	0, 114 and 572 RPM / 0, 10, 50 mm/s

Tab. 2: Table of all the eighteen possible combinations.

	Tissue orientation					
	0°			90°		
	Perpendicular velocity (mm/s)					
Insertion velocity (mm/s)	0	10	50	0	10	50
1	c1	c2	c3	c10	c11	c12
10	c4	c5	c6	c13	c14	c15
50	c7	c8	c9	c16	c17	c18

2.1.5 Design of the experiment

A factorial design for the experiment was chosen because it is an efficient way to investigate multiple factors. Three points for the rotational and the three points for the insertion velocities were used to give an indication of the friction/velocity curve. The choice of the insertion and rotational velocities were based on experimental studies with needles found in literature and such that some combinations result in the same resultant velocity [3, 5, 6, 7, 8].

Practically, a (steerable) needle will cross tissue in all directions. For this reason the effect of the fiber orientation on the friction is investigated. Insertions parallel and perpendicular to the fibers were performed. The three rotational velocities, three insertion velocities and the two tissue orientations result in eighteen combinations as shown in table 2 which were applied in random order.

It was difficult to make a prediction of the required repetitions to obtain a sufficient statistical power because of the multiple factors of the experimental design. For this reason it was chosen to perform as much as possible measurements within the budget and within the available time.

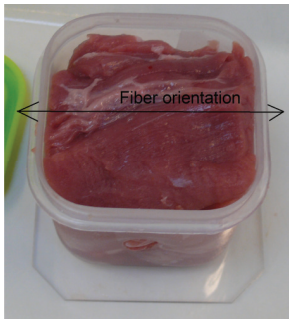

Fig. 5: The container filled with meat. The meat is arranged such that the fibers are orientated in horizontal direction.

2.1.6 Procedure

The first step was to prepare a phantom by cutting approximately a 50 mm-cube shaped sample from a tenderloin which was placed in the container. The sample was placed in the container such that the insertion is parallel or perpendicular to the muscle fibers (see figure 5). If necessary an additional piece of meat was added to completely fill the container. The phantom was acclimatized for two hours before it was used.

The second step was to make a hole in the phantom with a shortened trocar needle (18G/1.27 mm COOK ref. G02901) in combination with a special tool (see figure 6) in the right fiber orientation assigned by the MATLAB program. The tool, attached a hole in the container, has nine holes and guides the needle in a straight path through the tissue. A non used hole had to be chosen and in this way 18 holes had to be made in total for the two orientations. Every hole was used two times, so 36 measurements could be performed with one phantom.

After the needle was placed thought the tissue, the guide tool was removed. Now, the catheter was place over the needle and the catheter with needle was pushed through the tissue after which the needle was removed. The container was then attached to the plateau with a clamp and the first run with random settings could be performed.

Before each measurement was started, the maximum rotational velocity was performed for 2 seconds, to make sure that there was no stationary contact (appendix D). After traveling 125 mm during the measurement, the stage was returned to its initial position with 10 mm/s. When the stage was back to its initial position.

The second run, which took place in the same hole, is now started by tapping the space bar.

Then everything from step 3 onwards was repeated until every combination was performed twice, so 36 measurements. In total 16 appropriate runs were performed resulting in 576 measurements.

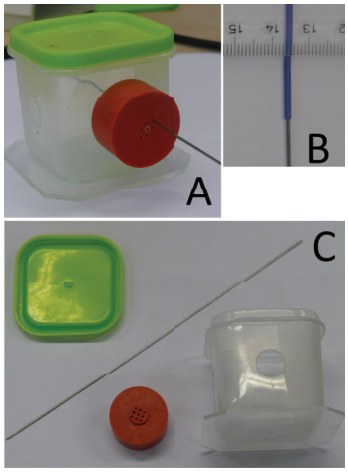

Fig. 6: A: Needle inside guide tool. B: Needle inside catheter with ruler in the background C: Overall picture of container with cover, needle and tool

2.2 Data analysis

The insertion force measurements show different step response curves (see figure 9). However on these curves several oscillations could be found. A pilot experiment with a gel phantom was performed to figure out if the oscillations are related to the properties of the meat (appendix G). These measurements also show oscillations (see figure 7 & 8).

A spectral analysis shows oscillations around 1.9, 9.5 and 43 Hz (appendix G). These frequencies match the natural frequencies of the setup (see appendix E.2). The container can oscillate with a natural frequency of 43 Hz caused by the leaf springs, force sensor and mass of the gel. Due to the rotational velocity, the system starts to oscillate with 1.9 or 9.5 Hz (appendix E.2). However this frequency is within the range of interest. A low pass (Butter-worth, zero phase) of 30 Hz is used to filter out the natural frequency of the setup. The contribution of the natural frequency is normally higher than of the rotations. The filtered data is used for the analysis. However, for the analysis of the settling time (discussed in the next section), a moving average filter (150 samples, zero phase) is used instead of a frequency filter to smooth irregularities.

2.2.1 Insertion force in time

Mainly three types of step response curves can be found for the insertion forces as shown in figure 9. Overshoot can be found in settings with no rotation or where the insertion velocity is higher than or equal to the rotational velocity. Settings where the rotational velocity is higher than the insertion velocity show normally curves similar to the step response without overshoot except the settings with 1 mm and 572 RPM. This setting is represented by a horizontal line at the steady value.

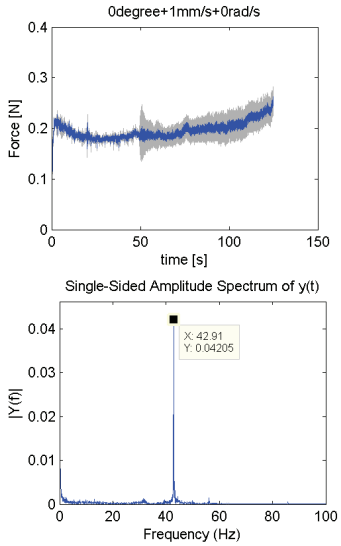

Fig. 7: **TOP:** Plot of a measurement of the insertion force with the setting 0°, 1 mm/s and 0 RPM in gel. In blue data filtered with a 30 Hz low pass zero phase filter and in gray the unfiltered data. **Bottom:** Fast Fourier transform plot of the above insertion force.

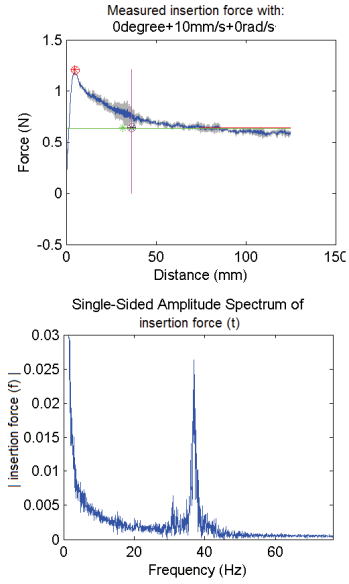

Fig. 8: **TOP:** Plot of a measurement of the insertion force with the setting 0°, 10 mm/s and 0 RPM in meat. The green line is the steady value, the pink line the settling time and the red dot the maximum value. **Bottom:** Fast Fourier transform plot of the above insertion force.

The data is analyzed with the step response analysis function of MATLAB 'stepinfo.m'. The first and last 1/25th part of the data is not used

by this function. The median of the last 2/5th part of the data is used as steady value. The settling time is stated as the time to reach and stay within 10% plus an amount of 0.1 N of the steady value. The maximum threshold is 100%. The distances to reach a steady value are calculated from the settling times by multiplying them by the insertion velocities that were applied.

The characteristics of the curves, the steady value, the overshoot or maximum and the settling distance, are presented in the box plots of figure 10, figure 11 and figure 12. All 576 measurements are used for the calculations.

In total twelve measurements are marked as 'failed', ten exceed the 4 N and two had a deviant curve. These 'failed' measurements are replaced by the group medians [17]. In this way, the group medians are least influenced. The fact that this lowers the standard deviation [17] can be neglected. In exceptional cases, up to four values within a group are replaced by the group medians. For the settling time, an additional 16 measurements are replaced by the group median because the MATLAB function could not find the settling time time within the set boundaries.

Below each box plot, a table is mentioned with statistical tests of the settings. In the next section is discussed how they are obtained. The characteristics of the curves are discussed separately in the next chapter.

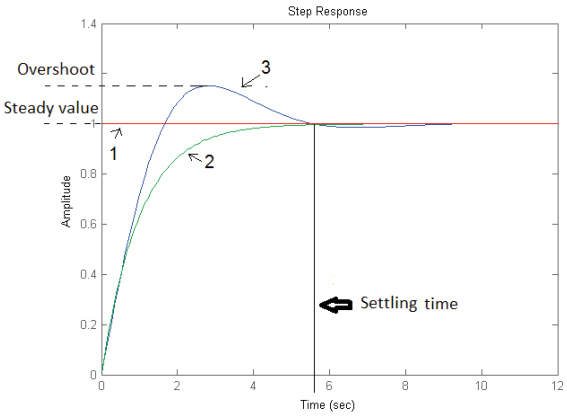

Fig. 9: 1: horizontal line at steady value, 2: step function without overshoot, 3: step function with overshoot.

2.2.2 Statistical tests

Below each set of box plots a table with an analysis of variance (ANOVA) is presented, which is performed in SPSS to investigate significant effects of the different parameters [17]. 'Failure' market measurements are replaced by the group medians (calculated without 'failures') [17]. A repeated measure is chosen because the effects of the settings within the phantoms are of interest [17].

The tables present two results. The first column is the outcome of ANOVA when it is assumed that the data is spherical. To meet sphericity, the variance between different levels should be equal. The second column contains the results of the Greenhouse Geiser. The Mauchly's test was performed which shows that some of the data is not spherical [17]. These are indicated by '*'. In these cases the results of the Greenhouse Geiser has to be chosen.

In a regular ANOVA it is assumed that the variation is equal in each group, so sphericity is met [17]. However when this is not the case, more or less overlap between the groups can be found, which is not assumed in the regular ANOVA. The Greenhouse Geiser test provides a correction factor which compensates the differences in variance and so the effect of the parameter can be investigated [17]. A significance level of 0.05 is used in all tests.

ANOVA shows if a factor has any effect but does not tell anything about the effect of the individual levels of the factor. As was discussed, sphericy is not always met and a regular post hoc test, where the effect of each individual level is investigated, could not be performed. For this reason several t-test were performed to compare the means of two groups with each other. A p-value below 0.005 shows that the means significantly differ. In the box plot can be seen which group is larger than the other group.

3 Results

In this chapter the results of the insertion force and torque measurements are presented. As was discussed, the insertion force measurements in time show different step responses. The characteristics are presented separately in the first sections. In the following section the results of the torque measurements are presented. The last section contains the resultant insertion force which is calculated from the steady insertion force and steady torque measurements.

3.1 Steady insertion force

Figure 10 shows box plots of the steady insertion force data and table 3 the statistical analysis of variance (ANOVA).

The box plot of figure 10 shows that groups were a rotation is applied have normally a lower median steady friction force compared to groups without rotations. This is also confirmed by the t-tests. Remarkable are settings with an insertion parallel to the muscle fibers in combination with equal insertion velocity and tangential velocity. Here, the median steady insertion force increases. The same combinations with perpen-

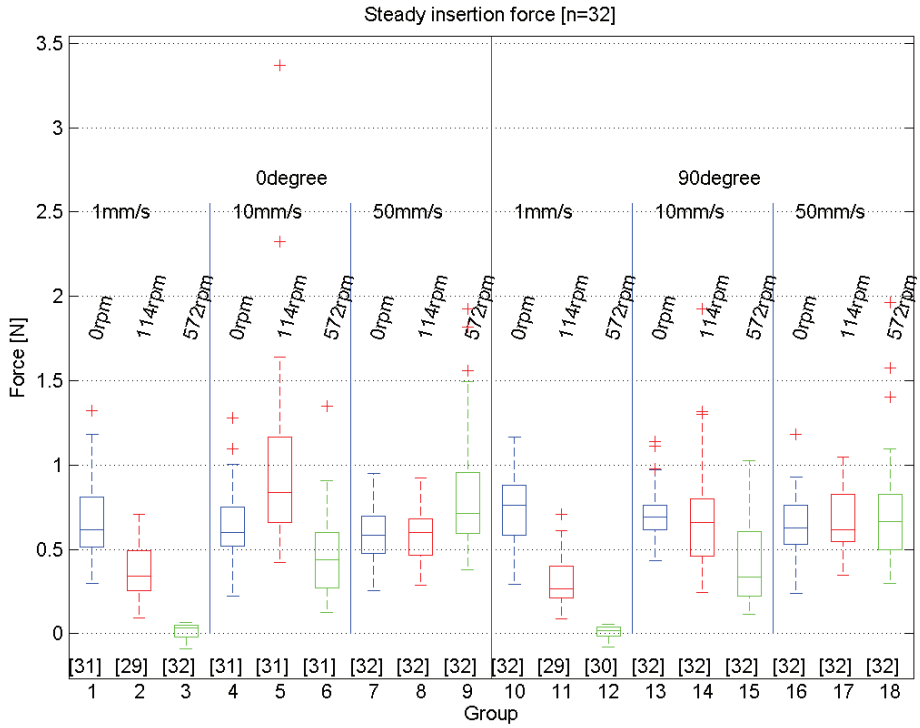

Fig. 10: Box plots of steady insertion forces for each combination. The box plots are of checked measurements without 'failures' ([n]). The groups are filled up to the group size of 32 by (32-n) times the group medians.

Tab. 3: Left: Table with two tests: Regular ANOVA where spherical is assumed and the Greenhouse Geisser where a correction factor is used to compensate non spherical. Factors with P-values lower than 5% affect the steady insertion force. Factors with other values do not have a significant affect on the insertion force. Sphericity of the data is tested with the Mauchly's test of sphericity. Non spherical factors are indicated by '*'. **Right:** Table with several t-tests. P-values lower than 5% show that the group means significantly differ.

Setting	Sphericy assumed	Greenhouse Geisser
Orientation	0.512	0.512
Insertion velocity	<0.001	<0.001
Rotational velocity	<0.001	<0.001
Orientation × ins. vel.	0.060	0.068
Orientation × rot. vel.	0.001	0.002
Ins. vel. × rot. vel.*	<0.001	<0.001
Or. × ins. vel. × rot. vel.*	0.007	0.023

Comparison	p-value	Comparison	p-value
Group 1 vs 2	<0.001	Group 10 vs 11	<0.001
Group 1 vs 3	<0.001	Group 10 vs 12	<0.001
Group 1 vs 4	0.394	Group 10 vs 13	0.406
Group 4 vs 5	0.001	Group 13 vs 14	0.910
Group 4 vs 6	0.006	Group 13 vs 15	<0.001
Group 4 vs 7	0.285	Group 13 vs 16	0.069
Group 7 vs 8	1.00	Group 16 vs 17	0.272
Group 7 vs 9	<0.001	Group 16 vs 18	0.067
Group 1 vs 7	0.055	Group 10 vs 16	0.006

dicular insertions do not have this effect. Here the rotation has little affect on the median steady insertion force. These findings were also verified by a t-tests. The differences between these two settings can explain the significance of the interaction effect between the orientation and rotational velocities mentioned in the table.

The table also shows that the steady insertion force is affected by the insertion and rotational velocities. Furthermore an interaction effect [1] between the insertion and rotational velocities as well as between the orientation of the fibers and rotational velocities can be found. Also an interaction effect on the steady insertion force of all parameters can be found. However, the reliability of results of a three way interaction are contestable.

Furthermore, some of the steady insertion forces are negative. The steady insertion forces are corrected with an offset value which repre-

[1] An interaction effect of x and y on z means that the influence of y on z is also influenced by the parameter x. The individual effects cannot be added together to get the overall effect.

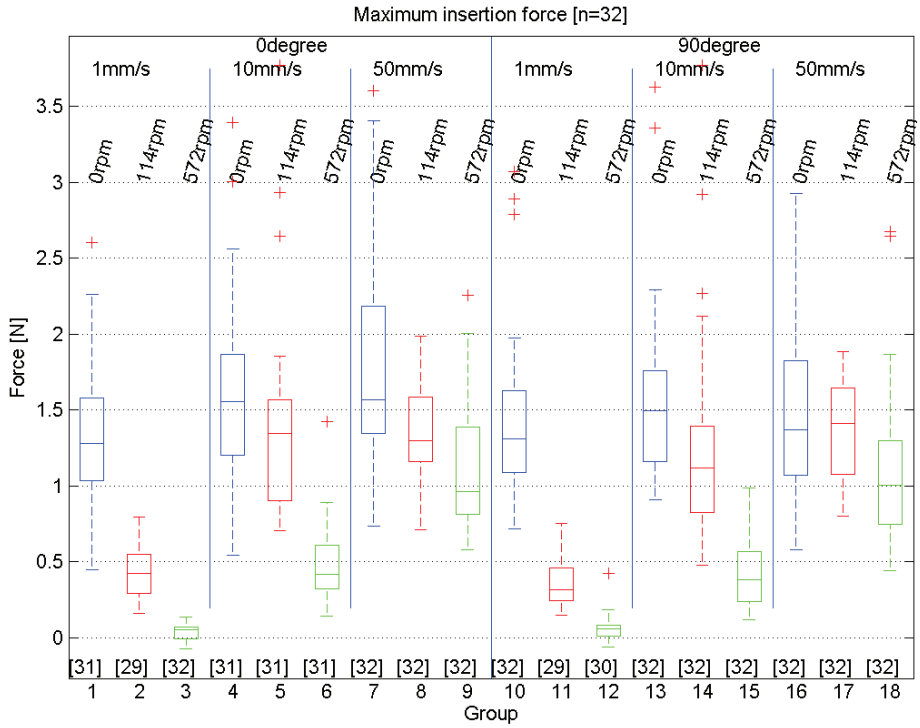

Fig. 11: Box plots of maximum insertion forces for each combination. The box plots are of checked measurements without 'failures' ([n]). The groups are filled up to the group size of 32 by (32-n) times the group medians.

Tab. 4: Left: Table with three tests: Regular ANOVA where spherecy is assumed, Greenhouse Geisser where a correction factor is used to compensate non spherecy. Factors with P-values lower than 5% affect the maximum insertion force. Factors with other values do not have a significant affect on the maximum insertion force. Sphericity of the data is tested with the Mauchly's test of sphericity. Non spherical factors are indicated by '*'. **Right:** Table with several t-tests. P-values lower than 5% show that the group means significantly differ.

Setting	Sphericy assumed	Greenhouse Geisser
Orientation	0.375	0.375
Insertion velocity*	<0.001	<0.001
Rotational velocity	<0.001	<0.001
Orientation × ins. vel.*	0.279	.277
Orientation × rot. vel.*	0.573	0.564
Ins. vel. × rot. vel.	<0.001	<0.001
Or. × ins. vel. × rot. vel.	0.205	0.217

Comparison	p-value	Comparison	p-value
Group 1 vs 2	<0.001	Group 10 vs 11	<0.001
Group 1 vs 3	<0.001	Group 10 vs 12	<0.001
Group 1 vs 4	0.026	Group 10 vs 13	0.203
Group 4 vs 5	0.121	Group 13 vs 14	0.007
Group 4 vs 6	<0.001	Group 13 vs 15	<0.001
Group 4 vs 7	0.330	Group 13 vs 16	0.374
Group 7 vs 8	0.001	Group 16 vs 17	0.183
Group 7 vs 9	<0.001	Group 16 vs 18	0.001
Group 1 vs 7	0.001	Group 10 vs 16	0.770

sents the measured force without load. This is an average value of three measurements and the offset can slightly vary due to the play of the setup. In turn, this can cause some of the values to be slightly below zero. Also noise will contribute to this.

The first nine settings and the last nine settings are roughly the same which can explain that the effect of the orientation is not significant. The insertion velocity especially has an effect in combination with a rotation. The differences between the settings with no rotation are small. Summarized:

- The median steady insertion force is reduced for settings where the tangential velocity is higher than the insertion velocity.
- Equal tangential and insertion velocities can result in an increased median steady insertion force.
- The median steady insertion force is not or is little affected by the insertion velocity and fiber orientation.

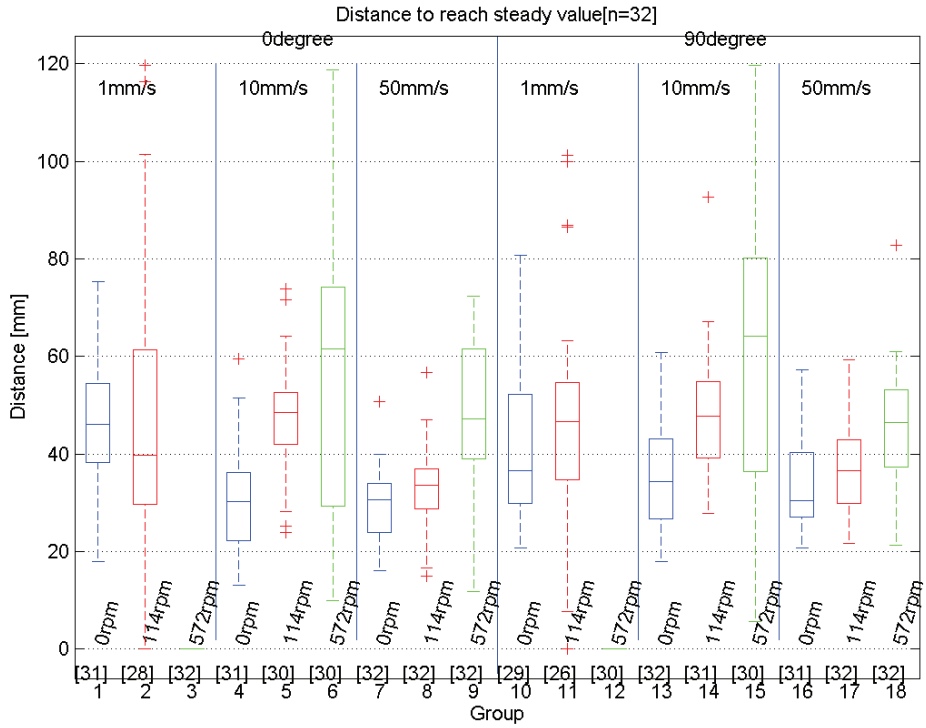

Fig. 12: Box plots of the distance to reach steady value for each combination. The box plots are of checked measurements without 'failures' ([n]). The groups are filled up to the group size of 32 by (32-n) times the group medians.

Tab. 5: Left: Table with three tests: Regular ANOVA where sphericy is assumed, Greenhouse Geisser where a correction factor is used to compensate non sphericy. Factors with P-values lower than 5% affect the distance to reach the steady insertion force. Factors with other values do not have a significant affect on this distance. Sphericity of the data is tested with the Mauchly's test of sphericity. Non spherical factors are indicated by '*'. **Right:** Table with several t-tests. P-values lower than 5% show that the group means significantly differ.

Setting	Sphericy assumed	Greenhouse Geisser
Orientation	0.501	0.501
Insertion velocity*	<0.001	<0.001
Rotational velocity*	<0.001	<0.001
Orientation × ins. vel.*	0.146	.156
Orientation × rot. vel.*	0.913	0.867
Ins. vel. × rot. vel.	<0.001	<0.001
Or. × ins. vel. × rot. vel.	0.653	0.600

Comparison	p-value	Comparison	p-value
Group 1 vs 2	0.298	Group 10 vs 11	0.226
Group 1 vs 3	<0.001	Group 10 vs 12	<0.001
Group 1 vs 4	<0.001	Group 10 vs 13	0.046
Group 4 vs 5	<0.001	Group 13 vs 14	<0.001
Group 4 vs 6	<0.001	Group 13 vs 15	<0.001
Group 4 vs 7	0.728	Group 13 vs 16	0.458
Group 7 vs 8	0.091	Group 16 vs 17	0.038
Group 7 vs 9	<0.001	Group 16 vs 18	<0.001
Group 1 vs 7	<0.001	Group 10 vs 16	0.038

3.2 Overshoot / maximum

The results for the overshoot or maximum insertion force (in cases where the overshoot is zero) are presented in figure 11 and table 4. The statistical test shows that the orientation does not affect the maximum insertion force, also not in combination with other parameters. Furthermore, it is shown that the maximum insertion force is affected by the insertion velocity as well as by the rotational velocity. Also an interaction affect between these two parameters can be found.

In the presented box plots, it is clear that an increased rotational velocity results in a reduced median maximum. This is also found by the t-tests with the exception of some groups. In comparison, an increased insertion velocity results normally in an increased median maximum. The t-tests show that this only holds for some of the groups with parallel insertions. It should be noticed that the median of the settings with no rotation and 10 mm/s compared to settings with no rotation and 50 mm/s, is the same. Settings with equal rotational velocity but with different inser-

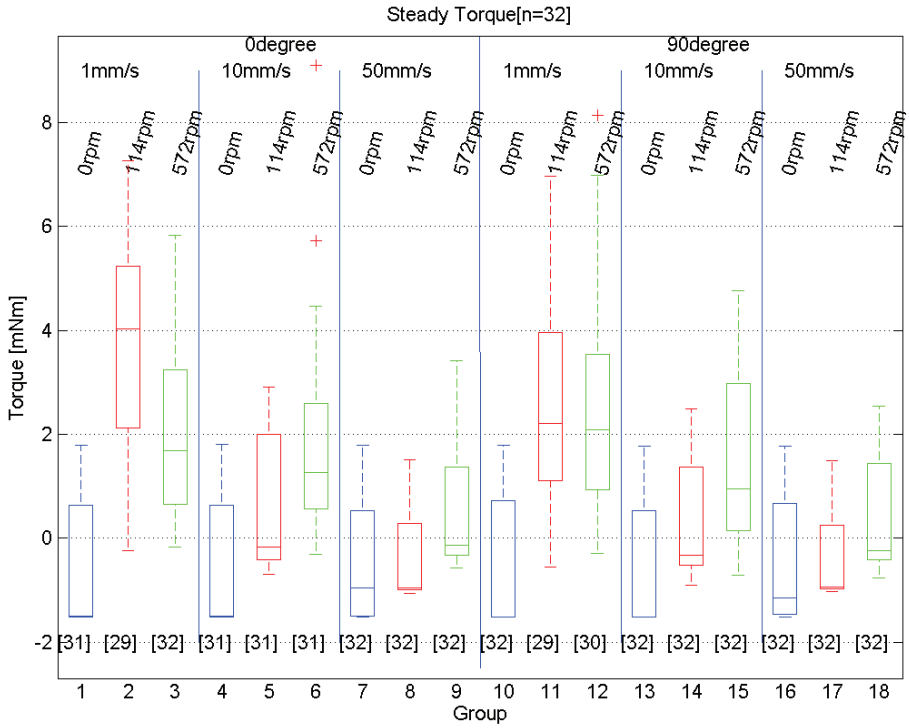

Fig. 13: Box plots of the steady torques for each combination. The box plots are of checked measurements without 'failures' ([n]). The groups are filled up to the group size of 32 by (32-n) times the group medians.

Tab. 6: Table with three tests: Regular ANOVA where spherecy is assumed, Greenhouse Geisser where a correction factor is used to compensate non spherecy. Factors with P-values lower than 5% affect the steady torque. Factors with other values do not have a significant affect on the steady torque. Sphericity of the data is tested with the Mauchly's test of sphericity. Non spherical factors are indicated by '*'. **Right:** Table with several t-tests. P-values lower than 5% show that the group means significantly differ.

Setting	Spherecy assumed	Greenhouse Geisser
Orientation	0.038	0.038
Insertion velocity*	<0.001	<0.001
Rotational velocity*	<0.001	<0.001
Orientation × ins. vel.*	0.165	.176
Orientation × rot. vel.*	0.003	0.004
Ins. vel. × rot. vel.	<0.001	<0.001
Or. × ins. vel. × rot. vel.	<0.001	0.001

Comparison	p-value	Comparison	p-value
Group 1 vs 2	<0.001	Group 10 vs 11	<0.001
Group 1 vs 3	<0.001	Group 10 vs 12	<0.001
Group 1 vs 4	<0.943	Group 10 vs 13	0.485
Group 4 vs 5	<0.001	Group 13 vs 14	<0.001
Group 4 vs 6	<0.001	Group 13 vs 15	<0.001
Group 4 vs 7	0.131	Group 13 vs 16	0.083
Group 7 vs 8	0.093	Group 16 vs 17	0.182
Group 7 vs 9	<0.001	Group 16 vs 18	<0.001
Group 1 vs 7	0.094	Group 10 vs 16	0.031
Group 2 vs 3	< 0.001	Group 11 vs 12	0.478
Group 2 vs 5	< 0.001	Group 11 vs 14	< 0.001
Group 3 vs 6	0.248	Group 12 vs 15	0.001
Group 5 vs 8	< 0.001	Group 14 vs 17	< 0.001
Group 6 vs 9	< 0.001	Group 15 vs 18	< 0.001
Group 2 vs 11	0.004	Group 5 vs 14	0.025
Group 3 vs 12	0.264	Group 6 vs 15	< 0.317

tion velocities, result in different median maximums. This explains the significant of the interaction effect of the rotational and insertion velocities in the table. Summarized:

- The maximum insertion force is not affected by the fiber orientation.
- An increased insertion velocity can results in an increased maximum insertion force.
- An increased rotational velocity results normally in a decreased maximum insertion force.
- The effect of the insertion and rotational velocity depends on each other.

3.3 Settling distance

The distance to reach a steady value, the settling distance, is defined as the settling time multiplied by the applied insertion velocity. The re-

sults in the box plot of figure 12 show that a rotational movement normally increases the median settling distance. Remarkable exceptions are settings with 1 mm/s and 572 RPM, where the median settling distance is zero.

Settings with equal rotational and insertion velocities but with different orientations results in roughly the same median settling distance. This indicate that the settling distance is not affected by the fiber orientation. This is also verified by the ANOVA presented in table 5. Also in combination with other parameters, the orientation does not affect the settling distance.

An increased insertion velocity normally results in a decreased median settling distance. This is also verified by the t-tests which shows that the means of most of the settings without rotations are different. The box plots and table indicate that there is a significant interaction effect of the insertion and rotational velocities. Summarized:

- The settling distance is not affected by the fiber orientation.
- An increased insertion velocity normally results in a decreased median settling distance.
- An increased rotational velocity normally results in an increased median settling distance.

3.4 Torque

Before the measurements are started, a rotation is applied. No clear curves could be distinguished as with the insertion force. For this reason only the results of the steady torque are presented in figure 13 and table 6. The steady torque is determined by the median of the last 2/5th part of the rough torque data. As with the insertion force, the 'failed' measurements are replaced by the group medians.

The box plots indicate that rotation increases the required torque. This is also verified by the t-tests, the means of groups with the same insertion velocity but with different rotational velocities are different. Remarkable are the settings without rotation where the torques are not zero. Due to the forward motion, rotation of the catheter can be induced. The motor controller acts against these rotations what can explain the non zero values. Other remarkable settings are at 1 mm/s velocity and 114 RPM rotation where the median torques are higher than settings with higher rotational velocities.

[2] With a significance level of 0.05.

The median torques normally decrease when the insertion velocities increase for settings with a rotation. This is also verified by the t-tests. The decrease in torque cannot be found for (all) settings without a rotation. These findings are verified by most of the results of the t-test.

The first nine settings in the box plot (with insertions parallel to the muscle fibers) follow the same pattern as the last nine (with insertions perpendicular to the muscle fibers). This can indicate that the torque is not affected by the fiber orientation. However some of the groups like group 2 vs 11 differ. Also the table with the statistical tests shows that the steady torque is affected by all parameters like the fiber orientation and they all have an interaction effect. An exception is the orientation in combination with the rotational velocity. So the torque is actually affected by the fiber orientation. Summarized:

- The steady torque can be affected by the fiber orientation [2].
- The median steady torque normally increases with an increased rotational velocity. Exceptions are settings with 1 mm/s and 114 RPM which have relatively high median torques compared to settings with 1 mm/s and 572 RPM.
- An increased insertion velocity results normally in a decreased median torque except for settings without catheter rotation.

3.5 Resultant insertion force

The steady insertion force and torque can be converted to a resultant force. This resultant force can provide information about the friction force itself. The resultant force is calculated by:

$$F_{res} = \sqrt{{F_{st}}^2 + \tau^2} \tag{2}$$

Where F_{st} is the steady insertion force and τ the steady torque. The resultant velocities are calculated by:

$$v_{res} = \sqrt{(v_{ins})^2 + (v_{pen})^2} \tag{3}$$

Where v_{ins} is the insertion velocity and v_{pen} the tangential velocity. The results of the resultant force are presented in figure 14.

Looking at the overall results and comparing them to the theory described in appendix C some contrasts can be found. First if the torque and insertion force could simply be combined to one resultant insertion force, the results with the same resultant velocities should have the same value. Groups with roughly the same resultant

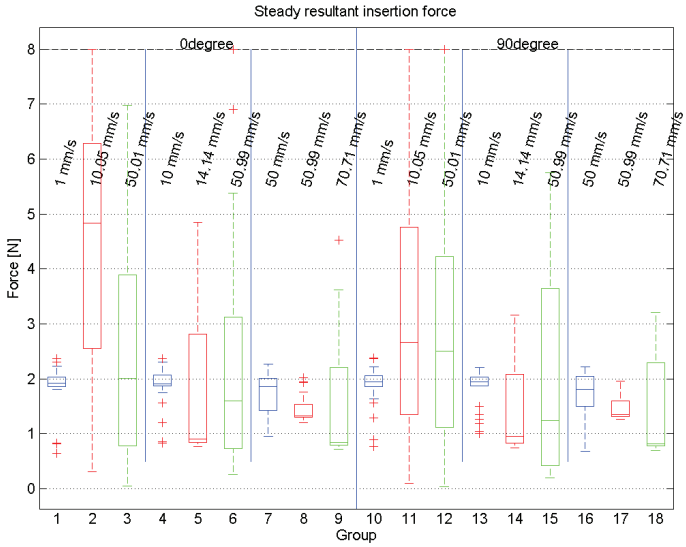

Comparison	p-value
Group 2 vs 4	<0.001
Group 3 vs 6	0.393
Group 3 vs 7	0.257
Group 7 vs 8	<0.001
Group 11 vs 13	0.018
Group 12 vs 15	0.016
Group 12 vs 16	0.080
Group 16 vs 17	0.001

Fig. 14: Left: Box plots of the steady resultant forces, calculated from the steady torque and steady insertion force. **Right:** Table with several t-tests. P-values lower than 5% show that the group means significantly differ.

velocities do not always have the same result. This is also verified by the t-tests. Most group means differ significantly from each other.

The friction in perpendicular direction could behave differently. Furthermore the resultant force is converted from the insertion force and torque which in turn is calculated from the motor current what can result in inaccuracy of the results. This makes it hard to make a prediction of the friction type.

4 Discussion

The viscoelastic behavior of the tissue appears at the friction force measurements (Appendix H). With constant insertion velocities and rotational velocities the friction forces change over time. Different combinations of settings show different curves over time. Basically three types of curves can be distinguished: a step response with overshoot, a step response without overshoot and a straight line. These curves show the presence of an initial state that changes over time to a steady state of the friction.

4.1 Effect of parameters

The results show that the fiber orientation does not affect the friction. Also is shown that the insertion velocity on its own has little effect on the final amount of friction force. However, comparing the same settings with different insertion velocities, differences in the amount of overshoot can be found. Insertion velocities of 10 mm/s or higher show higher peak values compared to the same settings with 1 mm/s. Higher velocities result in a higher shear rate and thus in a larger overshoot of the friction force.

In contrast, the rotational velocity can affect the final and initial friction force. An increased rotational velocity results in a decreased overshoot. The same holds partly for the final friction force. Settings were the tangential velocity is larger than the insertion velocity finally show a decreased friction force compared to other settings. Larger ratio's between the tangential velocity and the insertion velocity results in larger reductions.

4.2 Explanation friction reduction

However, this reduction is not due to the change of direction (as was discussed in appendix C). Settings with the same resultant velocity do not always have equal resultant friction forces. This means that the type of friction changes with the different settings.

Two types of friction were expected to occur during the insertion of the catheter: boundary lubrication and hydrodynamic lubrication. The amount of friction during hydrodynamic lubrication is normally much lower than during boundary lubrication. The difference between these types of friction is mainly the thickness of the lubricant layer between the tissue and the catheter.

4.3 Principle of sinter bearing

The friction of the catheter can possibly be described by the principle of a sinter bearing

[A. van Beek, personal communication, April 28, 2011]. A sinter bearing is build of a porous material of which the pores are filled with a lubricant [18]. Tissue that surrounds the catheter contains also a lubricant, primarily water, which is able to move through the tissue [12]. The lubricant layer in a sinter bearing is increased by a hydrodynamic pressure caused by the shaft rotation (see figure 15) [18]. Regarding the properties of the tissue it can be expected that the same can occur when the catheter is rotated: water is extracted from the surrounding tissue which increases the thickness of the lubricant layer. In turn, a transition from a Coulomb-like friction type to a more hydrodynamic-like friction type occurs.

No pressure is created in the insertion direction because the water is extracted with the catheter instead of trapped between the catheter and tissue. When the tangential velocity is higher than the insertion velocity, the film thickness is increased and the friction acts more hydro-dynamically resulting in a lower amount of friction.

Remarkable are the settings with 1 mm/s and 572 RPM where all parameters are relatively low compared to others. Note that for the settling time an error boundary of 10% of the steady value plus 0,1 N is used. Changes within these boundaries are not noticed which can explain the distance to reach a steady value to be zero. The other values of the other settings can be explained by the theory that above a certain velocity the viscosity lowers.

4.4 Limitations

It should be mentioned that the theory discussed above fits the results but additional experiments are required to verify if the theory also holds for other ranges of velocities. In additional experiments, the thickness and the presence of the lubricant layer could be measured with an ultra sound imaging device. Furthermore, most of the oscillations in the data are explained but still some oscillations are not.

Also dead pork tissue is used as phantom and results in living humans may differ. Differences in internal pressure, the amount of blood, temperature, metabolic processes, stiffness could be found. For example, at maximum 50% of the original amount of blood is present [19].

Additional, a catheter is used which is made of a polymer and the results with needles made of steel may differ. However, the properties of the tissue are mainly responsible for the predicted hypothesis and the same aspects can be expected to occur.

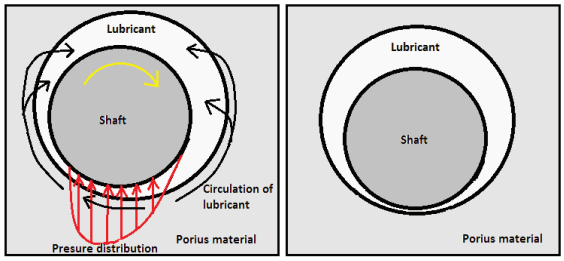

Fig. 15: Left: Sinter bearing during rotation. The rotation of the shaft creates a increased pressure below the shaft which increases thickness of the lubricate layer. **Right:** Sinter bearing with no rotation. No hydrodynamic pressure is created and the thickness of the lubricate layer is small.

5 Conclusion

A catheter, a flexible tube, was pulled through muscle tissue with different insertion and rotational velocities. Compared to needles, catheters are normally more flexible. This property could be used for a steerable needle, where the catheter (or flexible tube) could be considered as a needle shaft of a steerable needle. Insertions were performed perpendicular and parallel to the muscle fibers. During these insertions the insertion forces and torques were measured.

The results of the insertion forces in time reveal three types of curves: a straight line, a step response function without overshoot and a step response function with overshoot. The amount of overshoot, the steady value and the settling time are affected by the insertion and rotational velocities. The insertion velocity itself has little influence on the amount of steady insertion force. However, an increased insertion velocity increases the overshoot in most cases.

In comparison, an increased rotational velocity reduces the maximum or overshoot in most cases. The steady insertion force is reduced for settings were the tangential velocity is higher than the insertion velocity. The reduction in median steady friction due to rotation can be as large as 97% when comparing settings with minimum insertion velocity and maximum rotational velocity to insertions without rotation (0.76 N and 0.021 N P = $<$0.001). For settings were the tangential velocity is lower or equal to the insertion velocity, the steady insertion force is not affected or even increases.

Furthermore the results show that the insertion force is generally not affected by the fiber orientation. The most opportune settings are with 1 mm/s and 572 RPM, where the steady insertion force is almost zero. These settings have no overshoot and settling time, the resulting insertion force is a straight line. There is also little variation between the measurements which makes it easier to predict the insertion forces.

Overall can be concluded that catheter rotation can reduce the amount of friction considerably especially when the tangential velocity is much larger than the insertion velocity. This can improve the accuracy of needle or catheter placement and therefore the success of the intervention.

References

[1] N. Abolhassani, R. Patel, and M. Moallem, "Needle insertion into soft tissue: a survey.," *Medical engineering & physics*, vol. 29, pp. 413–431, May 2007.

[2] A. M. Okamura, C. Simone, and M. D. O'Leary, "Force modeling for needle insertion into soft tissue.," in *IEEE transactions on bio-medical engineering*, vol. 51, pp. 1707–16, Oct. 2004.

[3] M. A. Meltsner, N. J. Ferrier, and B. R. Thomadsen, "Observations on rotating needle insertions using a brachytherapy robot. In: Physics in medicine and biology, vol 52, pp. 6027-37," Oct. 2007.

[4] B. Maurin, L. Barbe, B. Bayle, P. Zanne, J. Gangloff, M. De Mathelin, A. Gangi, L. Soler, and A. Forgione, "In Vivo Study of Forces During Needle Insertions," in *Proceedings of the Scientific Workshop on Medical Robotics, Navigation and Visualization*, pp. 415–422, World Scientific Publishing Co. Pte. Ltd., 2004.

[5] N. Abolhassani, R. Patel, and M. Moallem, "Control of soft tissue deformation during robotic needle insertion.," *Minimally invasive therapy & allied technologies*, vol. 15, pp. 165–76, Jan. 2006.

[6] N. Abolhassani, R. Patel, and M. Moallem, "Experimental study of robotic needle insertion in soft tissue," *International Congress Series*, vol. 1268, pp. 797–802, June 2004.

[7] N. Abolhassani, R. Patel, and M. Moallem, "Trajectory generation for robotic needle insertion in soft tissue.," in *the Annual International Conference of the IEEE Engineering in Medicine and Biology Society*, vol. 4, pp. 2730–3, Jan. 2004.

[8] T. K. Podder, D. P. Clark, D. Fuller, J. Sherman, W. S. Ng, L. Liao, D. J. Rubens, J. G. Strang, E. M. Messing, Y. D. Zhang, and Y. Yu, "Effects of velocity modulation during surgical needle insertion.," in *27th Annual International Conference of the IEEE Engineering in Medicine and Biology Society.*, vol. 6, (Shanghai), pp. 5766–70, Jan. 2005.

[9] M. Mahvash and P. E. Dupont, "Fast Needle Insertion to Minimize Tissue Deformation and Damage.," in *IEEE International Conference on Robotics and Automation (ICRA)*, vol. 2009, pp. 3097–3102, July 2009.

[10] J. R. Crouch, C. M. Schneider, J. Wainer, and A. M. Okamura, "A velocity-dependent model for needle insertion in soft tissue.," in *Medical image computing and computer-assisted intervention (MICCAI)*, vol. 8, pp. 624–32, Jan. 2005.

[11] E. Marieb and K. Hoehn, *Human anatomy & physiology*, p. 317. San Francisco: Pearson Education, 7th ed., 2007.

[12] Y. Fung, *Biomechanics Mechanical Properties of Living Tissues*, pp. 251–252, 392–399. New York: Springer-Verlag, 2nd ed., 1993.

[13] T. Azar and V. Hayward, "Estimation of the Fracture Toughness of Soft Tissue from Needle Insertion," *Springer lecture notes in Biomedical Simulation*, vol. 5104, pp. 166–175, 2008.

[14] A. Jorres, *Management of Acute Kidney Problems*, p. 578. Berlin: Springer, 1st ed., 2010.

[15] J. Ferry, *Viscoelastic properties of polymers*, p. 3. John Wiley and Sons, 3rd ed., 1980.

[16] B. N. Persson, *Sliding friction : physical principles and applications*, p. 40. Berlin : Springer, 7th ed., 2000.

[17] A. Field, *Discovering statics using SPSS*. SAGE Publications Ltd, 3rd ed., 2009.

[18] J. R. Davis, *Copper and copper alloys*, pp. 107–109. USA: ASM international, 1st ed., 2001.

[19] R. Lawrie, *Lawrie's Meat Science*, p. 137. Woodhead, 7th ed., 2006.

APPENDIX

A

NEEDLE INSERTIONS

Several experimental studies have been performed to investigate the forces acting on a needle during insertion [4, 5, 6, 8, 10, 12]. Normally is assumed that the insertion force comprises three components: cutting, friction and deformation forces. Several attempts are made to model these parameters. These models can be used for the development of percutaneous devices, medical training and pre-intervention planning [4, 5, 10]. However the experimental studies are performed with needles, which introduce a cutting force. These cutting forces can influence the insertion force in a non continuous way what makes the actual behavior of the friction hard to obtained. In this appendix is discussed why existing studies not represent the actual behavior of the friction force. First some background information concerning the forces during the insertion of a needle are discussed. At the end, the actions that were taken to make sure that only the friction force is measured, are discussed.

A.1 Phases during insertion

During the insertion of a needle, several phases can be distinguished [4, 5, 6, 8, 10, 12]. These phases are related to the position of the needle compared to the position of the tissue [4, 5, 6, 12]. In the first phase, the pre-puncture phase, the needle tip is in contact with the surface of the tissue and exerts a force on it [5]. Due to the viscoelastic properties the tissue deforms with a certain amount [6]. The tissue is deformed until an equilibrium has been reached whereafter the needle suddenly cuts through the surface [4]. This is the deformation or post-puncture phase. This phase is normally characterized by a small reduction of the insertion force [4]. After the drop, the deformation phase switch to the insertion phase where the force increases with the distance of insertion [4, 5]. After the desired depth is obtained, the force stabilizes to a constant value . This is the relaxation phase. The last phase is the extraction phase where the needle is extracted. Summarized:

- Pre-puncture phase : the needle tip is in contact with the surface of the tissue which deforms due to the force exerted by the needle tip.
- Puncture phase: after a certain force has been reached, the needle suddenly cuts through the surface.
- Insertion phase: after the surface is penetrated, the force increases with the distance of insertion.
- Relaxation phase: after the needles has reached his attended depth, the force reduces to a steady value.
- Extraction phase: finally the needle is extracted.

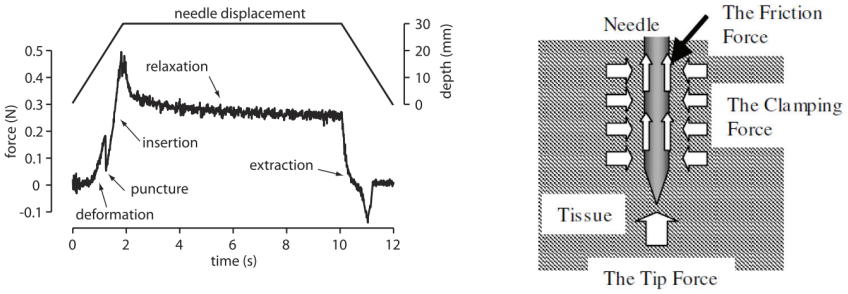

Figure A.1: Left: The different phases during the insertion of a needle [5]. **Right:** Forces during the insertion of a needle [8].

A.2 Forces during insertion

It is usually assumed that the force required to insert a needle consists of three components: cutting, friction and stiffness forces (equation A.1) [4, 12]. These components are also related to the different phases of the needle insertion as is shown in figure A.1. In the Pre-puncture phase the tissue is not penetrated and

no cutting and insertion forces are involved [4]. Only the stiffness of the needle and tissue contribute to the insertion force [12]. In the next phase the surface is cut whereafter the needle is inserted [4]. The cutting event is indicated by a drop of the insertion force [4]. During this phase cutting forces and clamping forces are involved [4]. In turn, the clamping forces affect the friction between the needle shaft and tissue [4]. Note that also forces related to the stiffness of the needle and tissue, the stiffness forces, contribute to the insertion force [12]. During the relaxation phase no cutting forces are involved but due to the properties of the tissue deformation forces occur. During the last phase, the extraction phase, only friction forces are involved [6]. Sometimes the elastic strain stored in the tissue is added in this phase [5]. The insertion force of the needle can be described as:

$$F_{insertion} = F_{stiffness} + F_{friction} + F_{cutting} \tag{A.1}$$

It should be noticed that the forces affect each other and can not simply be combined to one insertion force. For example the deformation of the tissue during the insertion phase is also affected by the friction between the surfaces of the tissue and needle shaft [4]. An increased friction also results in a larger tissue indentation. Furthermore the components are affected differently by parameters such as insertion velocity, temperature and structures. Cutting forces variate due to structures such as layers and affect the insertion force differently [4]. For this reason the insertion force should be described as:

$$F_{insac} = f(F_{stiffness}, F_{friction}, F_{cutting}) \tag{A.2}$$

A.2.1 Cutting forces

The cutting force is defined as the force required to separate the tissue [4]. Usually, it is stated that the deformation of the tissue in front of the needle tip also contributes to the cutting force [5, 6, 12]. The cutting force is in most cases modeled as a constant [8, 12] however inhomogeneity of tissue as well as the variation between individual persons makes this prediction doubtful [4].

The amount of cutting force is affected by the type of tissue, needle shape and needle diameter for example [4, 8]. Different needle tips and sizes result in different cracks [5]. This results in different amounts of clamping forces exerted by the tissue on the needle shaft which in turn affects the amount of the friction force [8].

Kataoka et al. [8] performed an experiment with an inner and outer needle to determine the cutting and friction forces individually. The forces acting on the inner and outer needle are measured separately. The force acting on the inner needle is assumed as the cutting force. The friction force is calculated by subtracting the cutting force from the force of the outer needle. The results show both constant as well as exponential behavior of the cutting force. Besides the variable behavior, the friction between the two needles is neglected which can contribute to the measured forces.

A.2.2 Deformation forces

The deformation force, sometimes denoted as stiffness force, is due to the mechanical properties of the tissue and is determined as the force required to cut

through the surface of the tissue [4, 6, 12]. Most tissues behave viscoelastic [7] which means that the amount of force is dependent on the penetration velocity. This is verified by experiments [4, 9]. Furthermore, it can be expected that the tip shape and size affect the amount of deformation. Sharper and smaller tips will cut the tissue sooner which results in less deformation.

A.2.3 Friction forces

The friction force is due to the interaction between the needle shaft and the surrounding tissue. The type of friction is usually considered as Coulomb friction, or combinations of Coulomb and viscous friction [4, 8]. In some models, also adhesive forces are considered besides the other types of friction [12]. However, in this report the friction is considered as boundary lubricated friction or as viscous friction, as was discussed in chapter 1. The presence of free water makes it plausible that a type of lubricated friction will occur.

In several experimental studies was show that needle rotation decreases the friction during the insertion [1, 2, 3, 11, 13]. This in turn reduces the tissue indentation which is beneficial for an accurate needle placement. Accurate needle placement is required during interventions such as brachytherapy where a specific target has to be treated. All experiments show that needle rotation reduces the friction force and tissue indentation. Abolhassani et al. [1, 2, 3] conclude that a controlled motion where the forces are kept orthogonal to the insertion direction, is the best approach for friction reduction and tissue indentation. In comparison, Podder et al. [13] and Meltsner et al. [11] hypothesize that there is a certain optimal combination of insertion and rotational velocities where both the friction as well as the tissue indentation is as low as possible . Besides the different hypotheses also different reductions were found. However this can be caused by the different needles, velocities and phantoms that were used. Furthermore it should be noticed that the insertions were performed with needles and therefore cutting forces are involved which could affect the measured friction forces.

A.3 Choices and reasoning

The interaction between the three types of forces makes it hard to study their individual aspects and behavior. The individual components are measured in several ways. Sometimes, the friction force is considered as the force required to extract a needle. However, when the needle is retracted before complete relaxation, a hysteresis of the friction might occur. The tissue is deformed with other initial values resulting in other behavior of the friction force. The retraction of a needle after complete relaxation also differs from an insertion without cutting force. Compared to regular insertions the friction is dynamic, also at the start. This in comparison to a retraction of a needle after relaxation where the friction starts with a static situation.

Several actions are taken to prevent other forces to contribute to the measured forces. First, a catheter is pulled through the tissue instead of inserted. The catheter is in the initial situation already placed through the tissue and is pulled further through the tissue at the start. In this situation, no cutting forces are involved during the insertion. Second, the experiment presented in

this report is performed with a dynamic insertion. The maximum rotation is applied before the start of each measurement to make sure that no stationary contact occurs. Third, meat phantoms of the the same sizes are used to fix the insertion depth. Because the friction force is related to the insertion depth. Furthermore, the tissue is enclosed by a container to fix it at a specific place and so the displacement of the catheter is referred as the actual displacement. With these actions, only the friction force is measured. Note, that the friction force in this situation can also be affected by the deformation of the tissue as well as of the catheter.

As was discussed in the introduction of this appendix, sometimes vulnerable tissues like nerves have be to avoided. Catheters are made of polymers instead of metals whereby they are normally more flexible compared to needles [14]. Polymers as well as metals are viscoelastic although in different amounts [14]. The idea was to develop a needle which used this property and is able to make curves with small radii [14]. The needle consist of a catheter as shaft and a steerable cutting device as tip [14]. The results of the experiment can provide information about the friction forces acting on the polymer shaft.

Bibliography

[1] N Abolhassani, R Patel, and M Moallem. Experimental study of robotic needle insertion in soft tissue. *International Congress Series*, 1268:797–802, June 2004.

[2] Niki Abolhassani, Rajni Patel, and Mehrdad Moallem. Trajectory generation for robotic needle insertion in soft tissue. In *the Annual International Conference of the IEEE Engineering in Medicine and Biology Society*, volume 4, pages 2730–3, January 2004.

[3] Niki Abolhassani, Rajni Patel, and Mehrdad Moallem. Control of soft tissue deformation during robotic needle insertion. *Minimally invasive therapy & allied technologies*, 15(3):165–76, January 2006.

[4] Niki Abolhassani, Rajni Patel, and Mehrdad Moallem. Needle insertion into soft tissue: a survey. *Medical engineering & physics*, 29(4):413–431, May 2007.

[5] Toufic Azar and Vincent Hayward. Estimation of the Fracture Toughness of Soft Tissue from Needle Insertion. *Springer lecture notes in Biomedical Simulation*, 5104:166–175, 2008.

[6] L Barbe, B Bayle, M de Mathelin, and A Gangi. Needle insertions modeling: Identifiability and limitations. *Biomedical Signal Processing and Control*, 2(3):191–198, 2007.

[7] Y.C. Fung. *Biomechanics Mechanical Properties of Living Tissues*. Springer-Verlag, New York, 2nd edition, 1993.

[8] Hiroyuki Kataoka, Toshikatsu Washio, Kiyoyuki Chinzei, Kazuyuki Mizuhara, Christina Simone, and Allison M Okamura. Measurement of the Tip and Friction Force Acting on a Needle during Penetration. In *MICCAI '02 Proceedings of the 5th International Conference on Medical Image Computing and Computer-Assisted Intervention-Part I*, pages 216–223. Springer-Verlag, 2002.

[9] Mohsen Mahvash and Pierre E Dupont. Fast Needle Insertion to Minimize Tissue Deformation and Damage. In *IEEE International Conference on Robotics and Automation (ICRA)*, volume 2009, pages 3097–3102, July 2009.

[10] B. Maurin, L. Barbe, B. Bayle, P. Zanne, J. Gangloff, M. De Mathelin, A. Gangi, L. Soler, and A. Forgione. In Vivo Study of Forces During Needle Insertions. In *Proceedings of the Scientific Workshop on Medical Robotics, Navigation and Visualization*, pages 415–422. World Scientific Publishing Co. Pte. Ltd., 2004.

[11] M A Meltsner, N J Ferrier, and B R Thomadsen. Observations on rotating needle insertions using a brachytherapy robot. In: Physics in medicine and biology, vol 52, pp. 6027-37, October 2007.

[12] Allison M Okamura, Christina Simone, and Mark D O'Leary. Force modeling for needle insertion into soft tissue. In *IEEE transactions on bio-medical engineering*, volume 51, pages 1707–16, October 2004.

[13] T K Podder, D P Clark, D Fuller, J Sherman, W S Ng, L Liao, D J Rubens, J G Strang, E M Messing, Y D Zhang, and Y Yu. Effects of velocity modulation during surgical needle insertion. In *27th Annual International Conference of the IEEE Engineering in Medicine and Biology Society.*, volume 6, pages 5766–70, Shanghai, January 2005.

[14] J P van der Maas. Tube insertion. Literature report, 2011.

APPENDIX

B

PILOT EXPERIMENT

For selecting the right force sensor and motor configuration, the force and torque that is required to move the catheter through the tissue have to be determined. The force is determined by extracting a deflectable puncture needle from beef and pork tenderloin.

B.1 Maximum friction force

Especially the maximum force that will occur during the insertion of the catheter is of interest, because the force sensor and motor should not be overloaded to prevent failure. As is discussed in the literature report, the friction during the insertion is history and time dependent [1]. It can be expected that the friction before sliding is higher than during sliding due to the deformation of the surfaces as well as of deformation of the lubricant. Also the time of stationary contact is of importance, the tissue tends to relax back to its original position after it is displaced. After the needle is placed into the tissue, the contact surface between the needle shaft and the tissue increases with time until an equilibrium is reached. Furthermore the normal force exerted by the tissue will increase with time until an equilibrium is reached due to phenomena such as viscoelastic creep (literature report section 7.2) [1].

B.2 Choices pilot experiment

An available deflectable puncture needle with a diameter of 1.829 mm (15G Daum ref. 10277) is chosen because this diameter was the most comparable to the diameter of the catheter. Beef and pork tenderloin were chosen as phantoms because they were commercially available and they are comparable to human muscle tissue as will be discussed in appendix D.4.

B.3 Procedure & materials pilot experiment

For the experiment a scale, the needle, a piece of wire, a small empty plastic bottle (0.5 l), a measuring cup, a ruler, a funnel and meat from the local supermarket were used. The first step was to attach one end of the wire to the back of the needle and the other end to the neck of the bottle (see figure B.1). Secondly, the needle was placed through the tissue at a random place and in a random direction.

Then the length of the needle that was in contact with the tissue was measured by the use of a ruler (figure B.1). Then the piece of pork or beef was slowly lifted and held in the air as in figure B.1 for 5 seconds. The hands were placed 1 cm besides the needle. If the needle was not extracted, the meat was laid down and an additional 5 ml water was added to the bottle. This process was repeated until the needle was extracted by the weight of the bottle. After extraction, the mass of the bottle was determined with the scale and the result was written down. The whole process was performed 14 times in pork and 12 times in beef.

B.4 Results pilot experiment

The mass in grammes is converted to a forces by:

$$F_g = M_{bottle} g \tag{B.1}$$

Where g is the free-fall acceleration ($9.81 m/s^2$) and M_{bottle} the mass of the bottle. The results are presented in figure B.2: 50% of the pork measurements

Figure B.1: Left: Materials that were used during the pilot experiment. A wire is attached with one end to the back of the needle and one end to the neck of the bottle. **Right:** Representation of the pilot experiment. When the mass of the bottle with water is high enough, the needle will be extracted. The real pilot experiment is performed above a table.

are between the 0.6 and 1.1 N, 50% of the beef measurements are between the 0.5 and 1.2 N. The medians of both types of tissue are 0.6 N. The largest force measured with beef, was 1.4 and with pork 1.2 N.

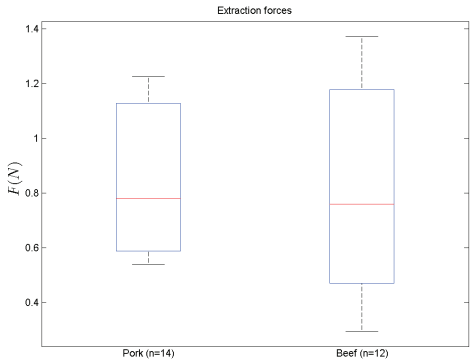

Figure B.2: Results of the extraction forces. The forces are determined by the weight of the bottle.

From experimental studies with needles as from friction models can be expected that the friction is affected by the insertion depth [1, 2]. In the case of boundary lubrication, which usually occurs at the start of sliding friction [3], the amount of friction is not directly dependent on the contact area of the needle shaft and tissue [4]. However the tissue is viscoelastic [5] and the more tissue is deformed, the more normal force is exerted on the needle shaft, like the compression of a spring, which increases the friction. For this reason the extraction forces were converted to force per unit length. The results are presented in (fig-

ure B.3). The median of pork, 14.4 N/m, differs from the median of beef, 18.4 N/m. However the measurements are performed in different directions, with different value and the friction could be affected by the fiber orientation which makes the results hard to compare.

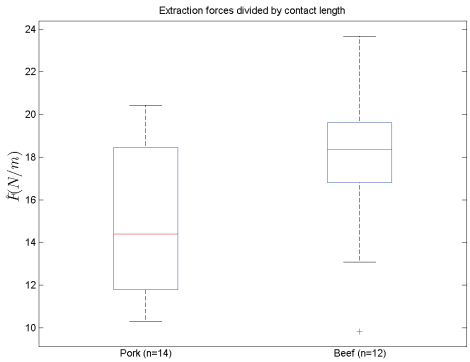

Figure B.3: Results of extraction forces divided by contact length. The results are determined by the extraction forces divided by the contact length between the needle shaft and tissue.

The results could be converted to the forces for the used tissue thickness in the experiment. However it is not sure that the relation between the friction and area of contact is linearly proportional. Therefore the maximum measured extraction force is used as required force for the experiment to make sure that force sensor will not be overloaded and that the motor is powerful enough. The forces never exceed the 1.5 Newton and with a safety factor of 50% a force of 2.25 N can be expected.

Bibliography

[1] J. P. van der Maas, "Tube insertion. Literature report," 2011.

[2] T. Azar and V. Hayward, "Estimation of the Fracture Toughness of Soft Tissue from Needle Insertion," *Springer lecture notes in Biomedical Simulation*, vol. 5104, pp. 166–175, 2008. [Online]. Available: http://dx.doi.org/10.1007/978-3-540-70521-5_18

[3] B. N. Persson, *Sliding friction : physical principles and applications*, 7th ed. Berlin : Springer, 2000.

[4] W. Z. Wang, L. Y. Wang, Z. X. Zhang, and H. B. Chen, "Boundary Lubrication Model under Square Surface Contact Condition," *Applied Mechanics and Materials*, vol. 29-32, no. 20094404120002, pp. 1396–1401, Aug. 2010. [Online]. Available: http://www.scientific.net/AMM.29-32.1396

[5] Y. Fung, *Biomechanics Mechanical Properties of Living Tissues*, 2nd ed. New York: Springer-Verlag, 1993.

APPENDIX

C

EXPECTATION OF FRICTION REDUCTION

In this appendix, the underlying thought of the friction reduction during the insertion of the catheter is discussed.

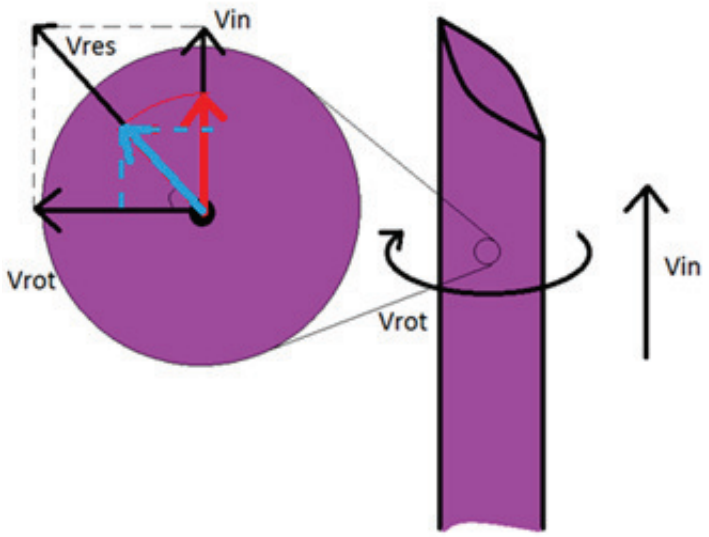

Figure C.1: Resultant velocity of a very small part of the surface of a needle. It is assumed that this velocity represents the sliding velocity between the catheter and tissue surface. The red arrow indicates the Coulomb friction without rotation and the blue arrow indicates the Coulomb friction when a rotation is applied.

C.1 Relation of insertion & rotation

When a rotation is applied during the catheter (tube) insertion, the direction of the resultant velocity changes as well as the magnitude of the resultant velocity looking at an infinitely small piece of the catheter as is illustrated in figure C.1. Friction, due to the interaction between sliding surfaces, acts in opposite direction to the displacement. When it is assumed that the friction force is not affected by the velocity, the friction force in the direction of the movement will reduce as is shown in figure C.1.

C.2 Friction during catheter insertion

Although the friction reduction during the insertion of a needle could be explained by a Coulomb friction model, Coulomb friction is not expected to occur. The regular Coulomb friction model, is a simplified model were the friction is described as the coefficient of friction times the normal force.

Because tissue contains hydrophilic gels, it is expected that two types of lubricate friction will occur: boundary lubrication and hydrodynamic lubrication. In the case of boundary lubrication the surface of the catheter or needle and the surface of the tissue are largely or completely separated by a lubricant layer of only a few particles thick. The interaction between catheter or needle, tissue and the fluid are of most importance for the amount of friction [1].

C.2.1 Boundary lubrication

The behavior during boundary lubrication can be typified as Coulomb friction where the friction coefficient exists of two parts [2]. The first part is related to the interaction between the particles of the fluid and the surfaces, the second part to the direct interaction of the surfaces [2]. For boundary lubrication, the amount of friction can be determined by [2]:

$$S_b = \mu N \tag{C.1}$$

with,

$$\mu = \beta\mu_m + (1-\beta)\mu_s \tag{C.2}$$

The force required to slide the surfaces over each other (S_b) depends on the coefficient of friction (μ) and the normal force (N). The coefficient of friction is the summation of the coefficient (μ_s) for the area where the surfaces are in direct contact ($1-\beta$) and the coefficient (μ_m) for the area that is separated by the lubricant (β).

As with Coulomb friction, the friction is little affected by the insertion and rotational velocity, when the the normal force and sliding velocity is not to high [2]. However the direction of the resultant friction is affected by the rotation and insertion velocity. This can reduce the friction in the insertion direction as shown in figure C.1.

C.2.2 Hydrodynamic lubrication

In comparison, for hydrodynamic lubrication, the interaction between the particles of the fluid itself is more important for the amount of friction. The amount of friction during this situation can be described by a fluid dynamic model [1]:

$$S_v = \frac{\eta A v_0}{h_0}\lambda \tag{C.3}$$

Where η is the viscosity of the lubricant, A the contact area (of the lubricant), v_0 the stationary velocity between the two surfaces, h_0 the smallest film thickness and λ the coefficient for the lubricant profile. This coefficient is calculated by:

$$\lambda = \frac{1}{\xi - 1}[4\ln\xi - \frac{6(\xi-1)}{\xi+1}] \tag{C.4}$$

Where $\xi = h_1/h_0$, the ratio between the smallest and largest film thickness. In the model it is assumed that the lubricant layer is at least 10 μm thick, that the lubricant flow is laminar and that no side leakage occurs.

When it is assumed that all parameters are constant, it can be expected that a higher velocity will result in a larger friction force. The friction is proportional to the resultant velocity and the friction in the direction of the insertion is in turn also proportional to the resultant velocity. The black arrows in figure C.1 show the behavior in this case.

The friction reduction by applying a rotation during the insertion of a needle, as was found by several experimental studies [3, 4, 5, 6, 7], cannot be explained. However it is expected that only the contact area is constant. The viscosity and

the film thickness are related to the resultant insertion velocity and the history of it. However, these relations do not necessarily be linearly proportional. This can explain the reduction found during insertions of needles.

Bibliography

[1] B. N. Persson, *Sliding friction : physical principles and applications*, 7th ed. Berlin : Springer, 2000.

[2] W. Z. Wang, L. Y. Wang, Z. X. Zhang, and H. B. Chen, "Boundary Lubrication Model under Square Surface Contact Condition," *Applied Mechanics and Materials*, vol. 29-32, no. 20094404120002, pp. 1396–1401, Aug. 2010. [Online]. Available: http://www.scientific.net/AMM.29-32.1396

[3] M. A. Meltsner, N. J. Ferrier, and B. R. Thomadsen, "Observations on rotating needle insertions using a brachytherapy robot. In: Physics in medicine and biology, vol 52, pp. 6027-37," pp. 6027–37, Oct. 2007. [Online]. Available: http://www.ncbi.nlm.nih.gov/pubmed/17881817

[4] N. Abolhassani, R. Patel, and M. Moallem, "Control of soft tissue deformation during robotic needle insertion." *Minimally invasive therapy & allied technologies*, vol. 15, no. 3, pp. 165–76, Jan. 2006. [Online]. Available: http://www.ncbi.nlm.nih.gov/pubmed/16785183

[5] ——, "Experimental study of robotic needle insertion in soft tissue," *International Congress Series*, vol. 1268, pp. 797–802, Jun. 2004. [Online]. Available: http://linkinghub.elsevier.com/retrieve/pii/S0531513104005394

[6] ——, "Trajectory generation for robotic needle insertion in soft tissue." in *the Annual International Conference of the IEEE Engineering in Medicine and Biology Society*, vol. 4, Jan. 2004, pp. 2730–3. [Online]. Available: http://www.ncbi.nlm.nih.gov/pubmed/17270841

[7] T. K. Podder, D. P. Clark, D. Fuller, J. Sherman, W. S. Ng, L. Liao, D. J. Rubens, J. G. Strang, E. M. Messing, Y. D. Zhang, and Y. Yu, "Effects of velocity modulation during surgical needle insertion." in *27th Annual International Conference of the IEEE Engineering in Medicine and Biology Society.*, vol. 6, Shanghai, Jan. 2005, pp. 5766–70. [Online]. Available: http://www.ncbi.nlm.nih.gov/pubmed/17281568

APPENDIX

D

PRELIMINARY MEASUREMENTS

In this appendix the preliminary measurements are discussed. Two sets of preliminary measurements were performed. Based on these results several choices were made. The first set of measurements show different initial values. It is expected that the initial values are affected by the time of stationary contact between the tissue and catheter. To avoid this the maximum rotational velocity is applied for two seconds before the start of the measurements in all subsequent experiments. The second set of preliminary measurements shows much variation. It is expected that the acidification process (rigor mortis) is responsible for this variation (appendix D.4). To reduce the variation, it was chosen to use meat of two days old to make sure that the acidification has stopped.

D.1 Methods & materials preliminary measurements

The preliminary measurements consists of two sets of measurements that were performed with the same methods and materials as with the subsequent regular measurements apart from some exceptions. First, all preliminary measurements were performed with a less accurate force sensor. The chosen force sensor was not available at the time due to distribution problems. The same type of force sensor was used but with a different range, the Futek Lsb200 22.2 N (5 lb) in combination with a standard amplifier. Second,the first set of measurements was performed with meat from the supermarket and no rotation was applied before the start of the measurements. Although the force measurements of the individual groups with the same settings follow the same curve, there is much variation within each group. The variation within the groups are assumed to be caused by the time of stationary contact, which in turn affects the friction. Therefore the maximum rotational velocity was applied for two second before every subsequent (second set and regular) measurement. The maximum rotational velocity was also applied at the start of the second set of measurements. Furthermore, meat of 4 hours after slaughtering was used in the second set of measurements to represent the reality as much as possible.

D.1.1 Tissue properties & friction

Tissue behaves viscoelasticly and phenomena such as viscoelastic creep occurs. When the tissue is stressed, it slowly deforms until an equilibrium. This is called creep. When the stress is removed, it slowly deforms back to its initial position. These phenomena also occurred during the first experiment. After a hole was created by the needle, the catheter was placed through the tissue. At this moment the tissue was deformed by the insertion. Over time, the tissue will tend to go back to it initial position, resulting in a larger normal force exerted on the needle shaft.

It was expected that boundary lubrication or hydrodynamic lubrication would occur during the insertion. The amount of friction during boundary lubrication is linearly proportional to the normal force. An increased normal force on the needle shaft exerted by the surrounding tissue results in an increased friction force. In the case of fluid lubrication, the friction is not directly related to the normal force. However the viscosity of the lubricant layer between the needle shaft and the tissue can be related to the pressure. An increased pressure can result in an increased friction force. Furthermore, the normal force can cause the lubricant to be squeezed out. The amount of friction during fluid lubrication is related to the thickness of the lubricant layer. A reduced layer thickness results in an increased friction force.

D.1.2 Time of stationary contact

Looking at the properties of tissue and the friction models, it can be expected that the time of stationary contact increase the friction force. Different stationary contact times results in different amounts of friction. The behavior of the tissue, viscoelastic, can be modeled with dampers and springs. Depending on the properties and the force that is exerted, the relaxation of the tissue takes

time. Two measures can be taken to make sure that the initial properties of the meat are the same for every measurement. First, making sure that the time of stationary contact of each measurement is equal. This was difficult because the hole was created manually and also the catheter was placed manually. Depending on the properties of the meat, the differences between the time of stationary contact will result in differences in the force measurements. Furthermore, the properties of the individual pieces of meat as well as the different positions in the meat will result in different viscoelastic behavior. A second possibility is to wait until there is no relaxation anymore. After a certain moment the whole catheter shaft is surrounded by the tissue and no more tissue deformation can occur. For the start of each measurement, a certain amount of time has to be waited before the measurements can be started. If the waiting time is up to 15 minutes for example, the experiment would be very time consuming. For this reason the first method is preferred.

D.1.3 Phantom of second set

In the second set of preliminary measurements it was chosen to use meat that was as fresh as possible in order to represent reality as much as possible and to prevent variation in the measurements. Furthermore a rotation of two seconds (at the maximum rotational velocity) was applied before the start of each measurement to make sure that there was no stationary contact during insertion. A needle is normally also placed at once and no stationary contact occurs.

Several abattoirs were contacted but none of them were able to deliver fresh pork tenderloin. One option was to buy a whole leg but this was to expensive. Eventually a self slaughtering butcher was able to provide fresh pork tenderloins directly from the carcass. These were more expensive than regular tenderloins because opening the carcass would damage other parts of the pig.

After the pigs were killed, the tenderloins were removed. At this moment the tenderloins had a temperature around the body temperature. During the transport, the tenderloins were stored in plastic boxes with a solution of physiological salts. The solution had a temperature of 20° and after the tenderloins were placed into it, the temperature of the tenderloins lowered.

The transport itself took several hours longer than expected because of traffic jams. For this reason the experiment was performed 4 hours after the tenderloins were removed. The temperature of the tenderloins were at this moment still above room temperature which can affect the properties of the meat (appendix D.4).

D.2 Results & discussion of first set

In figure D.1 the results of four measurements of insertions parallel to the muscle fibers, 1 mm/s and no rotation are shown. The shape of each curve can be described by a step response without overshoot. The rise times as well as the steady values differ. Notable is that the curves are not starting at the same initial value. The initial values are sometimes even below zero. This can be caused by the manual placement of the catheter. After a hole is created in the tissue, the tissue is placed over the catheter. At this moment the catheter is still attached on the motor shaft. Sometimes the tissue is placed to far and the

position had to be corrected. This can result in a pulling force on the sensor due to the viscoelastic properties of the meat.

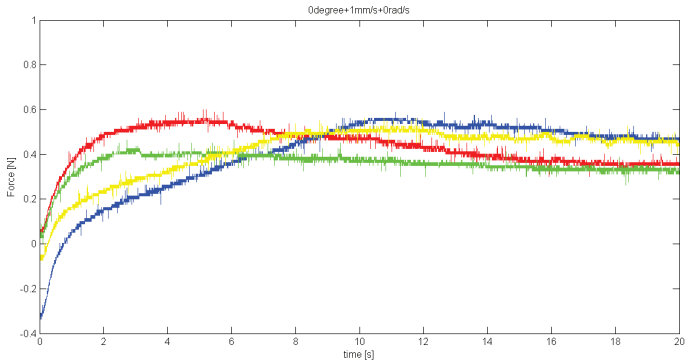

Figure D.1: Results of four (raw) insertion force measurements of first set with an insertion parallel to the muscle fibers, 1 mm/s and no rotation. The different colors indicate different measurements with the same settings. The meat phantom was made of pork tenderloin from the local super market.

The same can be found for other measurements. In figure D.2 four results with insertions parallel to the muscle fibers, 10 mm/s and no rotation are shown. Different shaped curves are found which can be described by a step response with overshoot. Again there is much variation within the measurements. The amounts of overshoot as well as the steady values differ. Furthermore, again the initial values are not the same.

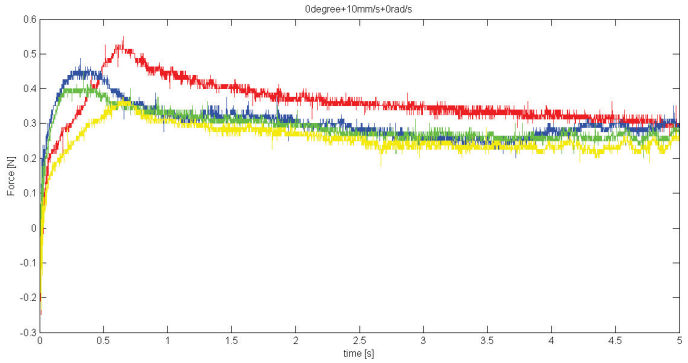

Figure D.2: Results of four (raw) insertion force measurements of first set with an insertion parallel to the muscle fibers, 10 mm/s and no rotation. The different colors indicate different measurements with the same settings. The meat phantom was made of pork tenderloin from the local super market.

Besides the two types of curves, also a third type can be found. Figure D.3 shows results of four measurements with insertions perpendicular to the muscle fibers, 1 mm/s and 10 rad/s. The shape of the curve of some measurements can be described by a straight line. Remarkable is that the insertion forces are almost zero. As was discussed in the paper, the rotation increases the lubricant

layer with a large friction reduction as result. The variation within this group is small, however the initial values still differ.

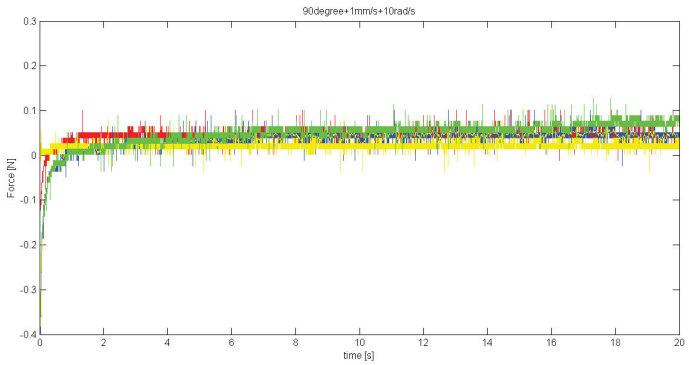

Figure D.3: Results of four (raw) insertion force measurements of first set with an insertion perpendicular to the muscle fibers, 1 mm/s and 10 rad/s. The different colors indicate different measurements with the same settings. The meat phantom was made of pork tenderloin from the local super market.

Overall can be concluded that different curves can be found for different groups, however there is much variation within the groups. The initial values are different as well as the steady values. To reduce the variation, it was chosen to apply a rotation before the start of a measurement and to use fresh unprocessed meat.

D.3 Results & discussion of second set

In this section the results of the measurements with fresh unprocessed meat directly from the abattoir are discussed. The used pork tenderloins were removed from the carcasses between 4 and 8 hours before the measurements. The tenderloins were partly covered by Epimysium, a strong layer of connective tissue (section E.2). The first runs failed because some parts of the Epimysium were trapped around the catheter. For this reason the Epimysium was completely removed. Due to the lack of time only one complete run could be performed were each setting is applied twice. Also a rotation of two seconds was applied before the start of each measurement. The results with insertions parallel to the muscle fibers, 1 mm/s and no rotation are shown in figure D.4. It can be seen that both curves start at the same initial value. The initial value does not exactly equal zero. This can be caused by the offset and inaccuracy of the force sensor. As with the other meat phantoms, a step response curve with overshoot can be found. The unprocessed fresh meat did not result in less variation for these settings.

The shape of the curves for settings with parallel insertions, 10 mm/s and no rotation, is the same as can be seen in figure D.5 and can be described by a step response with overshoot. Again there is much variation between the measurements. Remarkable is that there are small differences in the initial values. This can be caused by the inaccuracy and offset of the force sensor.

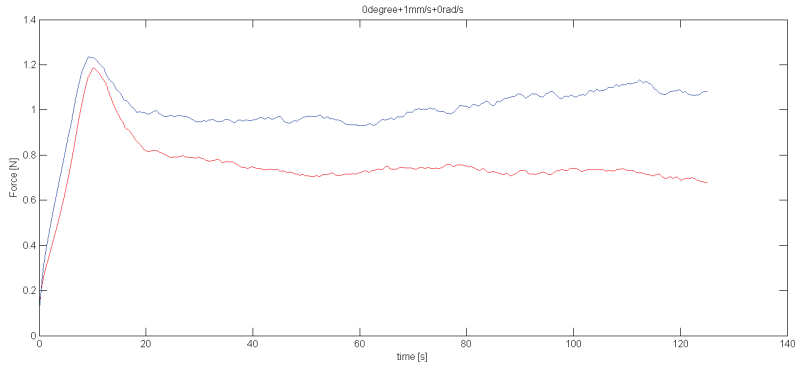

Figure D.4: Results of two (raw) insertion force measurements of second set with an insertion parallel to the muscle fibers, 1 mm/s and no rotation. Fresh meat was used and before the start of each measurement a maximum rotation of two seconds was applied to make sure that there was no stationary contact. Two different measurement were performed with the same settings which are indicated by different colors.

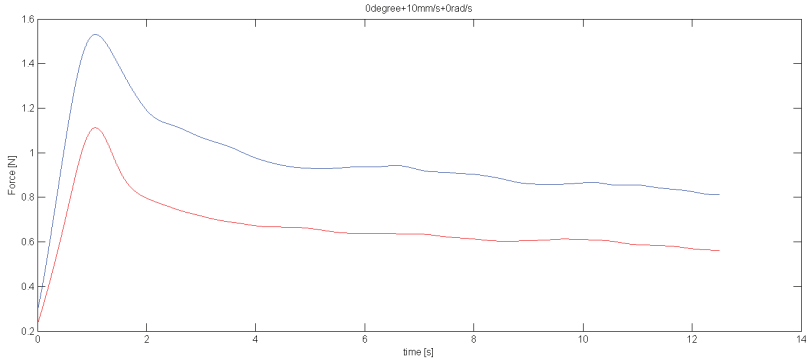

Figure D.5: Results of two (raw) insertion force measurements of second set with an insertion parallel to the muscle fibers, 10 mm/s and no rotation. Fresh meat was used and before the start of each measurement a maximum rotation of two seconds was applied to make sure that there was no stationary contact. Two different measurements were performed with the same settings which are indicated by different colors.

More variation was found between the measurements with settings with insertions perpendicular to the muscle fibers, 1 mm/s and 10 rad/s, as is shown in figure D.6. One of the curves can be described as a straight line through 0.2 N. The other curve can better be described by a step response without overshoot and with a steady value of 0.55 N.

D.4 Conclusion first & second runs

Overall there is much variation within the groups. The acidification process of pork meat takes normally between the 4 and 8 hours as is discussed in section E.4.1 and possibly the the meat was still acidifying (rigor mortis, appendix D.4). It can be expected that during the measurements the properties of the meat phantom had changed. This can explain the large variation in the

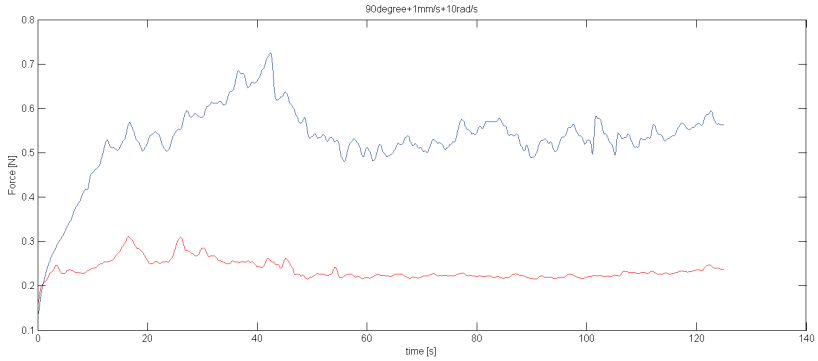

Figure D.6: Results of two (raw) insertion force measurements of second set with an insertion perpendicular to the muscle fibers, 1 mm/s and 10 rad/s. Fresh meat was used and before the start of each measurement a maximum rotation of two seconds was applied to make sure that there was no stationary contact. Two different measurements were performed with the same settings which are indicated by different colors.

measurements as well as the differences in the initial values. For this reason meat of at least two days old was used for all subsequent measurements to make sure that acidification had stopped. Looking at the results for this case, shown in figure D.7, it can clearly be seen that both curves start at the same initial value. Furthermore, there is little variation between the two measurements. However this is not valid for all the measurements as can be seen in figure D.8. These two measurements are performed with the same settings but with another meat phantom. However, both curves starts at zero and it can be expected that the variation, which can be found in the box plots of chapter 1, is due to the properties of the tissue. Tissue is a heterogeneous structure and depending on the place of insertion, different layers are crossed resulting in different amounts of friction as is discussed in section D.4.

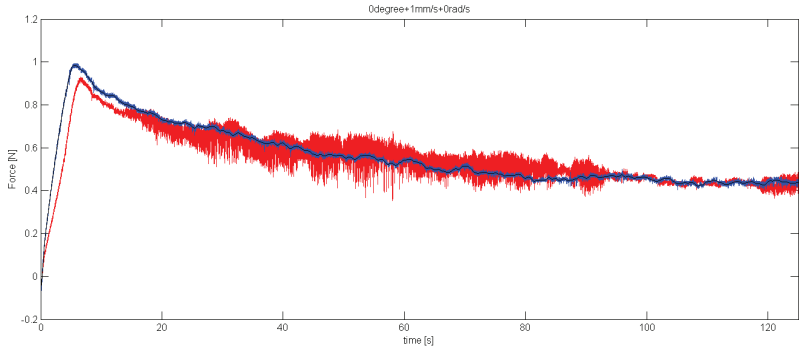

Figure D.7: Results of two (raw) insertion force measurements of regular set with an insertion perpendicular to the muscle fibers, 1 mm/s and no rotation. Meat of two days old was used for the phantoms. Two different measurement were performed with the same settings which are indicated by different colors.

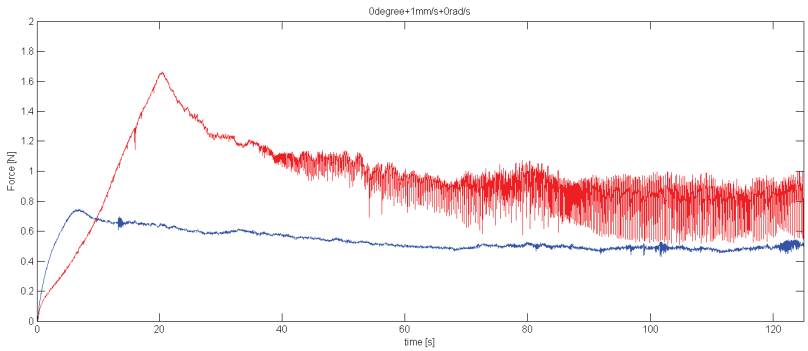

Figure D.8: Results of two (raw) insertion force measurements of regular set with an insertion perpendicular to the muscle fibers, 1 mm/s and no rotation. Meat of two days old was used for the phantoms. Two different measurements were performed with the same settings which are indicated by different colors.

APPENDIX

E

PROPERTIES OF MEAT

Pork tenderloin was used as phantom for the experiment, as it should represent human muscular tissue. In this appendix the reason why pork tenderloin can represent human muscular tissue are discussed. This piece is chosen because it it commercially available, soft, relatively homogeneous and cubic pieces of 50mm can be made from it. After the pig is killed several chemical processes stop. This in turn results in several changes in the muscle. These changes as well as the actions taken to prevent these changes are discussed in this appendix as well.

E.1 Anatomy of pigs

Looking at the anatomy of the human body and at the anatomy of pigs (figure E.1), both bodies are almost completely covered with muscular tissue [5]. For this reason muscular tissue is of interest for needle insertions [5]. Furthermore, the muscular tissue comprises on average between 36 and 42% of the weight of an adult [5]. Regarding the carcasses of pigs of 6 months old, this percentage is 48% for muscle tissue, 35% for fat and 10% for bone. Pigs are normally slaughtered at an age of 6 months. Note that blood, head, feet and organs are removed to obtain a carcass [4]. Furthermore, the concerned muscle tissue is mainly skeletal (or voluntary) muscle because other types such as smooth muscle and cardiac muscle are mainly present in the organs which were removed [4]. The difference between skeletal muscle and smooth muscle is that skeletal muscle has parallel fibres and smooth muscle does not [4].

Both, humans as well as pigs are mammalian and the anatomical structures are largely comparable for which pigs are used as human phantom [1, 4]. Although there are some differences between pigs and humans, the structure of the muscles are almost identical [4, 6]. Human muscle as well as pig muscle consist of around 75% water and 20% proteins like most animals [2, 4, 6]. The other contents of muscle include fat and free amino acids [4, 6]. The largest part of the proteins form the mechanical contraction mechanism which will be discussed in the next section [4, 6]. Variations in amounts can be found between species, age and sex. Also variation in amounts between the individuals of the same age, species and sex can be found [4].

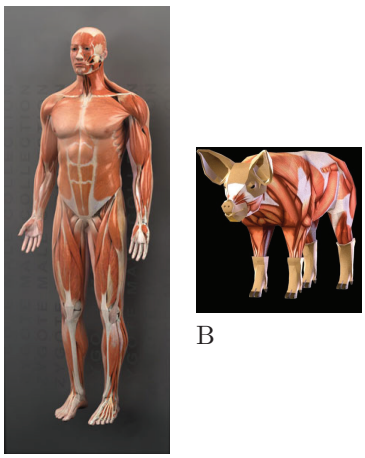

A B

Figure E.1: A: Model human muscular system. Source: 3D science.com. B: Model muscular system of pig. Source: the3Dstudio.com.

E.2 Muscle structure & contraction

Muscle of pigs as well as muscle of humans exists of long shaped cells, the muscle fibres with diameters between 60-100 μm and lengths up to 30 cm [3, 6]. Several

fibres are bundled into a bundle covered by sheaths of connective tissue called Perimysium [3, 4, 6] as shown in figure E.2. The muscle itself exists in turn of several muscle bundles and is covered by a strong sheath of connective tissue called the Epimysium [3, 4, 6]. These sheaths contain the large blood vessels and the nerves [4]. The individual fibres are also covered by connective sheaths, the Endomysium [3, 4, 6]. The Perimysium at the ends of the muscle turn over into a bundle of connective tissue, the tendon, which is normally attached to a bone [4, 6].

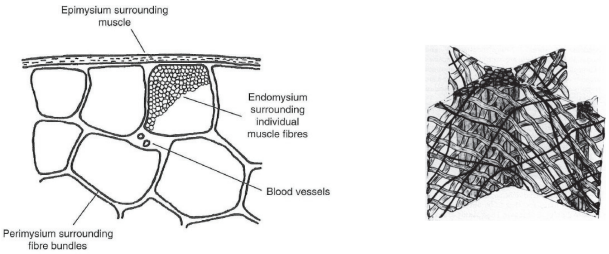

Figure E.2: Left: Sketch of cross-section of a muscle. The muscle fibres and different connective layers can be distinguished [6]. **Right:** 3D sketch of Perimysium that contain collagen fibres, elastin fibres and blood vessels [4].

The muscle fibres consist of up to 2000 fibrils with diameters of 1 μm as shown in figure E.3 which are together responsible for 80% of the volume of the fibre [6]. The fibrils are responsible for the contraction of the muscle [4, 5, 6]. Fibrils consist of thick and thin long ranged filaments mainly made of respectively myosine and actine forming chains of sarcomeres as shown in figure E.3 [4, 6]. These proteins are able to react with each other which shorten the length of the fibril [4, 6]. This in turn shortens the hole muscle as is illustrated in figure E.3. Calcium and ATP are required for the contraction of the filaments [4, 6]. When the muscle is activated by a stimuli, calcium is released from membrane systems surrounding the myofibril [4, 6]. This in turn causes the myosine and actine filaments to contract [4, 6]. The contraction stops until the calcium is pumped back into the membrane systems [4, 6]. This process requires energy in the form of ATP like the contraction of the muscle [6].

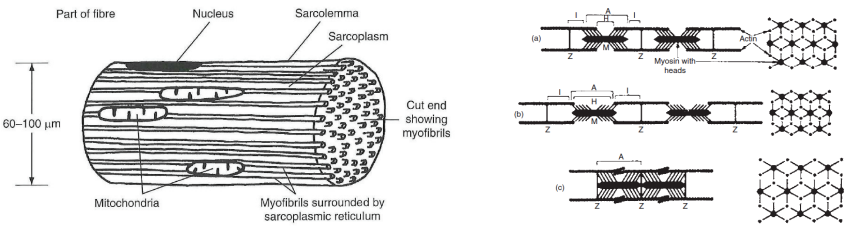

Figure E.3: Left: Schematically representation of a part of a muscle fibril [6]. **Right:** Sketch of sarcomeres at different stages: at rest (a), stretched (b) and contracted (c). [4]. On the left the longitudinal and right the cross sections.

E.3 Connective tissue

The strength of muscle tissue as well as the overall body is provided by connective tissue [3]. Connective tissue itself is strengthen by protein fibres, made of collagen and elastin [3, 4, 6]. Elastin is linearly elastic [3, 4, 6] in comparison to collagen which is not elastic [4, 6] or at most very little elastic [3]. Different types of connective tissue exist which can also be found in the different layers in muscle tissue.

The type depends on the presence of the types of collagen [3, 4, 6]. Three twisted polypeptide chains form a molecule of connective tissue [6]. Chains of the molecules form together the collagen fibre [6]. The type of collagen is determined by the amino acids forming together the polypeptide chain [6]. Amino acids are the building blocks of proteins and chains of 50 or more amino acids form a protein [4, 6]. Depending on the chain of amino acids, several cross-links between the molecules are formed which strengthen the connective tissue [6].

E.4 Meat properties

The cross-links between the molecules in connective tissue are affected by the age of the animal. Over time more cross-links are formed and the average diameter of the collagen fibres increases [4, 6]. The pork tenderloins originate from pigs with an age between the 6 and 7 months. The meat of young pigs is more tender than older pigs. Normally, meat is considered as muscle from dead carcasses but can also contain bone, connective tissue, fat and lean [6]. Furthermore, the meat is also affected by the storage temperature. Proteins can fall apart in smaller chains of amino acids by temperatures above the body temperature and acid conditions [6]. This process is called denaturation [6]. The properties of the proteins changes which can also affect the properties of the meat. In turn, this can also affect the tenderness as well as the water holding capacity of the meat as will be discussed in the next subsections.

E.4.1 Tenderness

The tenderness or toughness (softness) of the meat is affected by conditions of the animal during its live as well as by conditions post mortem [4, 6]. For example if the pigs are exposed to stressful conditions before slaughter, adrenaline is released into the blood circulation of the animal resulting in tough meat [4, 6]. The increased adrenaline level influences the aging process. Post mortem the properties of the muscle change when it is not frozen, this is the so called ageing process [4, 6]. Ageing is affected by the pH of the meat which is indirectly decreased by the release of adrenaline [4, 6]. The contraction of the muscle filaments as well as the strength of the connective tissue layers change during post mortem both affecting the tenderness of the meat [4, 6]. As was discussed in section E.2, the decoupling of the muscle filaments requires energy in the form of ATP [4, 6]. Directly after slaughtering the blood circulation of the animal is stopped resulting in a stopped oxygen supply [4, 6]. Only glycogen can be converted to ATP in this situation and lactic acids are created [4, 6]. This process is limited by the amount of glycogen that is present as well as by the pH

of the muscle [4, 6]. The conversion of glycogen decreases the pH of the muscle and below a certain value the process could not be sustained [4, 6]. The anaerobic (without oxygen) process is increased by adrenaline resulting in a directly increase in the pH after slaughtering. The critical pH level is reached sooner where after the muscle cannot relax anymore. This process is called acidification and is normally reached within 4 to 8 hours after the pig is killed [6].

In the absence of ATP the filaments form permanent cross-bridges and rigor mortis sets in [6]. For this reason the contractile condition of the muscle at rigor mortis is important for the tenderness of the meat [4, 6]. This process is also affected by the temperature [4, 6]. The calcium pumps, responsible for the activation of the muscle contraction, perform badly at temperatures below $10°C$ [4, 6]. This phenomenon is called cold shortening and results in more rough meat [6]. Furthermore the denaturation of the muscle proteins is affected by the temperature [4, 6]. The cross-bridges between the actine and myosine filaments are fragmented over time and the rate is higher at higher temperatures [6]. This process is stopped below zero temperature [6]. Also the connective layers present in the muscle denaturalizes over time [6]. This process elapse normally much slower and the effect is smaller [6]. Over time small changes in the structure of the connective layers and the collagen cross-links can be found [6].

E.4.2 Water holding capacity

Muscle consists of 75% water from which 10% is strongly bound to proteins, a large part is bound by chemical processes such as osmose and a small part can move freely [4, 6]. Water based suspensions are present in the connective tissue layers, in the muscle fibres, extracellular spaces as well as in the blood vessels [3, 4, 5]. When the muscle is removed from the carcass, water is lost from the muscle [4, 6]. The amount of drip is inversely related to the water holding capacity (WTC) [4, 6]. The WTC is influenced by the denaturation of proteins and pH resulting in two effects: the filaments shrink and the proteins lose their ability to combine with water [4, 6]. The free water is squeezed out from the filaments. Furthermore, when the muscle is cut, the fibres as well as the vessels are opened and free water can be lost [4]. The shrinkage of the filaments also affects the color of the meat [6]. Individual spaces between the muscle fibres increase resulting in a heterogeneous structure [6]. In these cases more light is reflected and the meat appears more paler [6].

E.5 Preservation of meat

Several methods like freezing, dehydrating, curing and sterilization exist to preserve meat for a long time [4]. However dehydrating and curing for example change the properties of the meat in such a way that it is not comparable to living human muscle tissue. The unprocessed meat could be supplied once a week and on the other hand the experiments could not be performed in one day. For this reason preservation was required.

E.5.1 Freezing

A regular way to preserve meat is by freezing it [4]. Meat is usually frozen to slow the growth of bacteria and to slow chemical changes [4]. For this reason the carcass should be frozen as quickly as possible. Freezing also reduces the weight loss by the vaporization of water from the meat [4]. However this will result in tough meat caused by cold shortening (section E.4.1) [4]. Cold shortening could be prevented by freezing the muscle after rigor mortis [4]. However, besides cold shortening, freezing is normally accompanied by drip [4]. Water expands at low temperature and in crystallized state (due the low temperature) the water rather damages the membranes than going through them [4]. Second, the water that is normally bound to proteins, can be released by the low temperature and become free water [4]. These processes can be partly prevented by additives such as glycerol and freezing within 75 minutes [4].

E.5.2 Refrigerate above zero

Like freezing, refrigerate above zero slows the growth of bacteria although with a smaller amount [4]. For this reason it is also beneficial to refrigerate the meat as soon as possible [4]. However due to the temperature difference, water may vaporize from the meat resulting in a decreased water content [4]. However the vaporization of water is reduced with decreased temperature [4]. Furthermore, cold shortening may occur when the meat is cooled before the onset of rigor mortis. However this can be prevented by storing the meat in the refrigerator after rigor mortis. It should be noticed that the growth of bacteria and vaporization of water is reduced but not stopped.

E.5.3 Packaging

Another method of preserving meat is packaging. Packaging can reduce the growth of bacteria and the loss of water [4, 6]. Furthermore it prevents the oxygen present in the air to react with pigments from the muscle [4, 6]. This in turn increase the growth of bacteria and result in a more brown colored meat [4, 6]. It should be noticed that packing does not prevent processes as cold shortening and that the growth of bacteria is not completely stopped. Bacteria present before packaging and anaerobic bacteria can still survive for a certain period resulting in deterioration of the meat [4].

E.6 Choices and measures

The main properties of the meat that change post mortem are the tenderness and water holding capacity. Both properties can influence the amount of friction that appears during the insertion of the catheter. Several actions are taken to prevent the changes in the meat. First, the meat was aged for one day before it was used. The acidification is already reached and regular meat can be used instead of opening the carcass before aging. while the meat was still at the abattoir, it was kept as natural as possible by avoiding additives and treatments to improve tenderness. Sometimes salt solutions are injected to increase the water holding capacity of the meat [6]. The first measurements were performed with meat of 4 hours after the pigs were killed as was discussed in appendix D, resulting

in univocal results. After acidification the tenderness of the meat still changes over time by the denaturation of proteins. The denaturation was minimized by conserving the meat at $7°C$. The reduced denaturation also reduces the loss of the water holding capacity of the meat. The pork tenderloins were vacuum packaged after removal to prevent dehydration. At arrival the pork tenderloins were stored into a water based suspension with physiological salts. Besides dehydration, this also reduces the denaturation because the pH is lowered. More water is added and the concentration of acids is lowered.

Bibliography

[1] Ashley Avenue and Sinclair Hormel. Comparative anatomy and physiology of the pig. *Scand. J. Lab. Anim. Sci.*, 25:11–21, 1998.

[2] J Bergstrom, P Furst, L Noree, and E Vinnars. Intracellular free amino acid concentration in human muscle tissue. *Journal of applied physiology*, 36(6):693–697, 1974.

[3] Y.C. Fung. *Biomechanics Mechanical Properties of Living Tissues*. Springer-Verlag, New York, 2nd edition, 1993.

[4] R.A Lawrie. *Lawrie's Meat Science*. Woodhead, 7th edition, 2006.

[5] J P van der Maas. Tube insertion. Literature report, 2011.

[6] P.D. Warris. *Meat science*. CABI, 2010.

APPENDIX

F

SET-UP CALCULATIONS

In this section, the performed calculations are discussed. First the force contribution of the leaf springs are calculated to investigate to what extent they contribute to the measurements. Second frequencies caused by the setup are calculated and discussed to explore the source of the oscillations in the measurements. Looking at the experimental setup, several frequencies can be expected to appear in the measurement as is discussed in this appendix.

F.1 Force contribution of leaf springs

The displacement of the catheter in the tissue results in a pulling force acting on the tissue caused by the friction between the catheter and the tissue as is illustrated in figure F.1. The pulling force is transmitted to the container that encloses the tissue which in turn is transmitted to the plateau. This pulling force causes the plateau (that supports the container) to displace. This plateau is supported by two leaf springs as is illustrated in figure F.1.

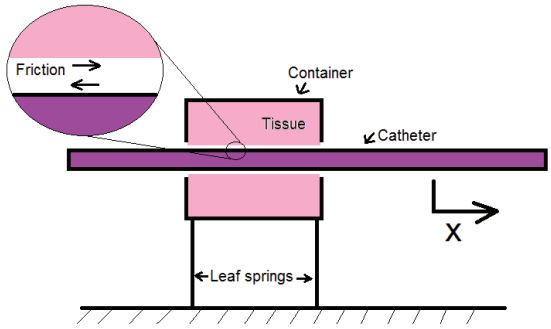

Figure F.1: Schematic view of the container during the insertion of the catheter.

The stiffness of the leaf springs affects the force measurements because the force sensor measures the forces indirectly by actually measuring the displacement (chapter 1). Although the displacement is very small (0.13 mm), the leaf springs increase the force required to displace the plateau. The contribution of the leaf springs is calculated by the use of a mechanical model of a homogeneous beam as shown in figure F.2 [1, 2].

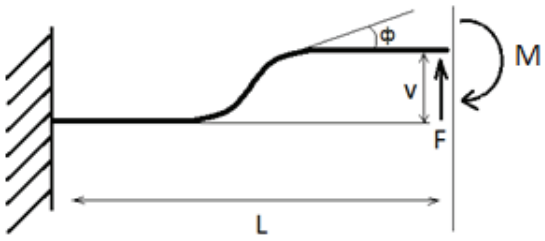

Figure F.2: Schematic view of a leaf spring considered as a homogeneous beam

Each leaf spring is modeled as a beam with length L, of which one end is clamped. The other end can be displaced but no rotation is possible. This results in the following constraint:

$$\phi = 0 \tag{F.1}$$

Where ϕ is the tip rotation of the beam. A force (F) and a moment (M) prevent the end from rotating. The tip rotation due to the force and the moment, as indicated by ϕ in figure F.2, has to equal zero. This results in the following

equation:

$$\phi = \frac{FL^2}{2EI} - \frac{ML}{EI} = 0[rad] \tag{F.2}$$

Where E is the modulus of elasticity, F the force acting on the tip, L the length of the leaf spring, M the moment acting on the tip and I the moment of inertia. This equation can be rewritten for the torque (M) in terms of the force (F) and length (L):

$$M = \frac{FL}{2} = 0[Nm] \tag{F.3}$$

The tip displacement (v) due to the moment and force can be calculated by:

$$v = \frac{FL^3}{3EI} - \frac{ML^2}{2EI}[m] \tag{F.4}$$

Substituting equation F.3 into equation F.4 yields:

$$v = \frac{FL^3}{3EI} - \frac{(\frac{FL}{2})L^2}{2EI}[m] \tag{F.5}$$

Rearranging equation F.5 to force (F) in terms of stiffness (k) and displacement (v) results in:

$$F = kv = \frac{12EI}{L^3}v[N/m] \tag{F.6}$$

With, moment of inertia I for a beam with a width, b, and height, h:

$$I = \frac{1}{12}bh^3[m^4] \tag{F.7}$$

The leaf springs are made of stainless steel and have a dimension of 0.025 (free length) $\times$ 0.072 $\times$ 0.00006 m. Filling in the values in equation F.7 yields:

$$I = \frac{1}{12}0.072 \cdot 0.00006^3 = 1.296 \cdot 10^{-15}[m^4] \tag{F.8}$$

The modulus of elasticity, E, of stainless steel is 210 MPa [2]. The maximum displacement of the force sensor is stated by the manufacturer as 0.127 mm (0.05 inches). Filling in these values and the value of equation F.8 into equation F.6:

$$F = k_{leaf}v = \frac{12 \cdot (210 \cdot 10^9) \cdot (1.296 \cdot 10^{-3})}{0.025^3} \cdot (0.127 \cdot 10^{-3}) = 27 \cdot 10^{-3}[N/m] \tag{F.9}$$

The displacement of the force sensor is linearly proportional to the force. The force exerted by the leaf springs is also linear proportional to the displacement. This means that the contribution of the two leaf springs is a continuous percentage. The percentage can be calculated by:

$$\varepsilon = \frac{2k_{leaf}}{k_{fs}} \tag{F.10}$$

To calculate the percentage, the stiffness of the sensor (k_{sensor}) is required. The maximum force is stated as 2.5 N and the maximum deflection as 0.127 mm. Note that the displacement of the plateau is restricted by the maximum

deflection of the force sensor. Considering the force sensor as a linear spring and filling the values:

$$k_{fs} = \frac{F_{smax}}{v_{smax}} = \frac{2.5}{0.127 \cdot 10^{-3}} = 19685[N/m] \tag{F.11}$$

Where k_{fs} is the stiffness of the force sensor, F_{smax} the maximum force that may be applied to the force sensor and v_{smax} the maximum deflection of the force sensor or maximum displacement of the plateau. Fill in the values into equation F.10:

$$\varepsilon = \frac{(2\frac{12 \cdot 210 \cdot 10^9 \cdot 1.296 \cdot 10^{-15}}{0.025^3})}{19685} = 2.1\% \tag{F.12}$$

These calculations show that a continuous contribution of 2.1% is added to the force measurements.

F.2 Frequencies of set-up

The results of the insertion force measurements reveal several oscillations which could not be explained. A blank experiment with a gel phantom was performed to investigate if the frequencies were due to the properties of the meat (appendix G). The results of this experiment show the same oscillations which makes it plausible that the frequencies are due to the construction. In the next sections the natural frequency of the construction and frequencies due to the rotation of the catheter are discussed. These calculated frequencies are compared to the frequencies found in the results in appendix G.

F.2.1 Natural frequency of construction

The meat is enclosed by a container. This container is attached on a plateau which is supported by leaf springs. The forward movement of the plateau is limited by the force sensor. If the force sensor and leaf springs are considered as a linear spring, than three springs are attached to the plateau (see figure F.3).

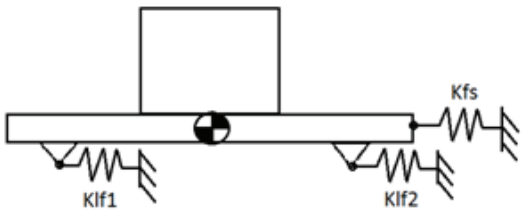

Figure F.3: Schematic view of the construction considering it as a mass with springs

The mass of the system (m) is considered as a point mass acting on the center of the plateau. This mass is the sum of the plateau, container and gel or meat. The system is a mass spring system and can be described by [3]:

$$m\ddot{x} + (k_{lf1} + k_{lf2} + k_{fs})x = F \tag{F.13}$$

Where k_{lf1} is the stiffness of the first leaf spring, k_{lf2} the stiffness of the second leaf spring and k_{fs} the stiffness of the force sensor. Rewriting equation F.13 into the general form [3] and with $k_{lf1} = k_{lf2}$:

$$\ddot{x} + \omega_0^2 x = \frac{F}{m} \tag{F.14}$$

with,

$$\omega_0 = \sqrt{\frac{2k_{lf} + k_{fs}}{m}} \tag{F.15}$$

Where ω_0 is the natural frequency of the system [3]. When an oscillating load is applied to the setup with the same frequency as the natural frequency of the system, the system starts to oscillate. Before the frequency can be calculated, the mass of the plateau (m_{pl}), clamp (m_{cl}), brackets (m_{br}), container (m_{co}) and gel or meat ($m_{gel/meat}$) have to be determined in order to determine the total mass of the system:

$$m = m_{pl} + m_{cl} + m_{co} + m_{gel/meat} + 2 \cdot m_{br} \tag{F.16}$$

The gel is considered as water and its mass is determined by:

$$m_{gel} = \rho_{water} \cdot b_{co} \cdot h_{co} \cdot l_{co} \tag{F.17}$$

Where ρ_{water} is the density of water, b_{co} the width of the container, h_{co} the height of the container and l_{co} the length of the container. The other masses are determined with a scale. Table F.1 show all the required information:

Parameter	**Symbol**	**Amount**
Mass container	m_{co}	26 gram
Density water	ρ_{water}	998 kg/m^3
With, length, height container	$h/l/b_{co}$	0.05 m
Mass clamp	m_{cl}	17.2 gram
Mass plateau	m_{pl}	106.8 gram
Mass bracket	m_{br}	5.66 gram

Table F.1: Required parameters for determining the natural frequency

The stiffness of the leaf springs and force sensor calculated in the previous section in equation F.12 are used to determine the natural frequency. Fill in all the values into equation F.15:

$$\omega_0 = \sqrt{\frac{2 \cdot 209 + 19685}{0.289}} = 265[rad/s] \tag{F.18}$$

The calculated natural frequency is the angular natural frequency and can be converted to ordinary frequency by:

$$f = \frac{\omega_0}{2\pi} \tag{F.19}$$

The calculated natural frequency of the system with a gel phantom is 42Hz. It is assumed that the meat phantom has roughly the same mass and the same natural frequency can be expected.

F.2.2 Frequencies due to rotations

The tube is strengthened with a carbon bar which is not perfectly straight. This in turn results in masses which are not perfectly centered and cause the tube to oscillate (see figure F.4). These oscillations can affect the insertion force as well as the torque required to insert the catheter.

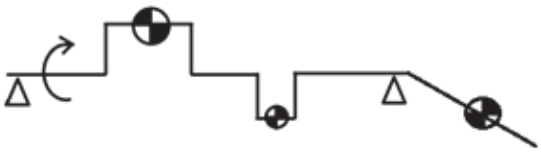

Figure F.4: Schematic view of the catheter with non-centered masses. When the catheter is rotating, the non-centered masses cause an oscillating motion.

In total two different rotational velocities (Ω) were applied, 1.906 and 9.530 rev/s. The period (T) of an oscillation is described by:

$$T = \frac{1}{\Omega}[sec] \tag{F.20}$$

The periods (T) can be converted to frequencies (f) by:

$$f = \frac{1}{T}[Hz] \tag{F.21}$$

So, the frequencies due to the rotations, equal the rotational velocities, 1.906 and 9.530 Hz.

Bibliography

[1] J. Gere, *Mechanics of Materials*, 5th ed., 2002.

[2] R. Hibbeler, *Sterkteleer voor technici [trans.]*, 1st ed., J. Rietdijk, Ed. Schoonhoven: Academic Service, 2002.

[3] J. Meriam and L. Kraige, *Engineering mechanics - Dynamics*, 4th ed. John Wiley and Sons, 1998.

APPENDIX

G

FREQUENCIES IN RESULTS

In this appendix the origin of the frequencies in the insertion force measurements are investigated. The calculated frequencies (section F.2) are compared with the frequencies in the results. The natural frequency of the setup, 43 Hz, should appear in the frequency analysis. Otherwise the frequencies are related to the properties of the meat. Furthermore a frequency of 1.9 Hz or 9.5 Hz, depending on the rotational velocity that was applied, should appear. Measurements with a gel phantom were performed to investigate the origin of the oscillations in the measurements. The frequencies in the measurements are investigated with a Discrete Fourier Transform. This method is discussed first. In the successive sections, the frequency analysis of the measurements with gel and those with meat are discussed separately.

G.1 Frequency analysis

The data acquisition device (NIDAQ) converts the continuous signals of the measuring devices to a digital signal. The data points were sampled with 1 kHz resulting in discrete measurements with a resolutions of 1000 measurements per second. The catheter was displaced over 125 mm and depending on the insertion velocity the measurements have durations of 2.5, 12.5 or 125 seconds. For the analysis of the curves, the signals were converted to a force per displacement. The time was multiplied by the applied insertion velocity. In this way the force measurements have the same lengths and show what the effect of the different settings are to reach a specific target. However the presence and the frequency of the oscillations on top of the curvatures cannot easily be seen. Not when the forces are plot against time as well as against displacement.

Oscillations appear as a periodic variation which means that values around the curvatures are structurally higher or lower. This property was used to examine the presence of oscillations and their frequencies. When the measurements are plotted versus frequency, the oscillations should cause a peak value in the plots. The periods of the amplitudes of the oscillations should all be the same and can be added to the same frequency because the frequency is defined as one divided by the period (equation F.21).

A continuous input or value $y(t)$ in the time domain can be converted to the frequency domain by the use of the Fourier transform which is defined as [1]:

$$Y(f) = \int y(t)e^{-j2\pi ft}dt \tag{G.1}$$

However, the signal is discrete and this transform can not be used. For this reason the discrete signal in the time domain was transformed to complex values in the frequency domain by the use of the MATLAB function 'fft'. This function gives the Discrete Fourier Transform (DFT) of the entered vector. The Discrete Fourier Transform is defined as [1]:

$$U(r) = \sum_{j=1}^{N} u(k)e^{-j2\pi rk/N} \tag{G.2}$$

Where N is the length of the vector and with integers,

$$r = [0, 1, 2, ..., N-1] \tag{G.3}$$

and,

$$k = [0, 1, 2, ..., N-1] \tag{G.4}$$

Only the changes in time around the steady value, the oscillations, are of interest and the median was extracted from the data vector. Note that besides the frequencies of the oscillations also frequencies for the rise time or settling time will appear. An force decrease or increase over time result in an amplitude in the frequency domain. In the next sections the DFT of force measurements in gel and meat is presented and discussed.

G.2 DFT of measurements

Measurements with a gel phantom were performed to investigate the source of the oscillations present in the results of the insertion force measurements. If

the oscillations can be attributed to the properties of the meat, they should not appear at the gel measurements. The gel was made by filling a container without holes almost completely with hot water wherein three gelatin sheets were dissolved. The suspension was hardened in the refrigerator for three hours. One run of 36 measurements following the same procedure as for meat was performed. The meat was replaced by the gel phantom which perfectly fits inside the container with holes. Note that the gel is homogeneous and that force measurements are not affected by the orientation.

G.2.1 DFT gel measurement

Oscillations are present in the insertion force measurements with gel as can been seen in the upper left graph of figure G.1 where the results of one gel measurement is shown. This graph shows the insertion force measurements with respect to time. The catheter was pulled with 1 mm/s through the gel without a rotation. Besides a plot of the insertion force also the velocity of the stage is shown. In this way the oscillations of the stage can be compared with the oscillations of the insertion force measurements and can be seen if they are related.

The DFT of the insertion force clearly shows a peak at 42.91 Hz. The frequency calculations shows that this frequency is due to the natural frequency of the construction which should be around the 42 Hz. This frequency is not present in the DFT of the linear stage velocity and it can be concluded that the stage does not influence the measurements.

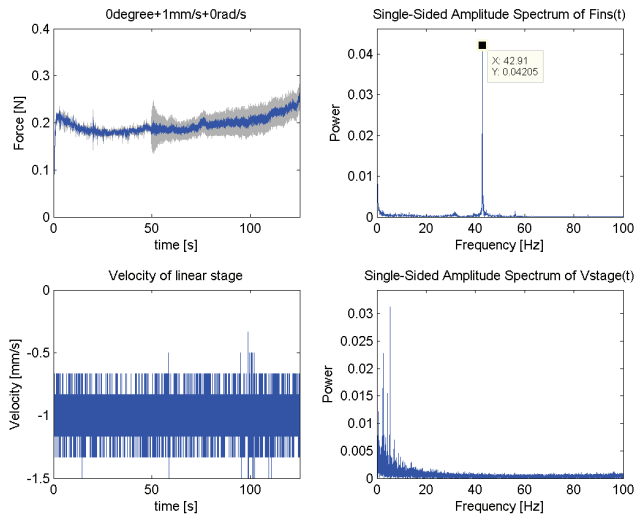

Figure G.1: : Upper left: Results of a force measurement with a gel phantom with 1 mm/s and no rotation. In gray the rough signal and in blue the filtered signal. Signals above 30 Hz were filtered out with a low pas zero phase filter. **Upper right:** Single-Sided Amplitude Spectrum of the insertion force which shows a peak around 42 Hz due to the natural frequency of the construction. **Lower left:** Velocity of the stage versus time. **Lower right:** Single-Sided Amplitude Spectrum of the velocity of the stage which shows a peak around 5 Hz due to the slight deviation of the spindle. The spindle has a pitch of 5 mm/rev.

From the frequency calculations can also expected that insertions with rotations should reveal additional frequencies. In the upper left graph of figure G.2 results of a measurement with 1 mm/s and 114 RPM is presented. Besides the large peak around 42 Hz a peak at 1.892 Hz can be found. This corresponds also to the frequency calculations of section F.2. A rotation of 114 RPM or 1.906 rev/s, adds oscillations with a frequency of around 1.906 Hz to the force measurements. The DFT of the velocity of the linear stage shows the same frequencies as without rotation and it is again expected that the linear stage not effect the force measurements.

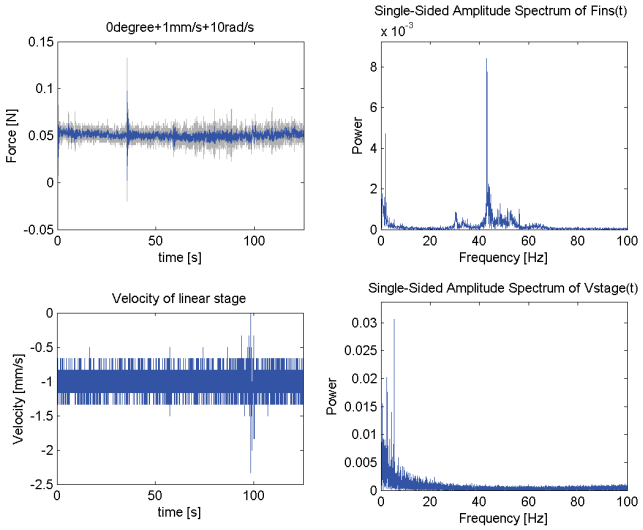

Figure G.2: : Upper left: Results of force a measurement with a gel phantom with 1 mm/s and 114 RPM. In gray the rough signal and in blue the filtered signal. Signals above 30 Hz were filtered out with a low pas zero phase filter. **Upper right:** Single-Sided Amplitude Spectrum of the insertion force. Besides the peak at 42 Hz, a peak at 1.9 Hz is present caused by the rotation of the catheter. **Lower left:** Velocity of the stage versus time. **Lower right:** Single-sided Amplitude Spectrum of the velocity of the stage which shows a peak around 5 Hz due to the slight deviation of the spindle. The spindle has a pitch of 5 mm/rev.

According to the calculations settings with rotational velocities of 572 RPM or 9.5 rev/s should reveal oscillations with a frequency of 9.5 Hz. Figure G.3 presents the results of a measurement with 1 mm/s and 572 RPM. Again the corresponding frequency due to the rotational velocity, 9.583 Hz, can be found in the DFT of the insertion force, as well as the natural frequency of the construction. Furthermore other frequencies can be found which can not directly be explained by the calculations. However during the experiment it was observed that small pieces of the gel were detached which were subsequently trapped between the surface of the catheter and gel. During the insertion the non-spherical pieces rolled between the surfaces which could affect the insertion force. Overall can be concluded that the natural frequency of the setup as well as the rotation of the catheter actually affect the insertion force measurements.

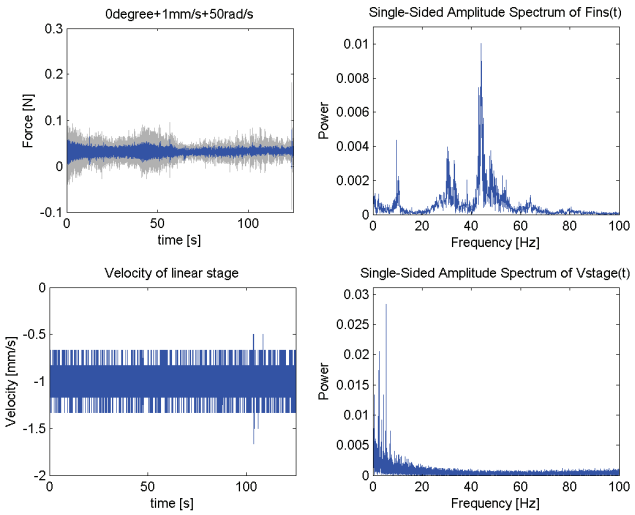

Figure G.3: : Upper left: Results of force a measurement with a gel phantom with 1 mm/s and 572 RPM. In gray the rough signal and in blue the filtered signal. Signals above 30 Hz were filtered out with a low pas zero phase filter. **Upper right:** Single-Sided Amplitude Spectrum of the insertion force. Besides the peak at 42 Hz, a peak at 9.6 Hz is present caused by the rotation of the catheter. **Lower left:** Velocity of the stage versus time. **Lower right:** Single-sided Amplitude Spectrum of the velocity of the stage which shows a peak around 5 Hz due to the slight deviation of the spindle. The spindle has a pitch of 5 mm/rev.

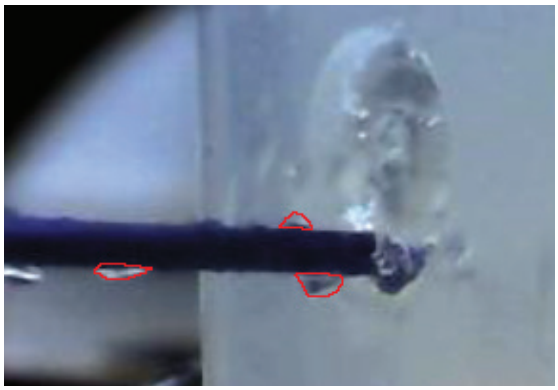

Figure G.4: Movie still of gel insertion. The non spherical pieces of gel that are attached to the catheter can be observed clearly.

G.2.2 DFT meat measurement

The insertion force measurements with meat can also be transformed to the frequency domain. The weight of a piece of meat, that fits the container, is comparable to the weight of the gel phantom. For this reason the same oscillations due to the natural frequency of the construction could occur in the insertion force measurements. Figure G.5 presents the results of a measurement with meat. The upper graph presents the insertion force measurements with respect to distance and the bottom the DFT of the insertion force measurements. The measurements were performed with an insertion velocity of 1 mm/s and without a rotation in the direction parallel to the muscle fibers. The DFT shows only a peak at 43.14 Hz due to the natural frequency of the construction.

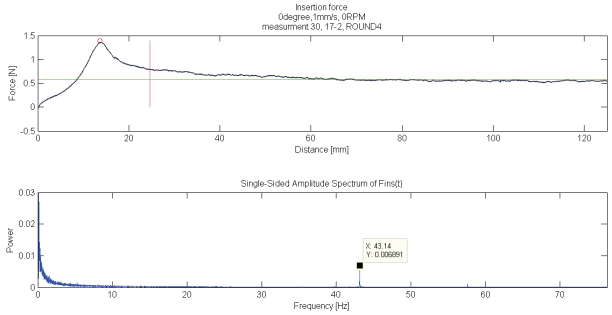

Figure G.5: Top: Results of insertion force measurements versus distance with a meat phantom. Insertions are performed parallel to the muscle fibers with 1 mm/s and no rotation. In gray the rough signal and in blue the filtered signal. Signals above 30 Hz were filtered out with a low pas zero phase filter. The horizontal green line indicates the steady insertion force. The vertical magenta line indicates the settling time. The red dot indicates the maximum value. **Bottom:** Single-Sided Amplitude Spectrum of insertion force which shows a peak at 43 Hz due to the natural frequency of the construction.

In the upper graph of figure G.6 the result of a measurement with a rotational velocity of 114 RPM is shown. The insertion was performed with 1 mm/s parallel to the muscle fibers. The bottom graph shows the DFT of the insertion force, the insertion force with respect to frequency. Besides a peak at 42 Hz, the results in the frequency domain also show a peak at 1.884 Hz which corresponds to the rotational movement of the catheter. So the calculated frequency of roughly 1.9 Hz appears also in measurements with meat.

The DFT of measurements with meat and rotational velocities of 572 RPM should reveal peaks at 9.5 Hz. Figure G.7 shows the results of a measurement with 1 mm/s and 572 RPM. The upper graph shows the insertion force and the bottom graph presents the DFT of the insertion force measurements. The DFT clearly shows peaks at 9.567 and 42 Hz which corresponds with the frequency calculations.

Until now only settings with 1 mm/s are shown. Figure G.8 shows the results of a measurement of the insertion force during insertion parallel to the muscle fibers with 10 mm/s and 572 RPM. The upper graph is again the insertion force measurement and the lower graph the DFT of the insertion force. The DFT shows two peaks one at 42 Hz, the natural frequency of the construction, and one at 9.5 Hz, due to the rotation of the catheter.

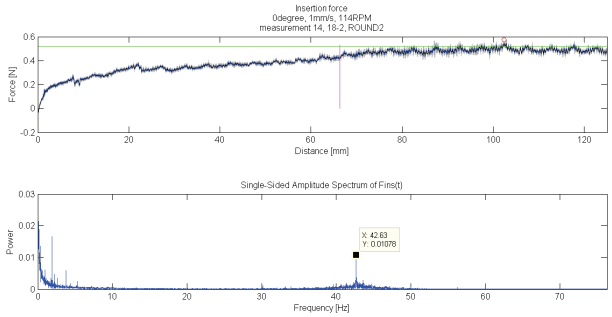

Figure G.6: Top: Results of force measurements versus distance with a meat phantom. Insertions are performed parallel to the muscle fibers with 1 mm/s and 10 rad/s. In gray the rough signal and in blue the filtered signal. Signals above 30 Hz were filtered out with a low pas zero phase filter. The horizontal green line indicates the steady insertion force. The vertical magenta line indicates the settling time. **Bottom:** Single-Sided Amplitude Spectrum of insertion force. Besides a peak at 42 Hz, a peak at 1.9 Hz is present caused by the rotation of the catheter.

G.3 Filtering signals

From the results it can be concluded that the insertion force measurements are affected by the natural frequency of the construction as well as by the rotation of the catheter. For this reason a low pass zero phase second order Butter-worth frequency filter of 30 Hz is used to filter out the natural frequency of the construction. A zero phase filter is chosen to prevent time delays in the measurements. The natural frequency can be slightly higher or lower than the calculated frequency due to the variation in mass of the meat phantom. For this reason a lower frequency than the calculated frequency is used for the filter.

This filter also reduces the chance of aliasing because the sample frequency is much larger than the 30 Hz [1]. A Butter-worth does not filter out frequencies above the cutt-off frequency abruptly. This filter gradually reduces the effect of frequencies above the cut-off frequency. This also reduces the chance on aliasing

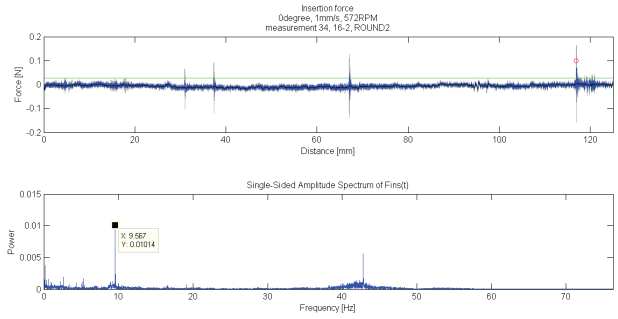

Figure G.7: Top: Results of force measurements versus distance with a meat phantom. Insertions are performed parallel to the muscle fibers with 1 mm/s and 50 rad/s. In gray the rough signal and in blue the filtered signal. Signals above 30 Hz were filtered out with a low pas zero phase filter. The horizontal green line indicates the steady insertion force. **Bottom:** Single-Sided Amplitude Spectrum of insertion force. Besides a peak at 42 Hz, a peak at 9.5 Hz is present caused by the rotation of the catheter.

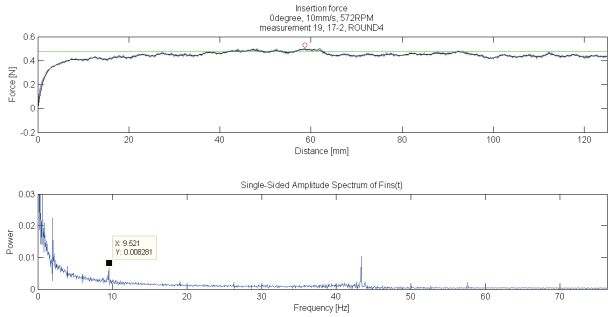

Figure G.8: Top: Results of force measurements versus distance with a meat phantom. Insertions are performed parallel to the muscle fibers with 10 mm/s and 50 rad/s. In gray the rough signal and in blue the filtered signal. Signals above 30 Hz were filtered out with a low pas zero phase filter. The horizontal green line indicates the steady insertion force. **Bottom:** Single-Sided Amplitude Spectrum of insertion force. Besides a peak at 42 Hz, a peak at 9.5 Hz is present caused by the rotation of the catheter.

of the frequencies around the cut-off frequency.

The frequencies due to rotations of the tube are not filtered out because the frequencies are within the range of interest and also relevant information about the behavior of the meat itself could be present at these frequencies.

The settling time is very sensitive to oscillations and for this reason an average filter is used instead of the frequency filter to filter out the oscillations due to the rotation as well as the unexplainable oscillations before the settling time is determined. A moving average filter of 150 samples is applied to the settling time data. The value of one sample is determined by the average of the 150 surrounding samples. Information above 6.7 Hz is averaged (due to the combination of sample rate and filter rate, $1/150 \times 1000 = 6.7$ Hz) and especially oscillations are smoothened. Note that the individual non periodic information above this boundary is not removed but the effect of it is lowered. For this reason it was not applied for the determining the maximum because this filter would smoothen the maximum peaks.

Bibliography

[1] A. de Vlugt, A. Schouten, W. Mugge, and A. Klomp, "Lecture notes: System Identification & Parameter Estimation (WB2301)," Delft University of Technology, Tech. Rep., 2009.

APPENDIX

H

MODELING INSERTION FORCE

As was discussed in the paper (chapter 1) different types of curves can be found for different groups. The experimental setup and the properties of tissue show elastic behavior and it can be expected that the behavior of the insertion force can be modeled with a mass-damper system. The processes that occur during the needle insertion, responsible for the conduct of the insertion force, are discussed in this appendix. Furthermore, models of the insertion forces for each individual group are discussed. The behavior and amount of force for each individual group can be predicted with these models.

H.1 Curves

Figure H.2 shows results of measurements with different settings. Each plot shows six individual measurements from three different runs. The measurements were filtered with a low pass zero phase filter of 30 Hz as was discussed in appendix G. In total eighteen different plots are shown with all the different combinations. Three types of curves can be found in the results of the insertion force measurements: a step response with overshoot, a step response without overshoot and a straight line (as is illustrated in figure H.1). Although the individual measurements show the same curve, the individual positions and sizes differ. As was discussed in appendix D.4, there is much variation in the properties between different pieces of meat as well as within the individual pieces. This can explain the variations found in the results.

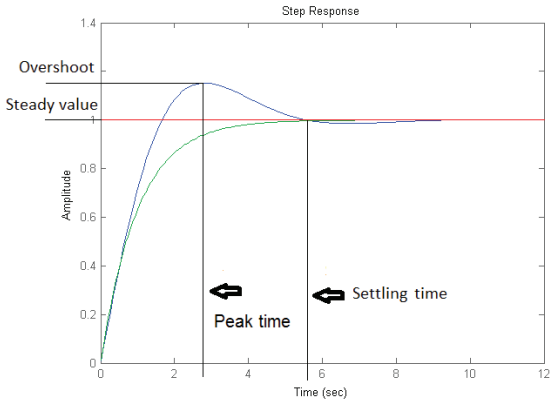

Figure H.1: Three step responses with indicated characteristics.

H.2 Modeling

Basically three types of curves can be found in the plots. Differences between groups can be found in the amount of overshoot, settling time and steady value as was discussed in chapter 1. Based on this information a model can be made for the individual groups. In turn, these models can be used for the simulation of a needle insertion. Note that only the friction is modeled and an additional model for the cutting forces is required.

The three curves can be characterized by four parameters as is shown in figure H.1 [1, 2]:

- Steady value : The final value.
- Settling time: Time for the response to reach, and stay in a boundary around the final value.
- Overshoot: Percentage that the peak value is larger than the final value.
- Peak time: The time to reach the peak.

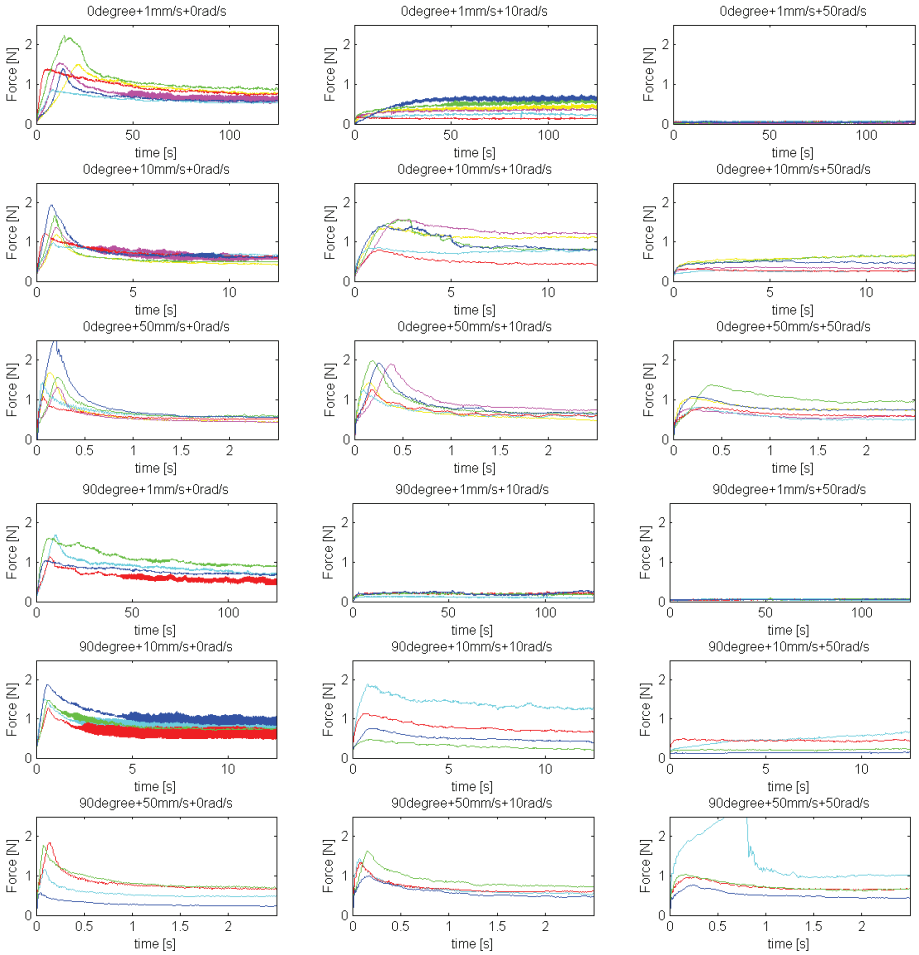

Figure H.2: Plots of insertion force measurements. Each plot contain six individual measurements performed in three different runs. The raw data is filtered with a zero phase 30 Hz low pas filter. Some of the measurements have still oscillations.

Note that a curve without overshoot does not have a peak time. The parameters of each individual curve are investigated with the MATLAB function 'stepinfo' as was discussed in section 3.1 of the paper (chapter 1). The group median of the parameters is used to model the curve for each individual group.

H.2.1 Mechanical model

As was discussed in chapter 1, the friction forces between the tissue and catheter cause the tissue to displace. However, the tissue is constrained by the container and the tissue cannot move. This results in a force exerted on the container which is eventually sensed by the force sensor as is illustrated in figure H.3. Tissue behaves viscoelastic and therefore it can be expected that the force exerted by the tissue dependents on the displacement and velocity of the catheter. This behavior could be modeled with a mass damper system as is shown in figure H.4. In turn, the friction force exerted on the tissue depends on the type of friction.

Before pulling the catheter, the maximum rotational velocity was applied for 2 seconds. This causes several things besides preventing stationary contact between the catheter and tissue. First, it is expected that the surface of the tissue is smoothened perpendicular to the insertion direction as is illustrated in figure H.5. Second, long ranged particles present in the lubricant are arranged perpendicular to the insertion direction. Third, the lubricant layer between catheter and tissue is increased as was discussed in chapter 1.

The displacement of the catheter at the start of each measurement also causes several things. The surface is smoothened in the insertion direction. The transition of perpendicular direction to the insertion direction takes time. The time of transition depends on the applied settings. Three situations can be distinguished: no rotation, a perpendicular velocity that is larger than the insertion velocity and all other situations.

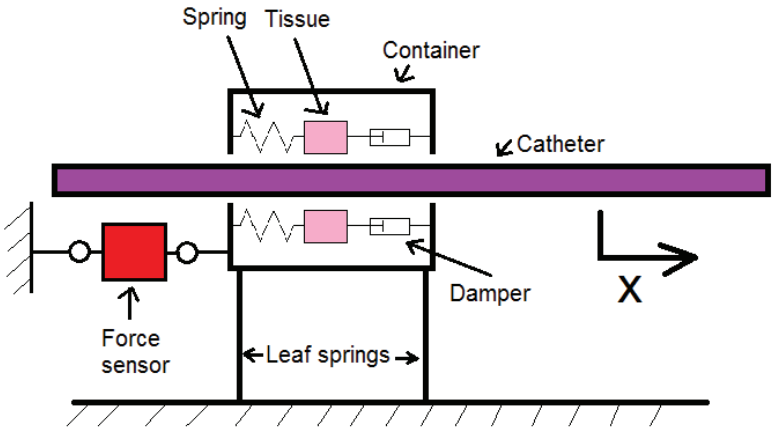

Figure H.3: Sketch of setup with the tissue phantom modeled as mass damper system.

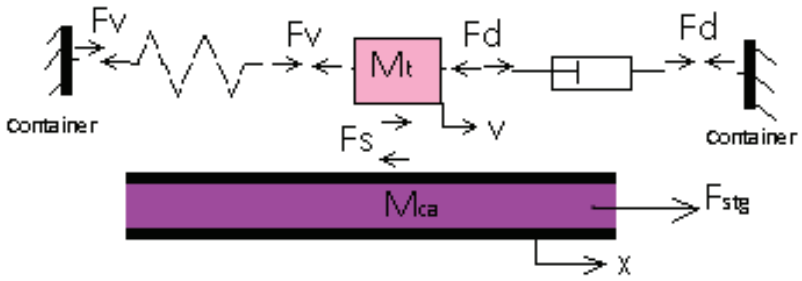

Figure H.4: Free body diagram of tissue and catheter. The displacement of the catheter results in a force that is exerted on the container.

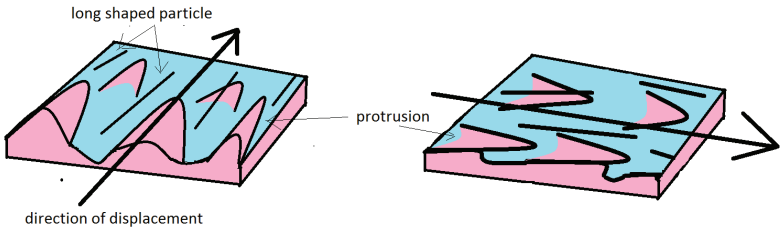

Figure H.5: Illustration of small pieces of tissue surface with protrusion, lubricant and long shaped particles which are in contact with the catheter surface. **Left:** The rotation of the catheter before the start of each measurements causes several events: the tissue surface is smoothen in perpendicular direction, long ranged particles are arranged in perpendicular direction and the lubricant layer is increased. **Right:** During sliding the surface is smoothen in the direction of the displacement and the long shaped particles arranged in the direction of the displacement.

H.2.2 Equation of motion

By the use of the Free body diagram (FBD) of figure H.4 an equation of motion can be formulated. The mass of the tissue and the mass of the catheter are considered as points masses. The linear stage exerts a force on the catheter and causes it to accelerate. The required force is increased due to the friction between the tissue and catheter shaft. The equation of motion for the catheter can be described as:

$$M_{ca}\ddot{x_{ca}} - F_{stg} = F_s \tag{H.1}$$

Where F_s is the friction force between the catheter shaft and tissue, x_{ca} the displacement of the catheter, F_{stg} the force exerted by the linear stage and tissue and M_{ca} the mass of the catheter.

The friction force is considered as boundary lubrication or as hydrodynamic lubrication and acts also on the tissue. This force also results in a displacement of the tissue. However the tissue is constrained by the container. In turn, the tissue is deformed and exerts a force on the container. The equation of motion for the tissue is formulated as:

$$M_t\ddot{x_t} + \xi\dot{x_t} + kv = F_s \tag{H.2}$$

Where M_t is the mass of the tissue, F_s the friction force between the catheter shaft and the tissue, x_t the displacement of the tissue, ξ the damping coefficient of the tissue and k the stiffness of the tissue. The equation of motion for both bodies can be described as:

$$\begin{bmatrix} M_{ca} & M_t \end{bmatrix} \begin{bmatrix} \ddot{x_{ca}} \\ \ddot{x_t} \end{bmatrix} + \begin{bmatrix} 0 & \xi \end{bmatrix} \begin{bmatrix} \dot{x_{ca}} \\ \dot{x_t} \end{bmatrix} + \begin{bmatrix} 0 & k \end{bmatrix} \begin{bmatrix} x_{ca} \\ x_t \end{bmatrix} = F_{stg} \tag{H.3}$$

The viscoelastic properties of the tissue play an important role in the amount of force that is exerted on the container that enclosed the tissue. This force is eventually measured by the force sensor.

From the equation of motion can be seen that the acceleration of the catheter cause additional forces. However, when the catheter is displaced with a constant velocity, the tissue is deformed (the mass of the tissue is displaced but the tissue itself cannot move because it is enclosed by the container) with a constant

amount. Also the rate of deformation contribute to the forces before the steady state has been reached.

At the steady state, only the force of the stage is transmitted via the tissue to the container and finally to the force sensor. At this stage, the velocity is zero and from equation H.1 it can be seen that the force of the stage is equal to the friction force.

Also the other forces during the initial stage are of interest. A needle always starts from rest and accelerates to a certain velocity. During the insertion, more tissue comes into contact with the needle and the velocity between the new tissue and the needle abruptly increases. So both the initial as well as the steady state are of interest.

Two types of friction are expected to occur: boundary lubricated and hydrodynamic friction. During both types of friction it is expected that an initial state and a steady state can be distinguished. In the next sections is explained why these stages are expected to occur.

H.2.3 Modeling groups without rotation

Before each measurement, the maximum rotation is applied which increases the lubricant layer. When no rotation is applied during the measurement, the lubricant layer will decrease directly after the start of the measurement. The hydrodynamic pressure that was created by the rotation is no longer sustained. The same holds for settings where the perpendicular velocity is lower then the insertion velocity. The number and sizes of direct contact points between the surface of the catheter and tissue is increased.

At the start the contact points move together with the surface of the catheter in the insertion direction. After a certain distance, the friction between the contact points is lower than the force required to further displace the contact points. This is characterized as the peak time in the curves. Until an equilibrium is reached, long ranged particles arrange in the insertion direction and the tissue surface is smoothened over time. This time is the settling time in the curves.

The first displacement until the peak time can be described by the viscoelastic behavior of the tissue. This behavior can be modeled with an under-damped mass-damper system [1, 2, 3]:

$$F_{ins}(x_{ca}) = C(1 - e^{-\sigma x}(cos(\omega_d x_{ca}) + \frac{\sigma}{\omega_d} sin(\omega_d x))) \tag{H.4}$$

With the real part of the system pole:

$$\sigma = \zeta\omega_n \tag{H.5}$$

and the damping frequency:

$$\omega_d = \omega_n\sqrt{1-\zeta^2} \tag{H.6}$$

and scale factor:

$$C = \frac{Peak}{F_{ins}(t_{peak})} \tag{H.7}$$

Normally the damping ratio ζ and natural frequency ω_n of the system are known. In this case the system properties are unknown. However the input-output is

known and the properties of the system can be determined. The peak time is known and the damping frequency ω_d can be determined by:

$$\omega_d = \frac{\pi}{t_{peak}} \tag{H.8}$$

The peak value and the steady value are known and the damping ratio can be determined:

$$\zeta = \frac{-\delta}{\sqrt{(2\pi)^2 + \delta^2}} \tag{H.9}$$

with overshoot indicator:

$$\delta = log(\frac{Peak}{steady} - 1) \tag{H.10}$$

The natural frequency can be determined by rewriting equation H.6:

$$\omega_n = \frac{\omega_d}{\sqrt{1 - \zeta^2}} \tag{H.11}$$

The overshoot parameter from equation H.5 may not exceed 1, otherwise the system cannot be described.

After the peak has been reached, the tissue and lubricant slowly reach an equilibrium at the settling time. The tissue is still at the maximum displacement. The insertion force is modeled as the function that follows the upper peaks of the oscillating function of equation H.4, the tissue is after all not oscillating:

$$F_{ins}(x_{ca}) = C(1 + e^{-\sigma x_{ca}}) \tag{H.12}$$

The overshoot is lager than 100% for some of the settings. Equation H.4 cannot describe step functions with overshoots larger than 100%. In these cases the maximum overshoot is obtained in two steps. First the overshoot is divided by two:

$$\delta = log(\frac{\frac{Peak}{steady} - 1}{2}) \tag{H.13}$$

The new overshoot parameter is substituted in equation H.9 and used to calculate the insertion force function without scale factor C. However the overshoot in this function is lower than required. To increase the overshoot, the function is multiplied by a correction factor which can be calculated by:

$$C_{corr} = (\frac{2\delta}{(\frac{F_{ins}(t_{peak})}{S_{steady}})} - 1)e^{-\frac{6}{125}} - 1 \tag{H.14}$$

with,

$$S_{steady} = \frac{(1 + e^{-125\sigma}) - (1 - e^{-125\sigma})}{2} + (1 - e^{-125\sigma}) \tag{H.15}$$

The steady value S_{steady} is determined as the line between the upper and lower peaks of the oscillating step function. The correction factor (C_{corr}) is a log function that goes from 1 at $x = 0$ to 0 at $x = 125$. This function is scaled such that the the required overshoot is obtained after multiplication of the function. The insertion force for overshoots larger than 100% can be calculated by:

$$F_{lOS}(x_{ca}) = C_{corr} \cdot F_{ins}(x_{ca}) \tag{H.16}$$

Note that $F_{ins}(x_{ca})$ is in these cases calculated with $\frac{\delta}{2}$. Finally the equation is scaled to fit the maximum and steady value as good as possible:

$$F_{fin}(x_{ca}) = C_{lOS} \times F_{lOS}(x_{ca}) \tag{H.17}$$

With,

$$C_{lOS} = \frac{Peak}{F_{lOS}(t_{peak})} \tag{H.18}$$

H.2.4 Modeling groups with rotation

In the case that the perpendicular velocity is larger than the insertion velocity, more hydrodynamic friction occurs. There are no or less direct contact points between the catheter surface and tissue surface. The friction drop is mostly due to rearrangement of the long ranged particles in the direction of movement. The lubricant is also viscoelastic as was discussed in chapter 1 and the insertion force is modeled as an over-damped system [1, 2, 3]:

$$F_{2ins} = F_{steady}(1 - e^{-\frac{4}{t_{setl}}x_{ca}}) \tag{H.19}$$

This describes an exponential function that starts at 0 and goes to the steady insertion force (F_{steady}) at the settling time (t_{setl}).

H.2.5 Modeling of exceptions

In cases where the perpendicular velocity is much larger than the insertion velocity, it can be expected that the friction is of a more hydrodynamic type and only the long ranged particles have to be arranged. However, before the start the maximum rotational velocity was applied and the direction of the movement does not change much after the start. The long ranged particles are already arranged in the direction of the resultant displacement (chapter 1). This is the cases for groups with insertion velocities of 1 mm/s and rotational velocities of 572 RPM. In these cases the insertion force is modeled as:

$$F_{3ins} = F_{steady} \tag{H.20}$$

H.3 Model verification

The functions (models) are determined with the characteristics of the first 16 measurements of each group. 'Failure' marked measurements (as was discussed in the paper) are replaced by the group median. The other 16 measurements are used for validation. The correctness of the functions are analyzed with Variance-Accounted-For (VAF) values which are calculated by [4]:

$$VAF = 1 - \frac{\sum_{i=1}^{N}(y(x_i) - \hat{y}(x_i))^2}{\sum_{x=1}^{N} y(x_i)^2} \tag{H.21}$$

For all time intervals,

$$x_i = 0, 0.1, 0.2...125 \tag{H.22}$$

Where $\hat{y}(x_i)$ are the predicted points calculated by the function (model) and $y(x_i)$ the measured points. The VAF value is calculated for each individual measurement that is not used for the model. An outcome of 1 indicates that the model fits the measured data perfectly. The predicted points and the measured points are the same which results in an output of one. Negative values indicate that the model and measured data are not correlated. The predicted points differ much from the measured points resulting in an negative output.

H.3.1 GROUP 1

The model of the group with insertions parallel to the muscle fibers with an insertion velocity of 1 mm/s and no rotation is shown in figure H.6 indicated by the thick green line. The shape of the modeled curve is roughly the same as most of the measured curves. However the steady value is much higher than most of the measured values. The average overshoot is larger than 100% and multiple correction factors are used to scale the curve. This can explain the high steady value. The table with the VAF values besides the graph shows that four curves are not correlated to the modeled curve. This corresponds with two 'failed' measurements and two deviant curves. The best value is 96% and most values are above 50%.

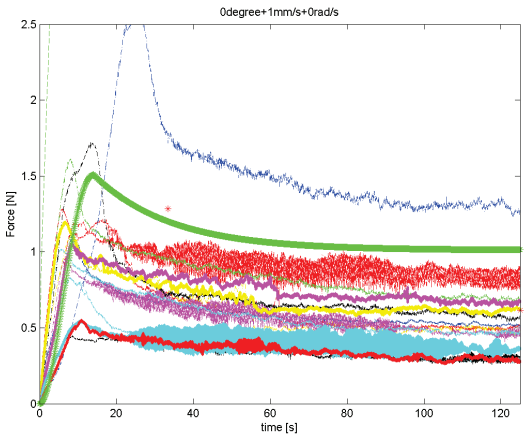

VAF
-2.2
0.53
0.54
0.37
-3.9
0.41
0.27
0.25
0.96
0.87
0.89
0.73
0.65
0.80
-1.6
-3.2

Figure H.6: Model and sixteen insertion force plots with insertions parallel to the muscle fibers, insertion velocities of 1 mm/s and without rotations. The thick green line is the model of this group. One 'failed measurement' and three deviant curves can be seen clearly resulting in negative VAF-values.

H.3.2 GROUP 2

The model of the group with insertions parallel to the muscle fibers with an insertion velocity of 1 mm/s and rotation of 114 RPM is shown in figure H.7 indicated by the thick green line. The shape of the modeled curve is roughly the same as most of the measured curves. Clearly two failed measurements can be

seen. The table with the VAF values besides the graph shows that three curves are not correlated to the modeled curve. Two of the uncorrelated curves are from the failed measurements and one measurement has a deviant curve. The best value is 98% and most values are above 75%.

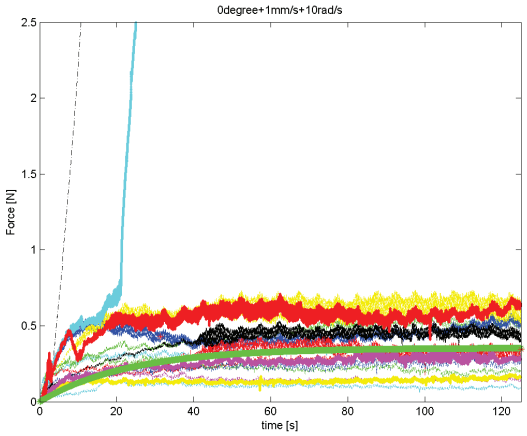

VAF
0.97
0.97
0.89
0.85
0.93
0.75
-0.18
-3.2
0.98
0.75
0.87
0.22
-0.60
0.95
0.26
0.78

Figure H.7: Model and sixteen insertion force plots with insertions parallel to the muscle fibers, insertion velocities of 1 mm/s and a rotation of 114 RPM. The thick green line is the model of this group. Two 'failed measurements' can be identified. One of the measurements shows a rough start. This results in three negative VAF-values.

H.3.3 GROUP 3

The model of the group with insertions parallel to the muscle fibers with an insertion velocity of 1 mm/s and rotation of 572 RPM is shown in figure H.8 indicated by the thick green line. All measured points are covered by the thick green line. Remarkable are the VAF values which are all zero. This can be caused by the fact that the group is modeled as a horizontal line through zero. When these zeros are filled in equation H.21 the outcome will be zero as well.

H.3.4 GROUP 4

The model of the group with insertions parallel to the muscle fibers with an insertion velocity of 10 mm/s and no rotation is shown in figure H.9 indicated by the thick green line. Most curves look like the modeled curve, however some differ. Also can be seen that some of the measurements show unexplainable oscillations. The table with the VAF values besides the graph shows that, two curves are not correlated to the modeled curve. The best value is 96% and most values are above 50%.

H.3.5 GROUP 5

The model of the group with insertions parallel to the muscle fibers with an insertion velocity of 10 mm/s and rotation of 114 RPM is shown in figure H.10 indicated by the thick green line. Most curves look like the modeled curve. Also

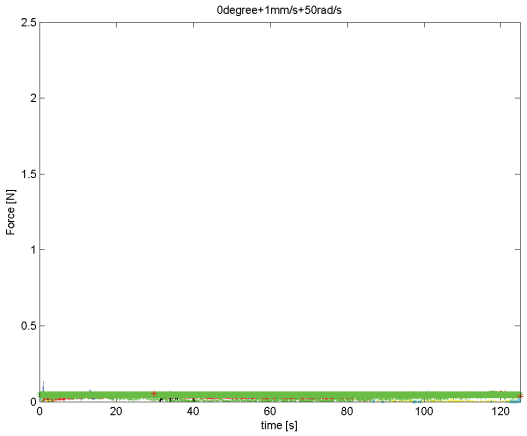

VAF
0
0
0
0
0
0
0
0
0
0
0
0
0
0
0
0

Figure H.8: Model and sixteen insertion force plots with insertions parallel to the muscle fibers, insertion velocities of 1 mm/s and rotation of 572 RPM. The thick green line is the model of this group.

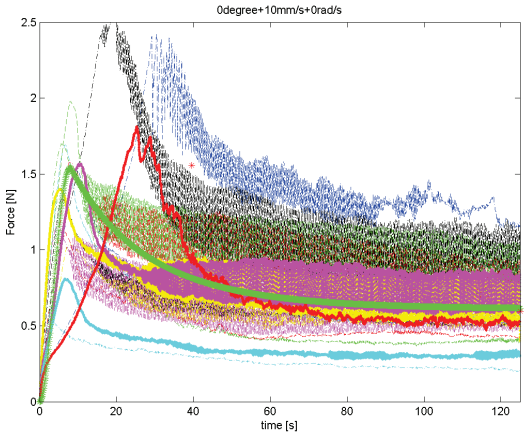

VAF
0.95
0.72
0.81
0.99
0.92
0.88
0.90
-2.5
0.94
0.91
0.71
0.82
0.95
0.97
-0.40
0.84

Figure H.9: Model and sixteen insertion force plots with insertions parallel to the muscle fibers, insertion velocities of 10 mm/s and without rotation. The thick green line is the model of this group.

can be seen that some of the measurements show unexplainable oscillations. Furthermore, one deviant curve can be indicated. The table with the VAF values besides the graph shows that, all curves are correlated to the modeled curve. The lowest value is 12%, the best value is 99% and most values are above 80%.

H.3.6 GROUP 6

The model of the group with insertions parallel to the muscle fibers with an insertion velocity of 10 mm/s and rotation of 572 RPM is shown in figure H.11 indicated by the thick green line. Most curves look like the modeled curve.

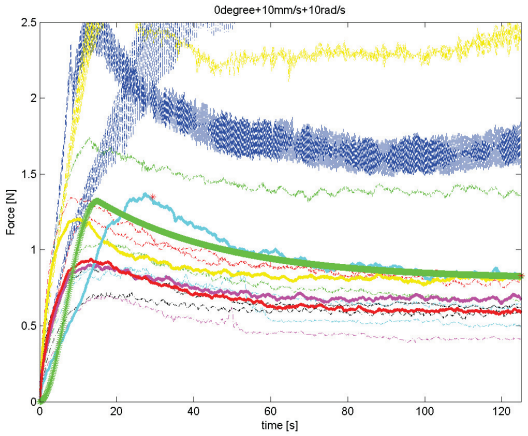

VAF
0.75
0.99
0.88
0.78
0.82
0.66
0.12
0.86
0.96
0.95
0.51
0.64
0.95
0.88
0.98
0.81

Figure H.10: Model and sixteen insertion force plots with insertions parallel to the muscle fibers, insertion velocities of 10 mm/s and a rotations of 114 RPM. The thick green line is the model of this group.

Three curves are not correlated as can be seen in the table with the VAF values besides the graph. The lowest value is 48%, the best value is 97% and most values are above 80%.

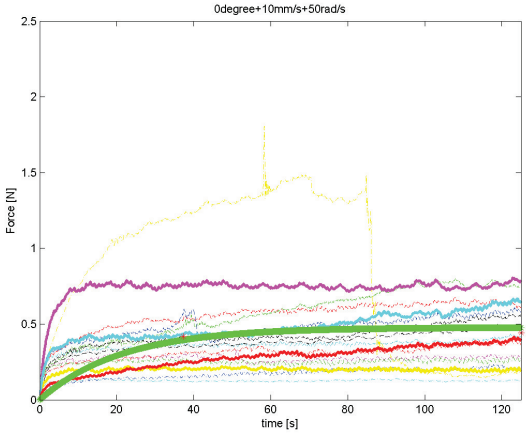

VAF
0.94
0.92
0.90
0.95
0.97
0.52
0.64
-4.4
0.86
0.48
-0.86
0.97
-0.28
0.77
0.95
0.80

Figure H.11: Model and sixteen insertion force plots with insertions parallel to the muscle fibers, insertion velocities of 10 mm/s and a rotations of 572 RPM. The thick green line is the model of this group.

H.3.7 GROUP 7

The model of the group with insertions parallel to the muscle fibers with an insertion velocity of 50 mm/s and no rotation is shown in figure H.12 indicated by the thick green line. The shape of the modeled curve is roughly the same as most of the measured curves. Some of the measurements show unexplainable

oscillations. Two curves are not correlated to the modeled curve. The best VAF value is 97% and most values are above 75%.

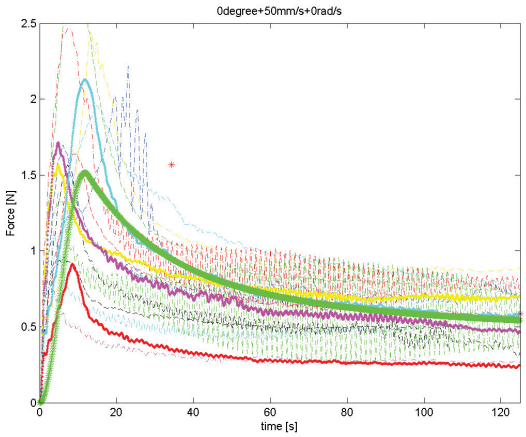

VAF
0.92
0.96
0.83
0.91
0.66
0.92
-1.6
0.46
0.85
0.78
0.94
0.78
0.91
0.87
0.97
-0.77

Figure H.12: Model and sixteen insertion force plots with insertions parallel to the muscle fibers, insertion velocities of 50 mm/s and without rotations. The thick green line is the model of this group.

H.3.8 GROUP 8

The model of the group with insertions parallel to the muscle fibers with an insertion velocity of 50 mm/s and rotation of 114 RPM is shown in figure H.13 indicated by the thick green line. The shape of the modeled curve is roughly the same as most of the measured curves. The table with the VAF values besides the graph shows that, two curves are not correlated to the modeled curve. The best value is 98% and most values are above 60%.

H.3.9 GROUP 9

The model of the group with insertions parallel to the muscle fibers with an insertion velocity of 50 mm/s and rotation of 572 RPM is shown in figure H.14 indicated by the thick green line. Most of the measured curves look like the modeled curve except two curves. These two curves corresponds with the two negative VAF values. The best VAF value is 99% and most values are above 90%.

H.3.10 GROUP 10

The model of the group with insertions perpendicular to the muscle fibers with an insertion velocity of 1 mm/s and without a rotation is shown in figure H.15 indicated by the thick green line. Some of the measurements have much larger overshoots. However most shapes are similar to the modeled curves except for one measurement. The table besides the graph shows two negative VAF values. The best VAF value is 99% and most values are above 75%.

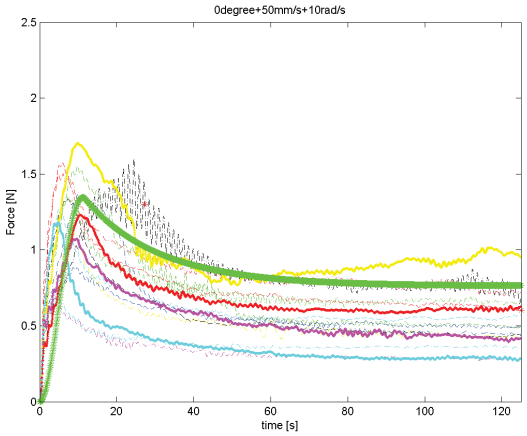

VAF
0.78
0.91
0.897
0.70
0.70
0.60
-1.4
-0.58
0.95
0.93
0.82
0.98
0.96
0.67
-0.54
0.92

Figure H.13: Model and sixteen insertion force plots with insertions parallel to the muscle fibers, insertion velocities of 1 mm/s and rotation of 114 RPM. The thick green line is the model of this group.

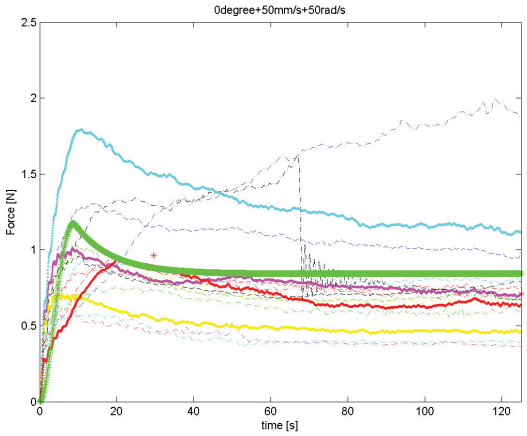

VAF
0.99
0.97
0.96
0.95
0.96
0.95
-0.062
-0.018
0.96
0.85
0.76
0.90
0.51
0.98
0.87
0.92

Figure H.14: Model and sixteen insertion force plots with insertions parallel to the muscle fibers, insertion velocities of 50 mm/s and rotation of 572 RPM. The thick green line is the model of this group.

H.3.11 GROUP 11

The model of the group with insertions perpendicular to the muscle fibers with an insertion velocity of 1 mm/s and with a rotation of 114 RPM is shown in figure H.16 indicated by the thick green line. Most curves look like the curve of the model. The table besides the graph shows one negative VAF value. The best VAF value is 99% and most values are above 75%.

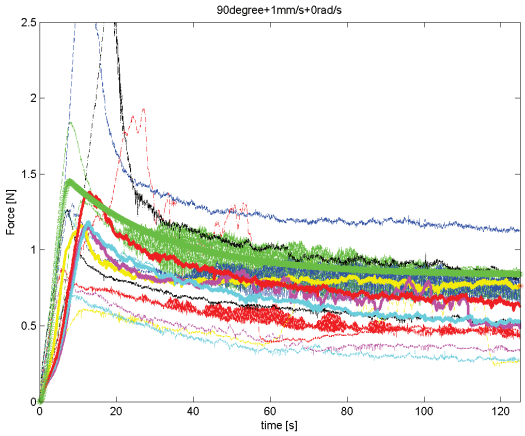

VAF
0.96
0.51
0.99
0.89
0.77
0.31
-0.22
-1.1
0.80
0.98
0.97
0.92
0.94
0.86
0.81
0.94

Figure H.15: Model and sixteen insertion force plots with insertions perpendicular to the muscle fibers, insertion velocities of 1 mm/s and no rotation. The thick green line is the model of this group.

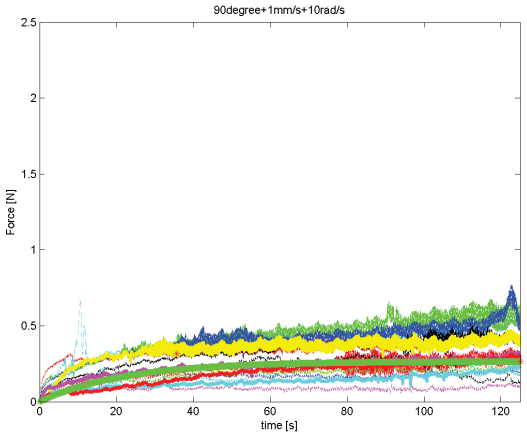

VAF
0.81
0.87
0.75
0.79
0.89
0.97
-1.8
0.61
0.97
0.93
0.85
0.95
0.86
0.99
0.57
0.96

Figure H.16: Model and sixteen insertion force plots with insertions perpendicular to the muscle fibers, insertion velocities of 1 mm/s and a rotation of 114 RPM. The thick green line is the model of this group.

H.3.12 GROUP 12

The model of the group with insertions perpendicular to the muscle fibers with an insertion velocity of 1 mm/s and with a rotation of 572 RPM is shown in figure H.17 indicated by the thick green line. As with the parallel insertion, the green line covers the measured data completely. The table besides the graph shows only zero VAF values. These could be explained in the same way as with the parallel insertions (GROUP3): the model is a horizontal line through zero.

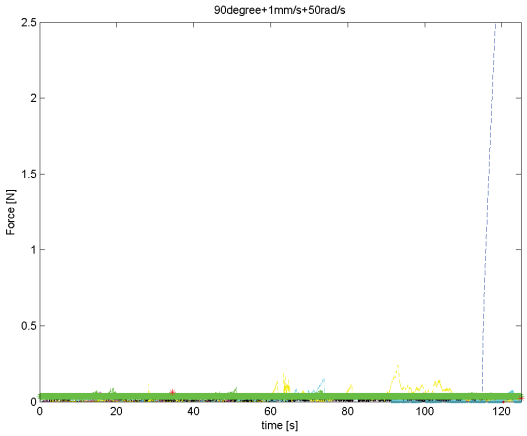

VAF
0
0
0
0
0
0
0
0
0
0
0
0
0
0
0
0

Figure H.17: Model and sixteen insertion force plots with insertions perpendicular to the muscle fibers, insertion velocities of 1 mm/s and a rotation of 572 RPM. The thick green line is the model of this group.

H.3.13 GROUP 13

The model of the group with insertions perpendicular to the muscle fibers with an insertion velocity of 10 mm/s and without rotation is shown in figure H.18 indicated by the thick green line. Some of the measured curves show oscillations. However most curve shapes are similar to the modeled curve. The table besides the graph shows that all measurements are correlated to the model. The lowest VAF value is 46% and the largest 99%.

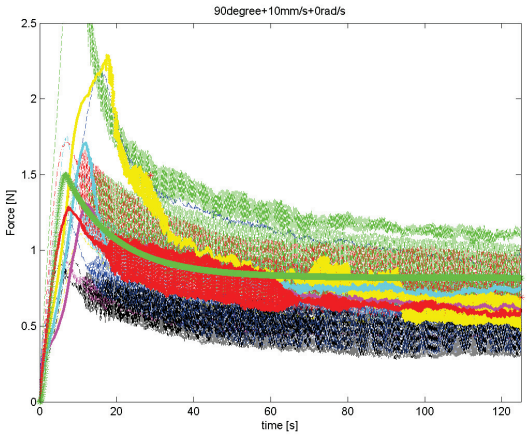

VAF
0.97
0.99
0.83
0.90
0.65
0.79
0.47
0.97
0.96
0.96
0.74
0.46
0.90
0.94
0.97
0.95

Figure H.18: Model and sixteen insertion force plots with insertions perpendicular to the muscle fibers, insertion velocities of 10 mm/s and no rotation. The thick green line is the model of this group.

H.3.14 GROUP 14

The model of the group with insertions perpendicular to the muscle fibers with an insertion velocity of 10 mm/s and with a rotation of 114 RPM is shown in figure H.19 indicated by the thick green line. One measurement shows oscillations. Most curve shapes are similar to the modeled curve, except for two which have a deviant shape. The table besides the graph shows no negative VAF values. Al curves are correlated to the model. The best VAF value is 99% and the lowest values is 15%.

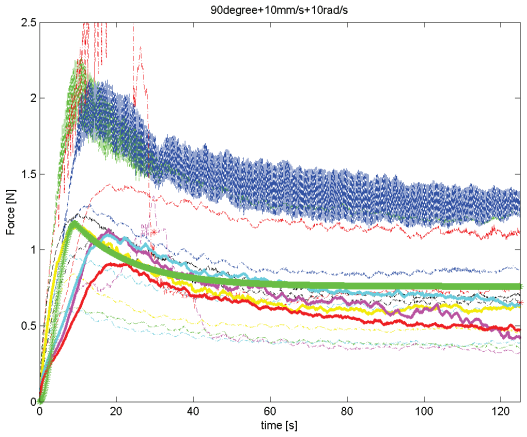

VAF
0.96
0.89
0.82
0.80
0.98
0.72
0.60
0.15
0.67
0.26
0.98
0.99
0.97
0.94
0.98
0.86

Figure H.19: Model and sixteen insertion force plots with insertions perpendicular to the muscle fibers, insertion velocities of 10 mm/s and a rotation of 114 RPM. The thick green line is the model of this group.

H.3.15 GROUP 15

The model of the group with insertions perpendicular to the muscle fibers with an insertion velocity of 10 mm/s and with a rotation of 572 RPM is shown in figure H.20 indicated by the thick green line. Two measurements have much higher values than the model. All curves have the same shape as the modeled curve but most measurements reach the steady state sooner. The table besides the graph shows four negative VAF values. The best VAF value is 97% and most values are above 50%.

H.3.16 GROUP 16

The model of the group with insertions perpendicular to the muscle fibers with an insertion velocity of 50 mm/s and without a rotation is shown in figure H.21 indicated by the thick green line. The figure shows two measurements with large oscillations. However the shape of most measurements is similar to the shape of the model. The table besides the graph shows three negative VAF values. The best VAF value is 98% and the lowest values is 75%.

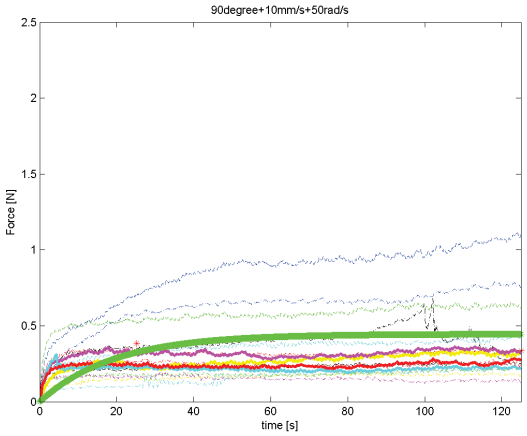

VAF
0.97
0.87
0.88
0.70
0.48
-0.94
-1.7
-0.94
0.57
-0.34
0.85
0.96
0.77
0.88
0.20
0.51

Figure H.20: Model and sixteen insertion force plots with insertions perpendicular to the muscle fibers, insertion velocities of 10 mm/s and a rotation of 572 RPM. The thick green line is the model of this group.

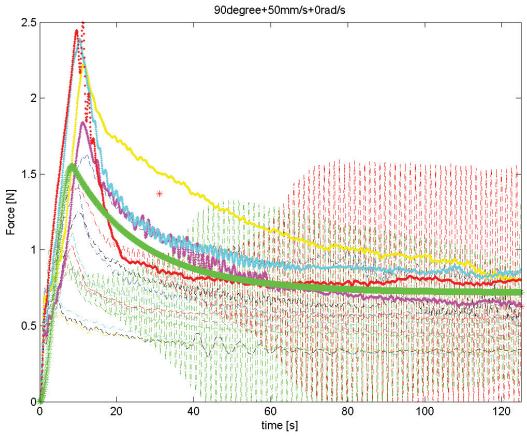

VAF
0.76
0.75
0.44
0.97
-0.77
-0.83
0.56
-0.60
0.82
0.60
0.92
0.95
0.90
0.98
0.96
0.96

Figure H.21: Model and sixteen insertion force plots with insertions perpendicular to the muscle fibers, insertion velocities of 50 mm/s and with a rotation. The thick green line is the model of this group.

H.3.17 GROUP 17

The model of the group with insertions perpendicular to the muscle fibers with an insertion velocity of 50 mm/s and with a rotation of 114 RPM is shown in figure H.22 indicated by the thick green line. All curve shapes are similar to the modeled curve. All measurements are correlated to the model. No negative VAF values can be found in the table next to the graph. The best VAF value is 99% and the lowest values is 11%.

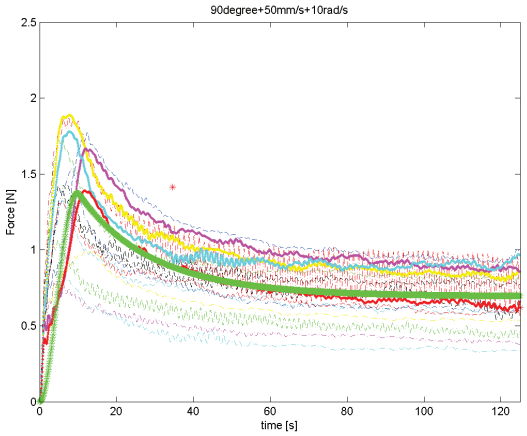

VAF
0.94
0.95
0.95
0.93
0.96
0.90
0.44
0.11
0.92
0.74
0.96
0.97
0.94
0.95
0.95
0.99

Figure H.22: Model and sixteen insertion force plots with insertions perpendicular to the muscle fibers, insertion velocities of 50 mm/s and a rotation of 114 RPM. The thick green line is the model of this group.

H.3.18 GROUP 18

The model of the group with insertions perpendicular to the muscle fibers with an insertion velocity of 50 mm/s and with a rotation of 572 RPM is shown in figure H.23 indicated by the thick green line. Most curve shapes are similar to the modeled curve. The table next to the graph shows three negative VAF values. The best VAF value is 98% and most values are above 75%.

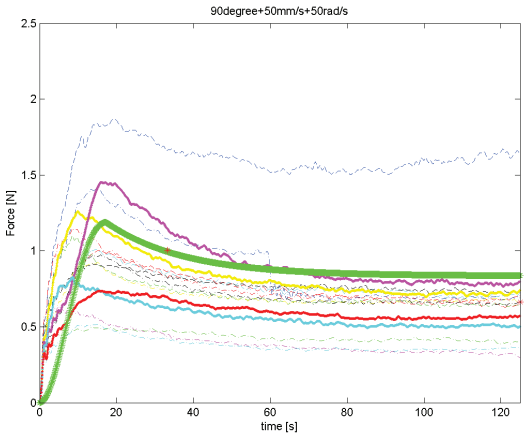

VAF
0.96
0.96
0.88
0.80
0.95
0.90
-0.55
-0.79
0.91
-0.11
0.91
0.92
0.95
0.98
0.64
0.76

Figure H.23: Model and sixteen insertion force plots with insertions perpendicular to the muscle fibers, insertion velocities of 50 mm/s and a rotation 0f 572 RPM. The thick green line is the model of this group.

H.4 Conclusion & Model implementation

The model verification shows that the behavior of the insertion force for each individual measurement can be modeled with a mass-damper system. These models can indicate the amount of friction. The models were divided into three types: a straight line, a step response with overshoot and one without. Within these three types, differences in the amount of overshoot, settling distance and steady value can be found. These characteristics are effected by the insertion and rotational velocities.

The relation between the characteristics and the applied velocities can be used to make a model of the amount of friction in terms of rotational and insertion velocity. In turn, these relations can be expressed as a function which can be substituted into the previous functions (models).

It should be noticed that the models are obtained from measurements where the contact area between the catheter and tissue (or insertion depth) is constant. In other situations, such as needle insertions where the contact area (or insertion depth) is not constant, the models should be adapted or the friction should be calculated iteratively with finite element models.

For example, the tissue can be divided into several elements as is illustrated in figure H.24. This is possible because the friction force is linearly related to the insertion depth, as can be seen from the friction models (appendix B.4) and experimental studies [5, 6].

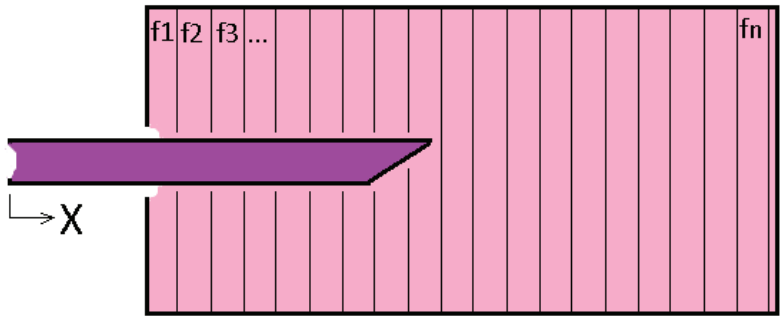

Figure H.24: Needle insertion into tissue where the tissue is divided into several elements. An approximation of the insertion force over insertion depth can be calculated by calculating the amount of force for each piece and adding them together.

During the insertion more elements come into contact with the needle. The force exerted by each element can be calculated and the total amount of insertion force is the sum of forces in all the elements. Each element has its own initial position relative to the needle from which the friction can be calculated.

When a element come into contact with the needle, the force, for this element, rises to a maximum where after the force goes to a steady value during further movement.

Bibliography

[1] G. K. Franklin, J. D. Powel, and A. Emami-Naeini, *Feedback Control of Dynamic Systems*, 5th ed. Pearson Education, 2006.

[2] N. S. Nise, *Control Systems Engineering*, 4th ed. John Wiley and Sons, 2004.

[3] J. Meriam and L. Kraige, *Engineering mechanics - Dynamics*, 4th ed. John Wiley and Sons, 1998.

[4] A. de Vlugt, A. Schouten, W. Mugge, and A. Klomp, "Lecture notes: System Identification & Parameter Estimation (WB2301)," Delft University of Technology, Tech. Rep., 2009.

[5] N. Abolhassani, R. Patel, and M. Moallem, "Needle insertion into soft tissue: a survey." *Medical engineering & physics*, vol. 29, no. 4, pp. 413–431, May 2007. [Online]. Available: http://www.ncbi.nlm.nih.gov/pubmed/16938481

[6] A. M. Okamura, C. Simone, and M. D. O'Leary, "Force modeling for needle insertion into soft tissue." in *IEEE transactions on bio-medical engineering*, vol. 51, no. 10, Oct. 2004, pp. 1707–16. [Online]. Available: http://www.ncbi.nlm.nih.gov/pubmed/15490818

APPENDIX

I

ADDITIONAL STATISTICAL TESTS

Not all groups in the measurements are normally distributed. This can affect the measurements, because the ANOVA assumes that the data is normally distributed. In this appendix, results of additional statistical tests with log scaled data is presented. The sections have the same structure as the sections in the paper. Only the sections that differ from the sections of the paper are presented. Section I.1 corresponds with section 2.2 of the paper and section I.2 with section 3 of the paper.

I.1 Data analysis

The insertion force measurements show different step response curves (see figure I.3). However on these curves several oscillations could be found. A pilot experiment with a gel phantom was performed to figure out if the oscillations are related to the properties of the meat (appendix E). These measurements also show oscillations (see figure I.1 & I.2).

A spectral analysis shows oscillations around 1.9, 9.5 and 43 Hz (appendix E). These frequencies match the natural frequencies of the setup (see appendix D.2). The container can oscillate with a natural frequency of 43 Hz caused by the leaf springs, force sensor and mass of the gel. Due to the rotational velocity, the system starts to oscillate with 1.9 or 9.5 Hz (appendix D.2). However this frequency is within the range of interest. A low pass zero phase filter (Butterworth, zero phase) of 30 Hz is used to filter out the natural frequency of the setup. The contribution of the natural frequency is normally higher than of the rotations. The filtered data is used for the analysis of the maximum insertion forces. For the analysis of the settling time (discussed in the next section), a moving average filter (150 samples, zero phase) is used to smooth irregularities.

I.1.1 Insertion force in time

Mainly three types of step response curves can be found for the insertion forces as shown in figure I.3. Overshoot can be found in settings with no rotation or where the insertion velocity is higher than or equal to the rotational velocity. Settings where the rotational velocity is higher than the insertion velocity show normally curves similar to the step response without overshoot except the settings with 1 mm and 572 RPM. This setting is represented by a horizontal line at the steady value.

The data is analyzed with the step response analysis function of MATLAB 'stepinfo.m'. The first and last 1/25th part of the data is not used by this function. The mean of the last 2/5th part of the (unfiltered) data is used as steady value. The settling time is stated as the time to reach and stay within 10% plus an amount of 0.1 N of the steady value. The maximum threshold is 100%. The distances to reach a steady value are calculated from the settling times by multiplying them by the insertion velocities that were applied.

The characteristics of the curves, the steady value, the overshoot or maximum and the settling distance, are presented in the box plots of figure I.4, figure I.5 and figure I.6. All 576 measurements are used for the calculations.

In total twelve measurements are marked as 'failed', ten exceed the 4 N and two had a deviant curve. These 'failed' measurements are replaced by the group means [1]. In this way, the group means are least influenced. The fact that this lowers the standard deviation [1] can be neglected. In exceptional cases, up to four values within a group are replaced by the group means. For the settling time, an additional 16 measurements are replaced by the group means because the MATLAB function could not find the settling time time within the set boundaries.

Below each box plot, a table is mentioned with statistical tests of the settings. In the next section is discussed how they are obtained. The characteristics of the curves are discussed separately in the next section.

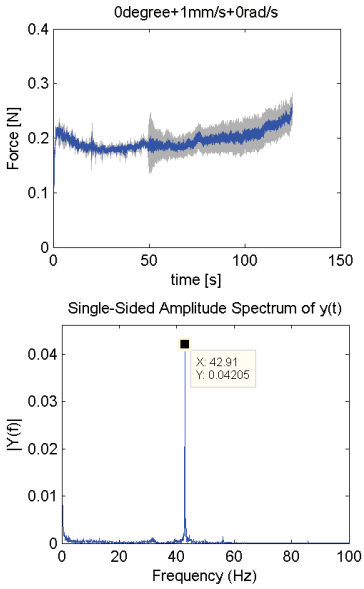

Figure I.1: TOP: Plot of a measurement of the insertion force with the setting 0°, 1 mm/s and 0 RPM in gel. In blue data filtered with a 30 Hz low pass zero phase filter and in gray the unfiltered data. **Bottom:** Fast Fourier transform plot of the above insertion force.

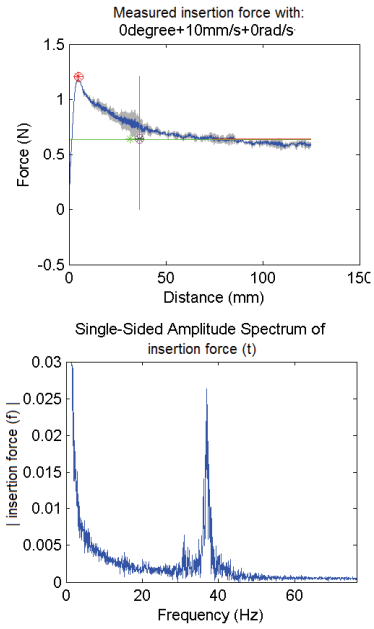

Figure I.2: TOP: Plot of a measurement of the insertion force with the setting 0°, 10 mm/s and 0 RPM in meat. The green line is the steady value, the pink line the settling time and the red dot the maximum value. **Bottom:** Fast Fourier transform plot of the above insertion force.

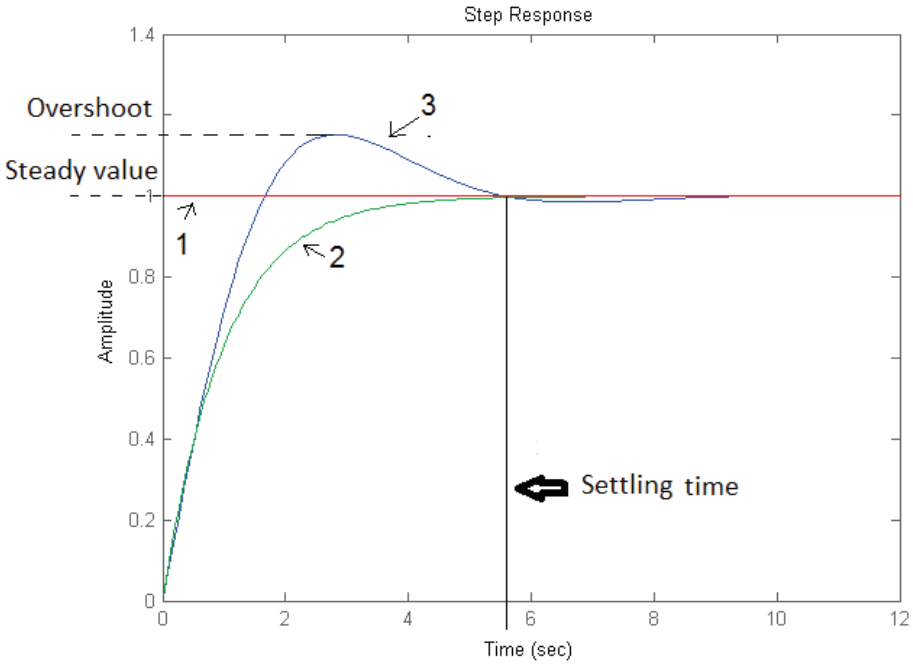

Figure I.3: Three step responses, 1: horizontal line at steady value, 2: step function without overshoot, 3: step function with overshoot.

I.1.2 Statistical tests

Below each set of box plots a table with an analysis of variance (ANOVA) is presented, which is performed in SPSS to investigate significant effects of the different parameters [1]. 'Failure' market measurements are replaced by the group means (calculated without 'failures') [1]. In turn, this data is transformed to a log scale to obtain normal distributed data [1]. All groups of the maximum and steady insertion force results are normally disturbed, except the two groups with insertions of 1 mm/s and 572 RPM. In the results of the settling distance and steady torque, more than ten groups are not normally distributed and this should be taken into account for the interpretation of the results. A repeated measure is chosen because the effects of the settings within the phantoms are of interest [1].

The tables present two results. The first column is the outcome of ANOVA when it is assumed that the data is spherical. To meet sphericity, the variance between different levels should be equal. The second column contains the results of the Greenhouse Geiser. The Mauchly's test was performed which shows that some of the data is not spherical [1]. These are indicated by '*'. In these cases the results of the Greenhouse Geiser has to be chosen.

In a regular ANOVA it is assumed that the variation is equal in each group, so sphericity is met [1]. However when this is not the case, more or less overlap between the groups can be found, which is not assumed in the regular ANOVA. The Greenhouse Geiser test provides a correction factor which compensates the differences in variance and so the effect of the parameter can be investigated [1]. For the multivariate test, no spherecy is required [1]. A significance level of

0.05 is used in all tests.

ANOVA shows if a factor has any effect but does not tell anything about the effect of the individual levels of the factor. As was discussed, sphericy is not always met and a regular post hoc test, where the effect of each individual level is investigated, could not be performed. For this reason several t-test were performed to compare the means of two groups with each other. A p-value below 0.005 shows that the means significantly differ. In the box plot can be seen which group is larger than the other group.

I.2 Results

In this section the results of the insertion force and torque measurements are presented. As was discussed, the insertion force measurements in time show different step responses. The characteristics are presented separately in the first sections. In the following section the results of the torque measurements are presented. The last section contains the resultant insertion force which is calculated from the steady insertion force and steady torque measurements.

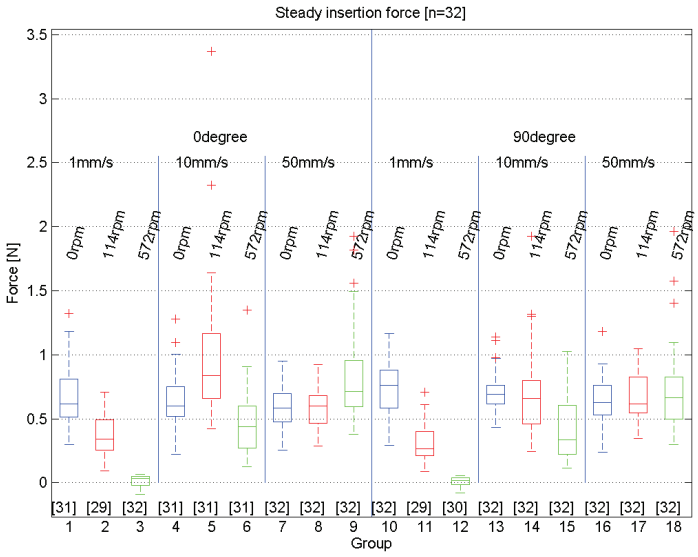

Figure I.4: Box plots of steady insertion forces for each combination. The box plots are of checked measurements without 'failures' ([n]). The groups are filled up to the group size of 32 by (32-n) times the group means.

I.2.1 Steady insertion force

Figure I.4 shows box plots of the steady insertion force data and table I.1 the statistical analysis of variance (ANOVA).

The box plot of figure I.4 shows that groups were a rotation is applied have normally a lower median steady friction force compared to groups without rotations. This is also confirmed by the t-tests. Remarkable are settings with

Table I.1: Left: Table with two tests: Regular ANOVA where sphericy is assumed and the Greenhouse Geisser where a correction factor is used to compensate non sphericy. Factors with P-values lower than 5% affect the steady insertion force. Factors with other values do not have a significant affect on the insertion force. Sphericity of the data is tested with the Mauchly's test of sphericity. Non spherical factors are indicated by '*'. **Right:** Table with several t-tests. P-values lower than 5% show that the group means significantly differ.

Setting	Sphericy assumed	Greenhouse Geisser
Orientation	0.732	0.732
Insertion velocity*	<0.001	<0.001
Rotational velocity*	<0.001	<0.001
Orientation × ins. vel.	0.072	0.078
Orientation × rot. vel.*	0.024	0.037
Ins. vel. × rot. vel.*	<0.001	<0.001
Or. × ins. vel. × rot. vel.*	0.013	0.023

Comp.	p-val.	Comp.	p-val.
Gr. 1 vs 2	<0.001	Gr. 10 vs 11	<0.001
Gr. 1 vs 3	<0.001	Gr. 10 vs 12	<0.001
Gr. 1 vs 4	0.465	Gr. 10 vs 13	0.590
Gr. 4 vs 5	<0.001	Gr. 13 vs 14	0.534
Gr. 4 vs 6	0.002	Gr. 13 vs 15	<0.001
Gr. 4 vs 7	0.361	Gr. 13 vs 16	0.057
Gr. 7 vs 8	0.961	Gr. 16 vs 17	0.228
Gr. 7 vs 9	<0.001	Gr. 16 vs 18	0.150
Gr. 1 vs 7	0.021	Gr. 10 vs 16	0.493

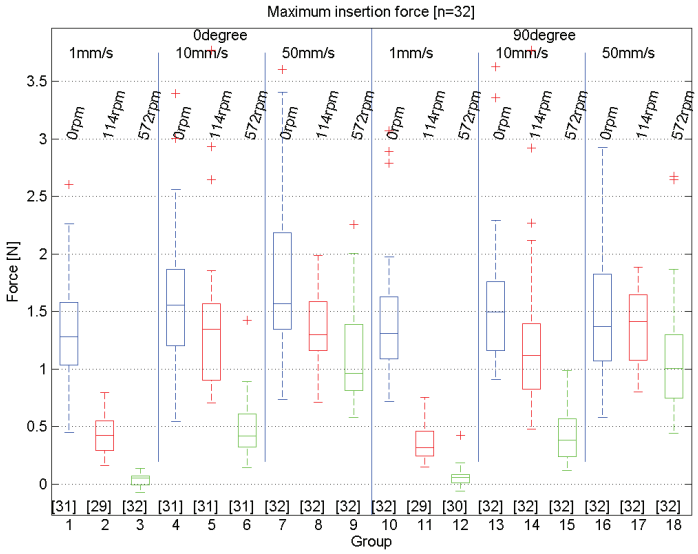

Figure I.5: Box plots of maximum insertion forces for each combination. The box plots are of checked measurements without 'failures' ([n]). The groups are filled up to the group size of 32 by (32-n) times the group means.

an insertion parallel to the muscle fibers in combination with equal insertion velocity and tangential velocity. Here, the median steady insertion force increases. The same combinations with perpendicular insertions do not have this effect. Here the rotation has little affect on the median steady insertion force. These findings were also verified by a t-tests. The differences between these two settings can explain the significance of the interaction effect between the orientation and rotational velocities mentioned in the table.

Table I.2: Left: Table with three tests: Regular ANOVA where sphericy is assumed, Greenhouse Geisser where a correction factor is used to compensate non sphericy. Factors with P-values lower than 5% affect the maximum insertion force. Factors with other values do not have a significant affect on the maximum insertion force. Sphericity of the data is tested with the Mauchly's test of sphericity. Non spherical factors are indicated by '*'. **Right:** Table with several t-tests. P-values lower than 5% show that the group means significantly differ.

Setting	Sphericy assumed	Greenhouse Geisser
Orientation	0.392	0.392
Insertion velocity*	<0.001	<0.001
Rotational velocity*	<0.001	<0.001
Orientation × ins. vel.	0.035	.035
Orientation × rot. vel.	0.331	0.325
Ins. vel. × rot. vel.*	<0.001	<0.001
Or. × ins. vel. × rot. vel.	0.090	0.099

Comp.	p-val.	Comp.	p-val.
Gr. 1 vs 2	<0.001	Gr. 10 vs 11	<0.001
Gr. 1 vs 3	<0.001	Gr. 10 vs 12	<0.001
Gr. 1 vs 4	0.026	Gr. 10 vs 13	0.140
Gr. 4 vs 5	0.067	Gr. 13 vs 14	0.001
Gr. 4 vs 6	<0.001	Gr. 13 vs 15	<0.001
Gr. 4 vs 7	0.354	Gr. 13 vs 16	0.251
Gr. 7 vs 8	0.001	Gr. 16 vs 17	0.511
Gr. 7 vs 9	<0.001	Gr. 16 vs 18	0.001
Gr. 1 vs 7	0.022	Gr. 10 vs 16	0.826

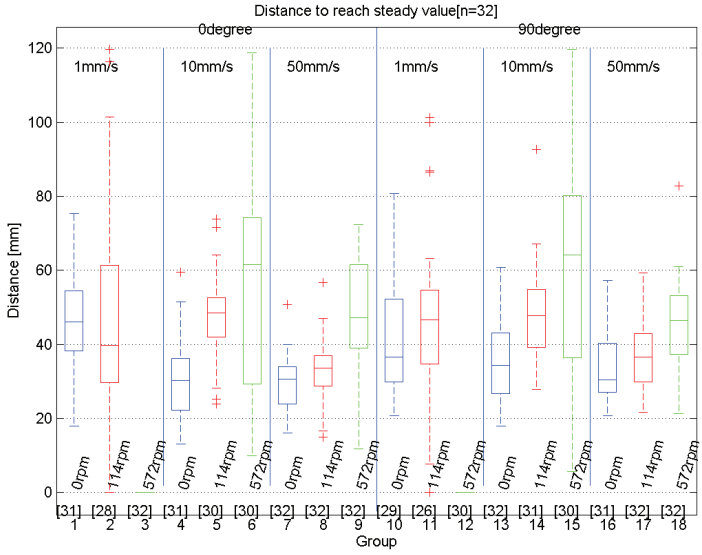

Figure I.6: Box plots of the distance to reach steady value for each combination. The box plots are of checked measurements without 'failures' ([n]). The groups are filled up to the group size of 32 by (32-n) times the group means.

The table also shows that the steady insertion force is affected by the insertion and rotational velocities. Furthermore an interaction effect [1] between the insertion and rotational velocities as well as between the orientation of the fibers and rotational velocities can be found. Also an interaction effect on the steady insertion force of all parameters can be found. However, the reliability

[1] An interaction effect of x and y on z means that the influence of y on z is also influenced by the parameter x. The individual effects cannot be added together to get the overall effect.

Table I.3: Left: Table with three tests: Regular ANOVA where sphericy is assumed, Greenhouse Geisser where a correction factor is used to compensate non sphericy. Factors with P-values lower than 5% affect the distance to reach the steady insertion force. Factors with other values do not have a significant affect on this distance. Sphericity of the data is tested with the Mauchly's test of sphericity. Non spherical factors are indicated by '*'. **Right:** Table with several t-tests. P-values lower than 5% show that the group means significantly differ.

Setting	Sphericy assumed	Greenhouse Geisser
Orientation	0.883	0.883
Insertion velocity*	<0.001	<0.001
Rotational velocity*	<0.001	<0.001
Orientation × ins. vel.*	0.250	.247
Orientation × rot. vel.*	0.787	0.710
Ins. vel. × rot. vel.*	<0.001	<0.001
Or. × ins. vel.* × rot. vel.	0.842	0.640

Comp.	p-val.	Com.	p-val.
Gr. 1 vs 2	0.423	Gr. 10 vs 11	<0.312
Gr. 1 vs 3	<0.001	Gr. 10 vs 12	<0.001
Gr. 1 vs 4	<0.001	Gr. 10 vs 13	0.072
Gr. 4 vs 5	<0.001	Gr. 13 vs 14	<0.001
Gr. 4 vs 6	<0.001	Gr. 13 vs 15	0.002
Gr. 4 vs 7	0.997	Gr. 13 vs 16	0.603
Gr. 7 vs 8	0.106	Gr. 16 vs 17	0.040
Gr. 7 vs 9	<0.001	Gr. 16 vs 18	<0.001
Gr. 1 vs 7	<0.001	Gr. 10 vs 16	0.071

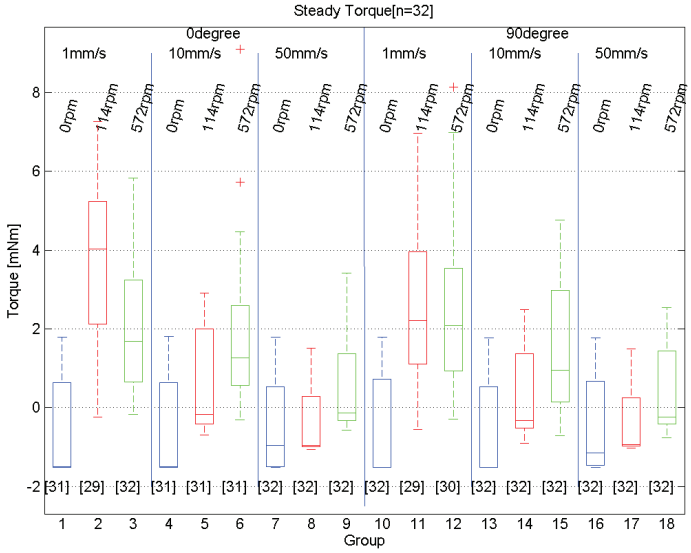

Figure I.7: Box plots of the steady torques for each combination. The box plots are of checked measurements without 'failures' ([n]). The groups are filled up to the group size of 32 by (32-n) times the group means.

of results of a three way interaction are contestable.

Furtheremore, some of the steady insertion forces are negative. The steady insertion forces are corrected with an offset value which represents the measured force without load. This is an average value of three measurements and the offset can slightly vary due to the play of the setup. In turn, this can cause some of the values to be slightly below zero. Also noise will contribute to this.

The first nine settings and the last nine settings are roughly the same which

Table I.4: Table with three tests: Regular ANOVA where sphericy is assumed, Greenhouse Geisser where a correction factor is used to compensate non sphericy. Factors with P-values lower than 5% affect the steady torque. Factors with other values do not have a significant affect on the steady torque. Sphericity of the data is tested with the Mauchly's test of sphericity. Non spherical factors are indicated by '*'. **Right:** Table with several t-tests. P-values lower than 5% show that the group means significantly differ.

Setting	Spherical assumed	Greenhouse Geisser
Orientation	0.826	0.826
Insertion velocity	<0.001	<0.001
Rotational velocity*	<0.001	<0.001
Orientation × ins. vel.	0.489	.468
Orientation × rot. vel.*	0.101	0.128
Ins. vel. × rot. vel.*	<0.001	<0.001
Or. × ins. vel. × rot. vel.*	<0.634	0.536

Comp.	p-val.	Comp.	p-val.
Gr. 1 vs 2	<0.001	Gr. 10 vs 11	<0.001
Gr. 1 vs 3	<0.001	Gr. 10 vs 12	<0.001
Gr. 1 vs 4	<0.711	Gr. 10 vs 13	0.413
Gr. 4 vs 5	<0.001	Gr. 13 vs 14	<0.001
Gr. 4 vs 6	<0.001	Gr. 13 vs 15	<0.001
Gr. 4 vs 7	0.051	Gr. 13 vs 16	0.004
Gr. 7 vs 8	<0.001	Gr. 16 vs 17	0.001
Gr. 7 vs 9	<0.001	Gr. 16 vs 18	<0.001
Gr. 1 vs 7	0.003	Gr. 10 vs 16	0.002
Gr. 2 vs 3	< 0.001	Gr. 11 vs 12	0.384
Gr. 2 vs 5	< 0.001	Gr. 11 vs 14	< 0.001
Gr. 3 vs 6	0.111	Gr. 12 vs 15	0.001
Gr. 5 vs 8	< 0.001	Gr. 14 vs 17	< 0.001
Gr. 6 vs 9	< 0.001	Gr. 15 vs 18	< 0.001
Gr. 2 vs 11	0.004	Gr. 5 vs 14	0.034
Gr. 3 vs 12	0.329	Gr. 6 vs 15	< 0.232

can explain that the effect of the orientation is not significant. The insertion velocity especially has an effect in combination with a rotation. The differences between the settings with no rotation are small. Summarized:

- The median steady insertion force is reduced for settings where tthe tangential velocity is higher than the insertion velocity.
- Equal tangential and insertion velocities can result in an increased median steady insertion force.
- The median steady insertion force is not or is little affected by the insertion velocity and fiber orientation.

I.2.2 Overshoot / maximum

The results for the overshoot or maximum insertion force (in cases where the overshoot is zero) are presented in figure I.5 and table I.2. The statistical test shows that the orientation does not affect the maximum insertion force, only in combination with the insertion velocity. Furthermore, it is shown that the maximum insertion force is affected by the insertion velocity as well as by the rotational velocity. Also an interaction affect between these two parameters can be found.

In the presented box plots, it is clear that an increased rotational velocity results in a reduced median maximum. This is also found by the t-tests with the exception of some groups. In comparison, an increased insertion velocity results in an increased median maximum. The t-tests show that this only holds for some of the groups with parallel insertions. It should be noticed that the median of the settings with no rotation and 10 mm/s compared to settings with no rotation and 50 mm/s, is the same. Settings with equal rotational velocity but with different insertion velocities, result in different median maximums. This

explains the significant of the interaction effect of the rotational and insertion velocities in the table. Summarized:

- The maximum insertion force is not affected by the fiber orientation.
- An increased insertion velocity can results in an increased maximum insertion force.
- An increased rotational velocity results normally in a decreased maximum insertion force.
- The effect of the insertion and rotational velocity depends on each other.

I.2.3 Settling distance

The distance to reach a steady value, the settling distance, is defined as the settling time multiplied by the applied insertion velocity. The results in the box plot of figure I.6 show that a rotational movement normally increases the median settling distance. Remarkable exceptions are settings with 1 mm/s and 572 RPM, where the median settling distance is zero.

Settings with equal rotational and insertion velocities but with different orientations results in roughly the same median settling distance. This indicate that the settling distance is not affected by the fiber orientation. This is also verified by the ANOVA presented in table I.3. Also in combination with other parameters, the orientation does not affect the settling distance.

An increased insertion velocity normally results in a decreased median settling distance. This is also verified by some of the t-tests which shows that the means of some settings without rotations are different. The box plots and table indicate that there is a significant interaction effect of the insertion and rotational velocities. Summarized:

- The settling distance is not affected by the fiber orientation.
- An increased insertion velocity can result in a decreased median settling distance.
- An increased rotational velocity normally results normally in an increased median settling distance.

I.2.4 Torque

Before the measurements are started, a rotation is applied. No clear curves could be distinguished as with the insertion force. For this reason only the results of the steady torque are presented in figure I.7 and table I.4. The steady torque is determined by the median of the last 2/5th part of the rough torque data. As with the insertion force, the 'failed' measurements are replaced by the group means.

The box plots indicate that rotation increases the required torque. This is also verified by the t-tests, the means of groups with the same insertion velocity but with different rotational velocities are different. Remarkable are the settings without rotation where the torques are not zero. Due to the forward motion, rotation of the catheter can be induced. The motor controller acts against these

rotations what can explain the non zero values. Other remarkable settings are at 1 mm/s velocity and 114 RPM rotation where the median torques are higher than settings with higher rotational velocities.

The median torques normally decrease when the insertion velocities increase for settings with a rotation. This is also verified by the t-tests. The decrease in torque cannot be found for (all) settings without a rotation. These findings are verified by most of the results of the t-test.

The table with the statistical tests (ANOVA) shows that the steady torque is not affected by all the fiber orientation. The test also shows that the torque is affected by both the insertion as well as the rotational velocities. Also an interaction effect between these two can be found. Summarized:

- The steady torque is not affected by the fiber orientation.
- The median steady torque normally increases with an increased rotational velocity. Exceptions are settings with 1 mm/s and 114 RPM which have relatively high median torques compared to settings with 1 mm/s and 572 RPM.
- An increased insertion velocity results normally in a decreased median torque except for settings without catheter rotation.

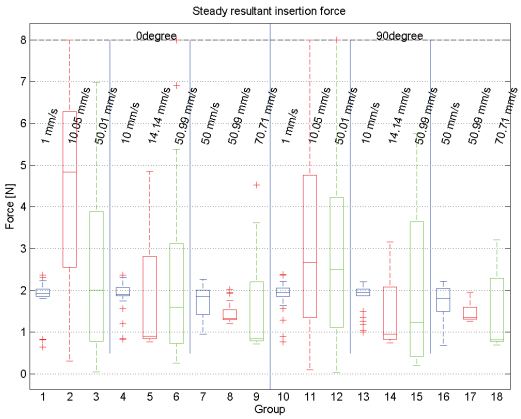

Comparison	p-value
Group 2 vs 4	<0.001
Group 3 vs 6	0.910
Group 3 vs 7	0.611
Group 7 vs 8	<0.001
Group 11 vs 13	0.278
Group 12 vs 15	0.250
Group 12 vs 16	0.925
Group 16 vs 17	0.003

Figure I.8: Left: Box plots of the steady resultant forces, calculated from the steady torque and steady insertion force. **Right:** Table with several t-tests. P-values lower than 5% show that the group means significantly differ.

I.2.5 Resultant insertion force

The steady insertion force and torque can be converted to a resultant force. This resultant force can provide information about the friction force itself. The resultant force is calculated by:

$$F_{res} = \sqrt{{F_{st}}^2 + \tau^2} \tag{I.1}$$

Where F_{st} is the steady insertion force and τ the steady torque. The resultant velocities are calculated by:

$$v_{res} = \sqrt{(v_{ins})^2 + (v_{pen})^2} \tag{I.2}$$

Where v_{ins} is the insertion velocity and v_{pen} the tangential velocity. The results of the resultant force are presented in figure I.8. The box plot show several outliers and for this reason the log of the resultant steady insertion force is used in the statistical test to minimize the effect of the outliers on the mean [1].

Looking at the overall results and comparing them to the theory described in the beginning of this paper some contrasts can be found. First if the torque and insertion force could simply be combined to one resultant insertion force, the results with the same resultant velocities should have the same value. Groups with roughly the same resultant velocities do not always have the same result. This is also verified by the t-tests. Several group means differ significantly from each other.

The friction in perpendicular direction could behave differently. Furthermore the resultant force is converted from the insertion force and torque which in turn is calculated from the motor current what can result in inaccuracy of the results. This makes it hard to make a prediction of the friction type.

I.3 Comparison & conclusion

Although the values of the statistical test with log scaled data differ, the same conclusions can be drawn. One exception is the effect of the fiber orientation on the steady torque. In the previous test, the ANOVA showed a p-value of 0.038 for the orientation which is just below 5%, so the fiber orientation affects the steady torque. In the ANOVA with a log-scale, the fiber orientation is not significant, which shows that the fiber orientation does not affect the steady torque. Because the result of the non-scaled data is around the significant level and the scaled test shows no affect, it is assumed that the steady torque is not affected by the fiber orientation.

Bibliography

[1] A. Field, *Discovering statics using SPSS*, 3rd ed. SAGE Publications Ltd, 2009.